KfK 4024
März 1986

SEFLEX
Fuel Rod Simulator Effects in Flooding Experiments

Part 1:
Evaluation Report

P. Ihle, K. Rust
Institut für Reaktorbauelemente
Projekt Nukleare Sicherheit

Kernforschungszentrum Karlsruhe

KERNFORSCHUNGSZENTRUM KARLSRUHE
Institut für Reaktorbauelemente
Projekt Nukleare Sicherheit

KfK 4024

SEFLEX - Fuel Rod Simulator Effects in Flooding Experiments
Part 1: Evaluation Report

P. Ihle and K. Rust

Kernforschungszentrum Karlsruhe GmbH, Karlsruhe

Kernforschungszentrum Karlsruhe GmbH
Postfach 3640, 7500 Karlsruhe 1

ISSN 0303-4003

Abstract

This report is a summary of an experimental investigation which is a part of the German LWR safety program. The aim of the SEFLEX program has been to quantify the influence of the design and the physical properties of different fuel rod simulators on heat transfer and quench front progression in unblocked and blocked rod bundles during the reflood phase of a LOCA in a PWR. Fuel rod simulators with Zircaloy claddings and a gas-filled gap between claddings and pellets exhibit lower peak cladding temperatures and shorter quench times than gapless heater rods with stainless steel claddings. Grid spacers cause significant cooling enhancement downstream during the time span at which maximum cladding temperatures occur. Ballooned Zircaloy claddings, forming e.g. a 90 percent blockage, are quenched substantially earlier than thickwall stainless steel blockage sleeves attached to the rods, and even earlier than undeformed rod claddings. A comparison of test data with results of the "Best Estimate" computer program COBRA-TF shows a good agreement with unblocked bundle data including grid spacer effects.

This report is accompanied by a unblocked bundle data report (KfK 4025) and a blocked bundle data report (KfK 4026). These three reports conclude the SEFLEX program.

SEFLEX-Brennstab-Simulator-Effekte in Flutexperimenten

Teil 1: Auswertebericht

Kurzfassung

Dieser Bericht ist eine Zusammenfassung einer experimentellen Untersuchung, die ein Teil des deutschen LWR Sicherheitsprogramms ist. Das Ziel des SEFLEX-Programms war die Quantifizierung des Einflusses von Aufbau und physikalischen Stoffdaten von verschiedenen Brennstabsimulatoren auf den Wärmeübergang und das Fortschreiten der Benetzungsfront in unblockierten und blockierten Stabbündeln während der Flutphase eines Kühlmittelverluststörfalles in einem LWR. Brennstabsimulatoren mit Zircaloy-Hüllrohren und einem gasgefüllten Spalt zwischen Hüllrohren und Pellets führen zu niedereren Maximaltemperaturen der Hüllrohre und zu kürzeren Wiederbenetzungszeiten als spaltlose Heizstäbe mit Edelstahlhüllrohren. Abstandshalter verursachen eine bedeutende Verbesserung der Kühlung in der Nachlaufströmung während der Zeitspanne, in der die Hüllrohre das Temperaturmaximum erreichen. Aufgeblähte Zircaloy-Hüllrohre, die z.B. eine Kühlkanalversperrung von 90 % darstellen, werden erheblich früher benetzt als dickwandige, an den Stäben angebrachte Blockadehülsen aus Edelstahl, und sogar früher als unverformte Hüllrohre. Ein Vergleich der Versuchsdaten mit Ergebnissen des "Best Estimate" Rechenprogramms COBRA-TF zeigt eine gute Übereinstimmung mit den Meßdaten der unblockierten Bündel einschließlich der Abstandshaltereffekte.

Zu diesem Bericht gehören zwei getrennte Berichte, Meßdaten von Experimenten mit unblockierten Bündeln (KfK 4025) und mit blockierten Bündeln (KfK 4026). Mit diesen drei Berichten ist das SEFLEX-Programm abgeschlossen.

TABLE OF CONTENTS

LISTING OF FIGURES

LISTING OF TABLES

PREAMBLE

This report is an overall summary of an experimental investigation which is a part of the German LWR safety program. Within the framework of this program the Kernforschungszentrum Karlsruhe (KfK) started the Project Nuclear Safety (PNS) in 1973 to investigate the fuel rod behavior of light water reactors (LWR) under loss-of-coolant accident (LOCA) conditions. Subjects of special importance were: The extent of core damage during a LOCA, the consequences of fuel rod failure on core coolability and fission product release, and the quantification of safety margins.

Two experimental programs of the PNS, performed in the Institut für Reaktorbauelemente (IRB) of the KfK, contributed to: (1) Zircaloy deformation behavior including interaction between fuel clad ballooning and thermal-hydraulics in a LOCA (REBEKA) and (2) Coolability of blocked rod bundles (FEBA). Comparison and analysis of the results of both programs indicated, that the two different types of rods used for simulation of nuclear fuel rods showed different behavior which needed to be quantified. Furthermore, the question arose how far the FEBA results concerning the coolability of severe blockages were applicable to ballooned fuel rod clusters.

The experience obtained from both programs was used for defining a new investigation in 1983:

"Fuel Rod Simulator Effects in Flooding Experiments (SEFLEX)

The publication of this report as well as two complementing data reports (KfK 4025, KfK 4026) marks the completion of this program.

Although many individuals have contributed to this program, we wish particularly to acknowledge the following:

Mr. H. Schneider — Modifications of the FEBA facility and of the REBEKA fuel rod simulators, management of rod bundle and test section assemblies, instrumentation and rig operations.

Mr. S. Barth — Data acquisition systems, instrumentation, data processing.

Mr. F. Erbacher Consulting and technical support.
Mr. A. Fiege General consulting and financial support by the PNS.

The main workshop VBW/HW of the KfK and the W. Bergmaier Co. at D-7520 Bruchsal 5 mainly for construction and instrumentation of the fuel rod simulators.

The authors gratefully acknowledge the support from the Nuclear Power Division of the Electric Power Research Institute (EPRI), USA, especially the efforts of Dr. W. B. Loewenstein, Dr. R. B. Duffey and Dr. A. Singh, for providing the opportunity to simulate selected FEBA and SEFLEX tests by using the COBRA-TF computer code. This analysis was sponsored by EPRI and carried out in cooperation with EPRI staff of the Safety Technology Department at the Palo Alto offices.

1. INTRODUCTION

The thermohydraulics in a nuclear reactor core during a loss-of-coolant accident (LOCA) of a pressurized water reactor (PWR) depends mainly on the location and the size of the break in the primary coolant system. However, the conditions of the plant at initiation of a LOCA as well as the design and the operation of the emergency core cooling system influence time dependent core cooling conditions as well.

During a large break in the cold leg, the water within the primary coolant circuit rapidly depressurizes leading to a flow reversal in the core. The flow direction from top to bottom of the core prevails at least towards the end of the blowdown phase, i.e. when the system pressure corresponds to the pressure in the containment. The upper part of Fig. 1 shows a simplified scheme of a 4-loop steam generator system of a PWR. The lower part of Fig. 1 shows the reactor pressure vessel and the installations.

During blowdown emergency core cooling systems (ECCS) are initiated following the transient of the system pressure. However, it is assumed that the reactor presssure vessel is empty at the end of the blowdown phase. The low pressure emergency core cooling system already operating is assumed to need some time to fill up the pressure vessel until the lower end of the core is beginning to be submerged in the rising water column (refill phase). At that moment the main flow direction through the core again is reversed to from bottom to top, prevailing during the reflood phase.

The nuclear decay of the fission products heats up the pellets and the claddings of the fuel rods until the ECCS becomes effective. Some of the fuel rods may reach temperatures which cause clad ballooning and burst. At beginning of the reflood phase the cladding temperatures are assumed to be above the Leidenfrost temperature. As the liquid level reaches the bottom end of the core and starts to rise around the fuel rods, complex transient heat transfer and two-phase flow processes occur. Ahead of the quench front the cladding temperatures are affected by the rate of steam generated upstream and the thermal-hydraulic behavior of entrained liquid droplets. The effect of this precursory cooling prevailing until quenching is characterized by a heat transfer coefficient decreasing with distance from the quench front. The local cladding temperature starts dropping when the precursory cooling ex-

ceeds the heat generated in the rods. The reflood phase is terminated when all rods are quenched over the whole length. Figure 2 shows schematically the pressure difference across the cladding and a range of temperature transients for different fuel rods in a 2F-cold leg break LOCA predicted by a conservative evaluation model.

The investigation presented contributes to answering the questions:
How fast are fuel rods cooled down realistically under given reflood conditions compared to swaged heater rods?
How and to what extend do coolant channel blockages (due to ballooned fuel rod claddings) influence the effectiveness of the reflood core cooling compared to blockages simulated by stainless steel sleeves?

A number of out-of-pile experiments were conducted in order to generate heat transfer and fluid flow data needed for the safety analysis of nuclear reactors. The thermal-hydraulic phenomena in unblocked as well as blocked rod bundle geometries were examined in reflood experiments such as FEBA [1], FLECHT-SEASET [2], THETIS [3], CEGB blockage tests [4], SCTF [5], CCTF [6] etc. The objectives of all these bundle tests have been to provide experimental reflood heat transfer and two-phase flow data in simulated PWR geometries for postulated LOCA conditions. The measured data were used to develop and validate physical models for computer codes providing qualified analytical tools for calculating realistic peak cladding temperatures and safety margins for unblocked and blocked bundle configurations.

Most of the experiments performed so far to understand the quench front progression and heat transfer in rod bundles were carried out using "solid-type" electrically heated rods for simulation of nuclear fuel rods. Such rods are characterized by a stainless steel cladding and a close thermal contact between cladding and the electric insulation filler material containing the embedded heating element.

However, during in pile tests such as the OECD Halden Reactor Project, it was observed that nuclear fuel rods, which are characterized by heat generating fuel pellets stacked in a Zircaloy tube with a radial gap between pellets and cladding, were quenched substantially earlier than electrically heated rods with a close contact between filler material and stainless steel cladding [7, 8, 9]. In the same project, REBEKA fuel rod simulators with a gas filled gap

between alumina pellets and Zircaloy claddings were observed to simulate closely the actual fuel rod behavior during a LOCA [10]. Similar results were obtained from NRU in pile tests [11].

Figure 3 shows a comparison of the transient cladding temperatures measured during four different tests carried out in the Halden Boiling Water Reactor (HBWR) under nearly identical test conditions. The temperatures were measured at an axial level of about 600 mm from the bottom end of the heated rod length of the nuclear rods and the SEMISCALE heater rods. Although limited in their validity, since three SEMISCALE heater rods of the seven rod bundle failed, the comparison indicates that during the blowdown and heatup phases the temperatures of the nuclear and the electrically heated rods essentially overlap each other. However, quenching of the SEMISCALE rods was significantly delayed compared to the nuclear rods. This behavior was confirmed when the SEMISCALE rod bundle was rebuilt and the test series was repeated.

Figure 4 shows a comparison of the transient cladding temperatures as measured at the peak power level of the nuclear fuel rods and the electrically heated REBEKA fuel rod simulators. Plotted are the envelopes of all temperature readings measured at the axial level mentioned. The REBEKA fuel rod simulators duplicate the temperature and quenching behavior of nuclear rods, as can be seen. The REBEKA fuel rod simulators have been developed for investigation of the plastic deformation behavior of pressurized Zircaloy-4 clad-ded fuel rod simulators under LOCA conditions. Results of single rod, full length 5 x 5 rod bundle and 7 x 7 rod bundle tests are summarized in Ref. 12.

Investigating the effects of cladding surface thermocouples and electrical heater rod design on quench behavior using REBEKA fuel rod simulators and FEBA heater rods, the different behavior of both the types of rods during simulated reflood conditions, known qualitatively, had been confirmed [13].

Furthermore, the influence of thermal properties of different cladding materials on the heat transfer and rewetting behavior was observed in experiments using single rods or tubes of stainless steel or Zircaloy, respectively, under falling film and bottom reflood conditions [14]. Similar bench-type reflood experiments were carried out with a 4-rod bundle to study the quench behavior of stainless steel and Zircaloy claddings [15, 16]. In the frame of the "Indirect Action Research Programme" of the Commission of the European

Communities upon "Safety of Thermal Water Reactors" the effects of cladding material and pin composition upon rewetting and quench phenomena were investigated [17, 18, 19].

The results of the different experiments confirmed qualitatively that the safety analysis based on reflood tests performed with conventional gapless heater rods overpredicts the extent of core damage. Approaching the safety margin quantitatively, computer code models for description of the thermal response of different fuel rod simulators need to be improved and tested. The validation of such models implemented in reflood codes needs experimental data obtained from different experiments. For a strict comparison of the effects of the design and the composition of different rods, such experiments should be performed under identical conditions varying only the composition of the fuel rod simulators.

Therefore the purpose of this investigation is to address the following open questions concerning bottom reflooding:

- Reflood timing and resultant peak cladding temperatures in fuel rod bundles under given reflood conditions in comparison to bundles of electrically heated rods, mostly used for out-of-pile experiments.

- Coolability of flow blockages caused by ballooned fuel rod claddings in comparison to blockages simulated by sleeves fixed on the outer surface of conventional heater rods.

2. S E F L E X REFLOOD PROGRAM

The aim of the SEFLEX (Fuel Rod Simulator Effects in Flooding Experiments) program has been to quantify the influence of the design and the physical material properties of different fuel rod simulators on quench front progression and heat transfer in unblocked as well as blocked rod bundles during the reflood phase of a LOCA in a PWR.

Forced feed bottom injection reflood tests have been performed using bundles of 5 x 5 REBEKA fuel rod simulators characterized by Zircaloy claddings, alumina pellets and a gas filled gap between cladding and pellets. For the tests the FEBA test facility has been used. These tests performed under various reflood conditions and the comparison of the results with corresponding tests of the FEBA program represent the SEFLEX program.

The FEBA tests were performed with swaged, solid type heater rods without gap between stainless steel cladding and filler material. Separate effect tests were carried out in eight test series with the objective to measure and to evaluate thermal-hydraulic behavior of grid spacers and of unblocked versus blocked rod bundle geometries with and without bypass. Flow blockages simulating ballooned fuel rod claddings were achieved with sleeves of stainless steel attached to the rods. The initial and reflood conditions varied were repeated systematically from series to series as close as experimentally possible to isolate the different geometrical effects. The bundle configurations tested are listed in Table 1.

For the conduction of the subsequent SEFLEX tests the main reflood parameters of the FEBA test program have been maintained; only the bundle of 5 x 5 conventional heater rods had been replaced by a bundle of 5 x 5 REBEKA rods which more closely represented the features that exist in the actual fuel rod design. The influence of the conductivity of the gap between Zircaloy cladding and pellet has been investigated replacing the helium gas filling by argon gas filling. Helium is the filling gas of nuclear fuel rods at beginning of life time. The heat conductivity of argon corresponds to that of the fission gas mixed with the helium after high fuel burnup. As for the FEBA program unblocked bundle tests served as base line tests. For blocked bundle tests a 90 percent flow blockage at 3 x 3 rods of the 5 x 5 rod bundle was applied having identical location and outer shape as that of the FEBA

Table 1

FEBA-program: Bundle geometry of test series I through VIII.
Axial arrangement of grid spacers and flow blockages.

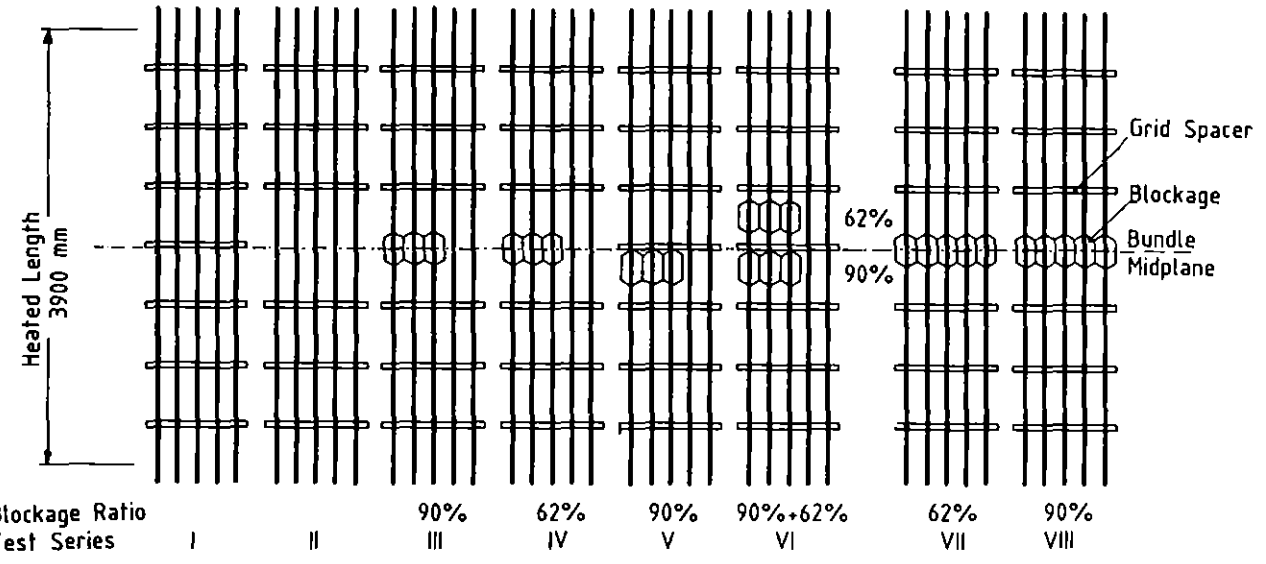

Series I: Baseline tests with undisturbed bundle geometry; seven grid spacers.

Series II: Investigation of the effects of a grid spacer; without grid spacer at the bundle midplane.

Series III: Investigation of the effects of a 90% flow blockage with bypass; blockage at the bundle midplane of 3 x 3 rods placed in the corner of the 5 x 5 rod bundle; without grid spacer at the bundle midplane.

Series IV: Investigation of the effects of a 62% flow blockage with bypass; blockage at the bundle midplane of 3 x 3 rods placed in the corner of the 5 x 5 rod bundle; without grid spacer at the bundle midplane.

Series V: Investigation of the effects of a 90% flow blockage with bypass combined with grid spacer effects; blockage immediately upstream of the bundle midplane at 3 x 3 rods placed in the corner of the 5 x 5 rod bundle; grid spacer at the bundle midplane.

Series VI: Investigation of the effects of 90% and 62% flow blockages with bypass combined grid spacer effects; 90% flow blockage immediately upstream of the bundle midplane; 62% flow blockage immediately downstream of the bundle midplane; both blockages at the same 3 x 3 rods placed in the corner of the 5 x 5 rod bundle; grid spacer at the bundle midplane.

Series VII: Investigation of the effects of a 62% flow blockage without bypass; blockage at the bundle midplane of all rods of the 5 x 5 rod bundle.

Series VIII: Investigation of the effects of a 90% flow blockage without bypass; blockage at the bundle midplane of all rods of the 5 x 5 rod bundle.

Table 2

SEFLEX-program: Bundle geometry of test series 1 through 4.
Axial arrangement of grid spacers and flow blockages.

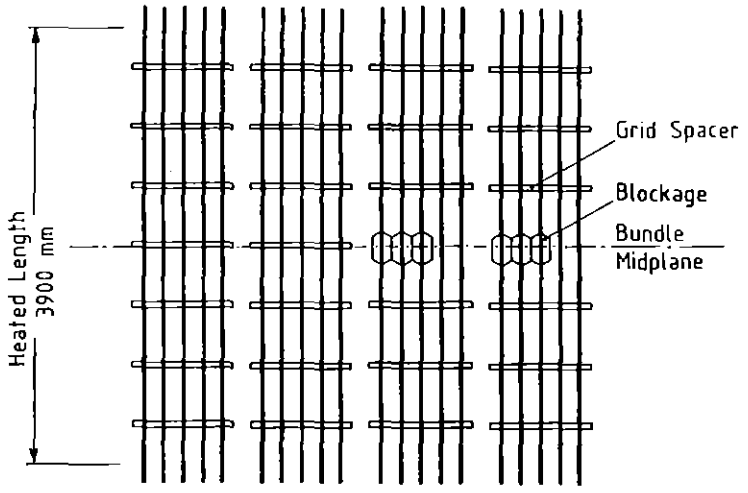

Gas Filling	Helium	Argon	Helium	Argon
Blockage Ratio			90%	90%
Test Series	1	2	3	4

Series 1: Rods with helium-filled gaps between Zircaloy claddings and alumina pellets; undisturbed bundle geometry with seven grid spacers.
Investigation of the effects of rod clad properties, conductivity of gas filled gaps, and grid spacers.
Comparison with FEBA test series I and SEFLEX test series 2.

Series 2: Rods with argon-filled gaps between Zircaloy claddings and alumina pellets; undisturbed bundle geometry with seven grid spacers.
Investigation of the effects of rod clad properties, conductivity of gas filled gaps, and grid spacers.
Comparison with FEBA test series I and SEFLEX test series 1.

Series 3: Rods with helium-filled gaps between Zircaloy claddings and alumina pellets; 90% flow blockage with bypass; blockage at the bundle midplane of 3 x 3 rods placed in the corner of the 5 x 5 rod bundle; without grid spacer at the bundle midplane.
Investigation of the effects of rod clad properties, conductivity of gas filled gaps, grid spacers, and flow blockage.
Comparison with FEBA test series III and SEFLEX test series 4.

Series 4: Rods with argon-filled gaps between Zircaloy claddings and alumina pellets; 90% flow blockage with bypass; blockage at the bundle midplane of 3 x 3 rods placed in the corner of the 5 x 5 rod bundle; without grid spacer at the bundle midplane.
Investigation of the effects of rod clad properties, conductivity of gas filled gaps, grid spacers, and flow blockage.
Comparison with FEBA test series III and SEFLEX test series 3.

tests. However, the flow blockages were realized by artificially ballooned Zircaloy claddings surrounding the pellet column.

The separate effect tests were carried out in four test series to measure and to evaluate the influence of four major factors on the reflood heat transfer and rod quenching:

- Rod clad properties
- conductivity of the gap between pellets and cladding
- grid spacers
- flow blockages.

The bundle configurations tested are listed in Table 2. The SEFLEX tests were conducted using REBEKA rod bundles in the FEBA test facility to minimize the influence of the boundary conditions of different test rigs. The initial and reflood conditions selected for the FEBA program were repeated as close as experimentally possible for the comparison of the difference in the behavior of the two rod designs on the basis of two-phase flow heat transfer phenomena of SEFLEX test series 1 through 4 and FEBA test series I and III.

3. TEST FACILITY

The FEBA test facility was designed for a separate effect test reflood program involving a constant flooding rate and a constant back pressure to allow investigation of the influence of grid spacers and coolant channel blockages independently of system effects. Since, the design of fuel rod simulators represents an experimental parameter similar to that of design and location of grid spacers or coolant channel blockages, the FEBA test facility as well as the operational procedure and the measurement technique of the FEBA tests have been maintained for the SEFLEX tests. Modifications necessary for replacing the 5 x 5 FEBA rod bundle by bundles of 5 x 5 REBEKA rods are described in Section 3.1.

3.1 Test Loop and Bundle Housing

Figure 5 shows schematically the FEBA test loop with its main components. It is a forced flow bottom injection reflood facility with a back pressure control system. Coolant water is stored in a tank (3). During operation, coolant is pumped (4) through a throttle valve (7) and a turbine meter (8) into the lower plenum region (10) of the test section (11). The coolant flow may be directed either upwards through the test assembly, or through the lower plenum (10) and water level regulation valve (9) back into the water supply. When reflood is initiated, coolant water rises in the test assembly and two-phase flow results when water reaches the hot zone of the fuel rod simulators. Entrained water droplets are transported upwards by the steam flow and may impinge on the steam water separator (13) placed above the test assembly. The liquid separated from the steam then drains into a collecting tank (17), where the water content is continuously measured. Steam passes around the droplet deflector and is then flowing through a buffer tank (19) and the back pressure control valve (10) to the atmosphere. A large external steam supply is connected to the buffer to heat up the total system and the buffer contents, and to maintain the system pressure.

For the performance of the FEBA test series [1], the heater rod instrumentation, which was completely embedded in the rod claddings, did exit from the lower end of the rod assembly as did the electric power connections for the heater rods. However, the instrumentation of the sleeve blockages was led to the top end of the housing such that the lead outs attached to the rod sur-

faces did not influence the two-phase mixture rising from the bottom.

For the performance of the SEFLEX test series, the heater rod instrumentation (15) and the electric power connections (14) for the heater rods were led out from the upper plenum (12). Therefore, the upper plenum (12) and the steam water separator (13) were modified as well as the lower plenum (10) where the REBEKA fuel rod simulators were filled with helium or argon gas, respectively, (21).

Figure 6 shows a photography of the FEBA test rig with its main components modified for the conduction of the SEFLEX tests.

Figure 7 shows a cross sectional view of the FEBA and the REBEKA rod bundle, respectively, placed in a square stainless steel (Standard No. 1.4571, ASTM 410) housing having an inner edge length of 78.5 mm and a wall thickness of 6.5 mm. The reasons for the use of a thick-walled housing were:

- To simulate surrounding heat generating hot rods by having sufficient heat storage in the wall prior to the individual tests (see Section 3.6).
- To facilitate assembling of the test rig.
- To allow easy penetration of the wall for instrumentation of the bundle with fluid thermocouples (see Section 3.4).

The dimensions of the housing inner cross section had been so chosen that the 5 x 5 rod bundle array and an infinite bundle were to have the same subchannel hydraulic diameter d_H:

$$d_H = \frac{4A}{C} = 13.47 \text{ mm}$$

where A: flow area; C: wetted perimeter.

The outer diameter of the rods was 10.75 mm and the rod pitch 14.3 mm for both, the FEBA heater rods as well as the REBEKA fuel rod simulators. Further dimensions of the rods and the bundles, respectively, are described in Section 3.2. Original PWR grid spacers were attached to the rods by friction. They were sliding in the bundle housing in axial direction when relative motion between rod bundle and housing occurred. The rods were bolted to the top of the test section. The lower ends of the rods were allowed to hang free for

FEBA as well as SEFLEX tests. For replacing the FEBA rod bundle by the REBEKA rod bundle the upper as well as the lower plenum were modified. The bundle housing was identical for both the bundles. Figure 8 shows a cross sectional view of the test section with the insulation at the housing outside for reduction of the heat losses to the environment.

The modification of the upper plenum is shown in Fig. 9. Whilst the FEBA rods were bolted to the top grid plate, the REBEKA rods were bolted to the top of the upper plenum, and penetrated the top grid plate through square holes which provided the same total cross section for coolant through flow as the circular holes between the FEBA rods for the FEBA grid plate. The two-phase flow leaving the rod bundles had to cross the REBEKA rods in radial direction. The cross flow in that portion of the plenum has probably led to slightly increased droplet evaporation compared with the FEBA flow conditions, i.e. without rods at that place. However, any effect of additional evaporation was rather small because of the short flow path along and across that - unheated - portion of the REBEKA rod bundle. After separation of the water from the steam, the flow path of the water to the water collecting tank was identical for both designs. The conditions for the steam flow, after separation from the water, did not affect the flow conditions upstream, since the pressure drop between bundle exit and buffer was very small.

Figure 10 shows the modification of the lower plenum. The FEBA rods penetrated the bottom of the plenum which was covered by a water film controlling the temperature of the lower plenum including the O-ring sealings to the temperature of the feedwater during heat up of the bundle. The REBEKA rods were hanging in a water-filled plenum. The water level was at the same elevation for both designs, and the water temperature was controlled to that of the feed water during the test. Therefore, no influence of the modification of the plenum on the reflood conditions was observed.

3.2 REBEKA Fuel Rod Simulator and FEBA Heater Rod

Fuel rod simulators of PWR dimensions were used to simulate the nuclear fuel rods. Figure 11 shows the cross section of a gapless FEBA heater rod which has an outer diameter of 10.75 mm. A spiral wound heating element of NiCr 80 20 (ASTM B 344-60) is embedded in the electrical insulator (magnesium oxide), and then encapsulated in the clad of NiCr 80 20 which has a wall thickness of

1.0 mm. In contrast to a nuclear fuel rod with a Zircaloy cladding and a gas filled gap, this heater rod is a solid type widely used for thermal-hydraulic tests. A close thermal contact between cladding and filler material results from swaging of the rods. More details including a working drawing are contained in Ref. [1].

Figure 12 shows the cross section of a REBEKA fuel rod simulator. This fuel rod simulator consists of an electrically heated rod of 6.02 mm outer diameter placed in the center of annular alumina pellets simulating fuel pellets. As for a nuclear rod, the pellets are encapsulated in the Zircaloy tube with a wall thickness of 0.725 mm. By pressurization of the rod with filling gas the gap between pellets and cladding is filled with helium or argon, respectively, to study the influence of the gap conductivity on the reflood behavior. The thickness of the Zircaloy cladding, the helium filling and the nominal gap width of 0.05 mm of a REBEKA rod are identical to a nuclear fuel rod at the beginning of life time. Heater rod and alumina pellets represent about 110 percent of the heat capacity of fuel pellets. The heat conductivity of argon corresponds roughly to that of the fission gas mixed with the helium after high fuel burnup. Figure 13 shows a working drawing of a REBEKA fuel rod simulator of nominal geometry modified for the SEFLEX tests.

The remaining characteristics of both types of fuel rod simulators, FEBA rod as well as REBEKA rod, were the same. Figure 14 represents an axial layout of the fuel rod simulators. The cosine power profile of the rods with a heated length of 3900 mm were approximated by seven steps of specific power. The axial power profile was flat with a peak-to-average ratio of 1.19. Seven grid spacers without mixing vanes (height 38 mm) were installed a 545 mm axial intervals throughout the bundles.

3.3 Blockage Design

The influence of the size and the shape of various coplanar blockages on local reflood heat transfer was already examined as part of the FEBA program. For most of the geometries, improved cooling was found downstream of such uniform blockages compared with base line tests without blockages conducted under the same flooding conditions. Only a 90 percent blockage with bypass led to about the same peak cladding temperatures downstream of the blockage compared with unblocked bundle data [1]. The most significant difference

between the temperatures so compared occurred after turnaround. Downstream of the blockage the temperatures decreased more slowly than in the unblocked portion of the bundles and a delayed quenching was observbed. However, the FEBA blockage configuration using sleeves was a compromise between flow channel constriction caused by ballooned claddings and the technical feasibility of such a simulation having sufficient life time for repeated tests. To examine and to isolate properly the blockage effects of FEBA and REBEKA rod bundles with 90 percent flow blockage with bypass, identical outer dimensions of the blockage geometries had to be selected.

The coplanar 90 percent blockage configuration with bypass used for the FEBA tests is shown in Fig. 15. Hollow sleeves of stainless steel were used to simulate ballooned claddings. The sleeves were attached to the rods. For the simulation of the heat resistance between pellets and lifted cladding a gap of 0.8 mm width filled with stagnant steam was provided between the outer surface of the FEBA rod and the inner surface of the sleeve. In addition, side plate devices were placed between the sleeves of the peripheral rods and the housing walls for constriction of the coolant subchannels between the 3 x 3 rod cluster and the housing.

Figure 16 shows a sectional view of the rod bundle with coplanar 90 percent flow blockage and bypass investigated in SEFLEX test series 3 and 4. The flow blockage was placed symmetrically to the bundle midplane (axial level 2025 mm) generating a local coolant channel constriction of nine subchannels of the 3 x 3 rod cluster. The balloons had an axial extension of 180 mm including the conical ends. The length of the 90 percent flow channel constriction amouted to 65 mm.

The outer shape and size of the blockages, i. e. the geometries and the surfaces exposed to the coolant, were the same for both, the SEFLEX and FEBA arrays. However, the heat capacities and the radial compositions underneath the cooled surfaces were different from each other.

Figure 17 shows a working drawing of REBEKA fuel rod simulators with artifically ballooned claddings as well as the instrumentation of the individual simulator types with thermocouples in axial and circumferential directions. The instrumention is described in detail in Section 3.4. To model a 90 percent flow blockage with bypass accordingly to the corresponding FEBA blocked

bundle configuration of test series III, three types of artificially ballooned Zircaloy claddings with different outer shape were produced. This was necessary to avoid side wall blockages as used for the FEBA tests. The cross sections of simulator type a and f, shown in Fig. 17, indicate the geometries of regular ballooned rods and ballooned rods placed at the housing wall of the 3 x 3 rod cluster, respectively. A third type of simulator was used to constrict the coolant subchannel in the corner of the housing (see cross section of rod No. 21 shown in Fig. 21). The required outer shape of the ballooned Zircaloy claddings was produced in a furnace by heating up the pressurized cylindrical tubes placed in correspondingly shaped molds. Subsequently, the ballooned claddings were cooled down very slowly to avoid any bursting or collapsing. During the reflood test series no deformation of the ballons took place. The blockage array after performance of the test series is shown in Fig. 18.

3.4 Instrumentation

Most part of the SEFLEX instrumentation consisted of thermocouples (Chromel-Alumel), since cladding (TS), heater sheath (TZ), grid spacer (TA), fluid (TF) and housing (TK) temperatures were to be measured at various positions. Figure 19 shows a schematic diagram of the axial levels of the thermocouples, the pressure and the differential pressure measuring positions. This diagram enables to relate the measuring positions to the blockage and the grid spacer positions as well as to the different specific power zones.

The cladding temperatures were measured with 0.36 mm sheath outer diameter thermocouples having insulated junctions. For test series 1 and 2 these thermocouples were embedded in grooves from the individual measurement position up to the top end of the rods. The grooves were milled into the outer surface of the Zircaloy claddings. The grooves were closed by peening over to avoid any disturbance of the coolant flow. For test series 3 and 4 these thermocouples were embedded in grooves of 20 mm length, which were milled into the outer surface of the Zircaloy claddings. The short grooves were closed by peening over as well. The remaining lead outs were attached to the outer surface of the Zircaloy claddings by very small and thin straps of Zircaloy which were spot welded to the claddings. For the instrumentation of the ballooned portion of the claddings the same method was applied with the difference that the thermocouple tips were not embedded in grooves but also were

attached to the rods by using straps (see Fig. 18). This external instrumentation was necessary with respect to the reduced wall thickness of the balloons. A separate effects experiment program [13] conducted in the LOFT Test Support Facility (LTSF) at the Idaho National Engineering Laboratory (INEL) with REBEKA fuel rod simulators to evaluate the effect of cladding external thermocouples on the quench behavior indicated: "Cladding external thermocouples have a negligible effect on the cooldown rate and quench behavior of a REBEKA fuel rod simulator over the range of LOCA-type, high pressure thermal-hydraulic reflood conditions examined."

As indicated in Figs. 12 and 21, some of the heater rods placed in the center of the alumina pellets were instrumented for the conduction of SEFLEX test series 3 and 4. The temperatures of the heater rod sheaths with an outer diameter of 6.02 mm were measured with 0.25 mm sheath outer diameter thermocouples having insulated junctions. These thermocouples were embedded in grooves which were milled into the outer surface of the Inconel rod sheath. The grooves were closed by peening over to keep the thermocouples at the provided measuring positions and to maintain the geometry of the alumina pellets. The leads were led out to the top end of the rod bundle close to the insulated connections of the electrical rod power supply.

The grid spacer temperatures were measured with 0.5 mm outer sheath diameter thermocouples having insulated junctions. The tips of these thermocouples (see indication TA on Figs. 20 and 21) were placed each at about 2 mm from the leading and the trailing edges, respectively, of the grid spacers. The thermocouples were attached to the grid spacers by very small and thin straps of stainless steel which were spot welded to the surface of the 0.4 mm thin grid spacer sheetings. The leads were led from the subchannels surrounding the central rod via trailing edge to the peripheral subchannels to avoid as far as possible any disturbance of the coolant flow.

The fluid temperatures were measured with unshielded thermocouples of 0.25 mm outer sheath diameter (see indication TF on Figs. 20 and 21). The junctions protruded into the center of the individual bundle subchannels. The ability of such fluid thermocouples for measuring steam temperature is demonstrated in Ref. 1.

The housing temperatures were measured with 0.5 mm outer sheath diameter thermocouples (see indication TK on Figs. 20 and 21) placed from the outside close to the inner surface of the 6.5 mm thick housing wall.

Pressures and pressure differences were measured with pressure transducers. In addition to the inlet and outlet pressure, the pressure differences were measured along the entire bundle length, along both the lower and upper portion of the bundle as well as along a short section at the bundle midplane. The flooding rate was measured with a turbo-flowmeter. The amount of water carried over was measured continuously by a pressure transducer at the water collecting tank.

All data were recorded with a scan frequency of 10 cycles per second using NEFF amplifiers, a PDP-11 mini-computer and disks for fast data recording.

3.5 Operational Procedure

The investigation of separate effects of core reflood during a PWR LOCA requires well defined system parameters for each test. The quality of the comparison among the tests depends mainly on the repeatability of the individual tests. Therefore, with respect to the real sequence of events during a LOCA, the following modification of the heat up period during refill of a reactor vessel had been made for the FEBA tests and maintained for the SEFLEX tests:

For about two hours prior to reflood, the fuel rod simulators were heated in stagnant steam to the described initial cladding temperature, using a low rod power. In the mean time the test housing was being heated up passively to the desired initial temperature by radiation from the rods. This led to a wall (6.5 mm thick) heat content of approximately the same as that of half a row of heater rods including the heat input during a test (rod power). The aim of choosing the "active wall" was to prevent premature quenching of the wall relative to the bundle quench front progression. The hot steam film at the surface of the wall acts somewhat like a layer of insulation for the two-phase flow in the bundle subchannels. The "passive wall" design using a thin wall of low heat capacity is an alternative method which allows fast heat up of the bundle and the housing. However, premature quenching may occur influencing the bundle heat transfer conditions. Furthermore, it complicates instrumentation and assembling.

Reflood was initiated by closing the water exit and the steam inlet valve at the lower bundle plenum and the drain valve of the water collecting tank (see Fig. 5). The bundle power was stepped up to the controlled decay heat transient, i.e. 120 percent ANS-Standard 40 seconds after shut down of a reactor for most of the tests. About 30 seconds prior to reflood the data recording system was started.

4. TEST MATRIX

The main test parameters varied are shown in Table 3:

- Bundle geometry
- Gap gas filling
- Flooding rate given as flooding velocity, i.e. the velocity of the rising water level in the cold bundle
- System pressure.

For the comparison of the reflood behavior of the two rod bundles consisting of either 5 x 5 FEBA or 5 x 5 REBEKA fuel rod simulators, the SEFLEX tests were carried out for flooding velocities of 3.8 cm/s and 5.8 cm/s (in the cold bundle) and system pressures of 2.1 and 4.1 bar. The test operational procedures were also similar (see Section 3.5). The power input was stepped up, when the rising water level reached the bottom end of the heated bundle length, to about 200 kW and decreased corresponding to the 120 percent ANS decay heat transient. Flooding velocity, system pressure, and feedwater temperature were kept constant during each test. The internal gas pressure was controlled to about 1 bar overpressure with respect to the system pressure.

Table 3

Test matrix of the SEFLEX-program

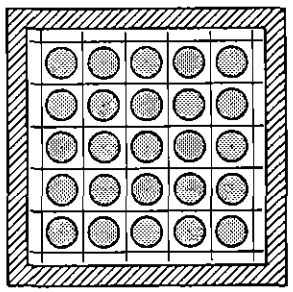

SEFLEX-Program
Test Series 1 and 2

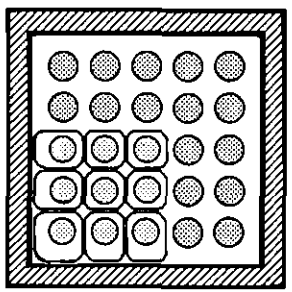

SEFLEX-Program
Test Series 3 and 4
90% Blockage
Ballooned claddings

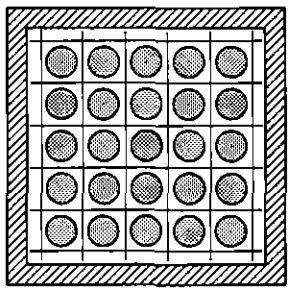

FEBA-Program
Test Series I

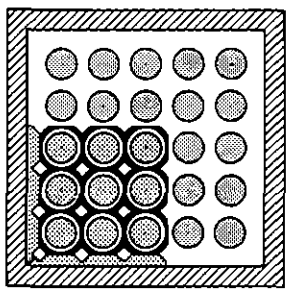

FEBA-Program
Test Series III
90% Blockage
Sleeve blockages

Program	Test Series	Test-No.	Rod Design	Cladding Material	Gap Gas Filling	Flooding Velocity cm/s	System Pressure bar	Feedwater Temperature °C	Reference Tests FEBA-Test	Reference Tests SEFLEX-Test
SEFLEX	1	05	REBEKA	Zircaloy	Helium	3.8	2.1	40	No. 223	No. 07
SEFLEX	1	03	REBEKA	Zircaloy	Helium	3.8	4.1	40	No. 216	
SEFLEX	1	06	REBEKA	Zircaloy	Helium	5.8	2.1	40	No. 218	
SEFLEX	1	04	REBEKA	Zircaloy	Helium	5.8	4.1	40	No. 214	
SEFLEX	2	07	REBEKA	Zircaloy	Argon	3.8	2.1	40	No. 223	No. 05
FEBA	I	223	FEBA	SS	gapless	3.8	2.1	40		No. 05 and 07
FEBA	I	216	FEBA	SS	gapless	3.8	4.1	40		No. 03
FEBA	I	218	FEBA	SS	gapless	5.3	2.1	40		No. 06
FEBA	I	214	FEBA	SS	gapless	5.8	4.1	40		No. 04
SEFLEX	3	32	REBEKA	Zircaloy	Helium	3.8	2.1	40	No. 241	
SEFLEX	3	35	REBEKA	Zircaloy	Helium	3.8	4.1	40	No. 239	
SEFLEX	4	33	REBEKA	Zircaloy	Argon	3.8	2.1	40	No. 241	
SEFLEX	4	34	REBEKA	Zircaloy	Argon	3.8	4.1	40	No. 239	
FEBA	III	241	FEBA	SS	gapless	3.8	2.1	40		No. 32 and 33
FEBA	III	239	FEBA	SS	gapless	3.8	4.1	40		No. 34 and 35

5. SEFLEX REFLOOD TEST RESULTS AND COMPARISON WITH FEBA DATA

The results of the SEFLEX test series 1 through 4 obtained with 5 x 5 REBEKA rod bundles [20, 21] are summarized and compared with results of corresponding FEBA tests [1]. This comparison, comprised within the SEFLEX program, deals with the overall bundle behavior, the grid spacer effects, the blockage effects and quench phenomena discussing data measured and evaluated.

Performing the SEFLEX program most of the individual results have been published successively [22 through 36].

5.1 Bundle Behavior

At initiation of the reflood phase the cladding temperatures of the rods are highly above the Leidenfrost temperature. As the liquid level reaches the bottom end of the bundle and starts to rise around the rods, complex heat transfer and two-phase flow processes occur. Ahead of the quench front the cladding temperatures are affected by the rate of steam generated upstream and the thermal-hydraulic behavior of entrained liquid droplets. The effect of this precursory cooling prevailing until quenching is characterized by a heat transfer coefficient decreasing with axial distance from the quench front. The local cladding temperature starts to decrease when the precursory cooling exceeds the heat generated in the rods.

For a proper comparison, the test conditions overtaken from the FEBA tests were systematically repeated for the individual tests of the SEFLEX series, e.g. initial cladding temperatures, power input, flooding rate, system pressure, inlet water subcooling etc.

The reflooding behavior of the two bundles consisting of either 5 x 5 FEBA or 5 x 5 REBEKA rods is significantly different. Figure 22 shows cladding temperatures versus time of three test runs performed with a flooding velocity of 3.8 cm/s and a system pressure of 2.1 bar in a FEBA rod bundle (square symbols), in a REBEKA rod bundle with helium-filled gaps (circular symbols), and in a REBEKA rod bundle with argon-filled gaps (triangular symbols). The temperature transients were measured at four different axial levels, in each case at about the half way between two grid spacer positions. Upstream of the bundle midplane (Plot A: axial level 2225 mm), the influence of the different

rod design on the peak cladding temperature is not yet pronounced, but the quench times of the REBEKA rods are almost 100 s, i.e. about 30 percent, shorter than that of the FEBA rods. Downstream of the bundle midplane (Plot B: axial level 1680 mm; Plot C: axial level 1135 mm; Plot D: axial level 590 mm), these differences become more pronounced towards the top end of the bundles.

The reasons for the lower cladding temperatures and the faster quench front progression of the REBEKA rod bundles are the lower heat capacity of the Zircaloy claddings and the more pronounced thermal decoupling of the cladding from the heat source, compared with the thick stainless steel claddings of the swaged FEBA rods.

For a temperature of 500 °C the products of specific weight and thermal capacity of Zircaloy-4 and NiCr 80 20 amount to [42]:

NiCr 80 20 $\rho \cdot c_p = 4.17$ W•s/(cm³•K)

Zircaloy-4 $\rho \cdot c_p = 2.15$ W•s/(cm³•K)

and the heat conductivities amout to [42]:

NiCr 80 20 $\lambda = 0.21$ W/(cm•K)

Zircaloy-4 $\lambda = 0.19$ W/(cm•K)

Taking into account the following cladding dimensions

FEBA (NiCr 80 20) $d_o = 10.75$ mm

$d_i = 8.65$ mm

REBEKA (Zircaloy-4) $d_o = 10.75$ mm

$d_i = 9.30$ mm

the internal energies per unit length are given by

FEBA cladding $E = 1.33$ W•s/K

REBEKA cladding $E = 0.49$ W•s/K

A comparison of the internal energies stored in FEBA and REBEKA rod claddings leads to a ratio of about 2.7.

The assumptions of a heat transfer coefficient of 3.0 W/(cm²•K) between filler material and FEBA rod cladding, a gap width of 0.05 mm between alumina pellets and REBEKA rod cladding, and a filling gas temperature of 500 °C in REBEKA rods result in the following ratios of the thermal conductances at the interfaces:

FEBA/REBEKA (He-filling)	5
FEBA/REBEKA (Ar-filling)	40
REBEKA (He-filling)/REBEKA (Ar-filling)	8

This comparison does not include the heat transfer by radiation between the ceramic and the cladding.

The comparison between a nuclear fuel rod and a SEMISCALE heater rod (see Fig. 4), shows the same trend concerning shorter quench time for Zircaloy cladded rods with gap. However, the SEMISCALE heater rod having a similar design as a FEBA rod did not lead to significantly higher peak cladding temperatures than the nuclear fuel rods. This finding only is consistent with the temperature transients measured in the lower portions of the FEBA and the REBEKA rod bundles, respectively (see Fig. 17, Plot A). It has to be mentioned that the heated length of the rods used in the OECD Halden experiments was only 1500 mm and the data shown were measured 600 mm from the bottom end of the heated length. For the FEBA and REBEKA rods in the SEFLEX tests the heated length amounted to 3900 mm. Since in the upper bundle portions the peak cladding temperatures are substantially lower for REBEKA rods than for FEBA rods, it can be assumed that the heated length of the rods used in the OECD Halden experiments was too short for promoting a similar behavior leading to lower peak cladding temperatures for e.g. the fuel rods in the OECD Halden experiment.

Analyzing the reasons for the lower peak cladding temperatures in the REBEKA rod bundle the question arises whether the precursory cooling is really better or the about 10 percent lower amount of heat stored in the REBEKA rods leads to lower peak cladding temperatures during precursory cooling.

The first indication for the differences between the transient heat transfer coefficients prevailing in the individual rod bundles can be found qualitatively reading the temperature transients of the bundle housing. Figure 23 shows the housing temperatures measured at the axial level 1680 mm during the tests discussed above. The housing, which is identical for the total of the tests, is cooled faster using the REBEKA rod bundles than using the FEBA rod bundle. Therefore, there is an increased reflood heat transfer for rods with Zircaloy claddings and helium gas filled gaps, e.g. SEFLEX test No. 03, compared with gapless heater rods with stainless steel claddings, e.g. FEBA test No. 223. The heat transfer again increases for increased heat resistance

across the gap, e.g. for the argon gas filled REBEKA rods, e.g. SEFLEX test No. 07.

The heat transfer analysis quantifies the cooling conditions for the different rod bundles. Heat transfer coefficients, rod surface heat flux, temperature distribution in a cross section of a rod and stored heat per unit of length of a rod have been calculated for various locations within the bundle. Input data for the one-dimensional inverse heat conduction calculation using the modified and supplemented HETRAP-computer code [41] are the measured local cladding temperature, the corresponding specific rod power, the saturation temperature related to the system pressure, the temperature-dependent material properties [42, 43] as well as the individual rod geometry. The FEBA rod cross section was defined by 11 radial nodes and the REBEKA rods by 14 radial nodes to obtain the transient temperature distributions in the rod cross sections.

The FEBA heater rod consists of four concentric rings of different material regions. Contact resistances between material regions were specified by constant uniform input data.

The REBEKA fuel rod simulator required to describe eight concentric rings of different materials. Again, contact resistances between two material regions were defined by constant uniform input data. The heat conductance of the gas filled gaps between heater rod and pellets as well as pellets and cladding was assumed to consist of two components: (1) Heat transfer due to thermal radiation and (2) Heat transfer due to conduction in the filling gas. Since the conduction model does not calculate the effects of power history of the rods, the gap width specified by input includes any changes from the as-built conditions. Therefore, it was assumed that the gap between heater rod and pellet was reduced from a nominal width of 0.04 mm to an effective width of 0.01 mm due to thermal expansion of the heater rod in radial direction.

The numerical procedure used in the conduction solution is based on a finite-difference resistance network approach.

The rod surface heat flux transients, evaluated for the tests discussed above, for the axial level 1680 mm, confirm increased precursory cooling in the REBEKA rod bundles as shown in Fig. 24. For the early portion of the

reflood phase the heat flux at the surface of the gapless heater rods of the FEBA tests is lower than that of the helium filled REBEKA rods of the corresponding SEFLEX tests. The highest heat flux density is evaluated for REBEKA rods with argon filling. The individual transients are approaching each other with increasing reflood time and reach about the same values after approximately 200 seconds. However, at that time the cladding temperatures are decreasing for all the cases shown, i.e. after the time of peak cladding temperatures. Cladding temperatures and corresponding surface heat fluxes are compared in Fig. 25 using an enlarged time scale for the first 140 seconds of the reflood phase. The transients are the same as plotted in Fig. 22 (Plot B) and Fig. 24.

The heat stored in a FEBA rod compared with that stored in REBEKA rods with either helium or argon filling is shown in Fig. 26 for axial level 1680 mm. It has to be mentioned that for the same initial cladding temperatures at beginning of the reflood phase the amount of heat stored in a FEBA rod is about 10 percent larger than that of the REBEKA rods (see values at t = 0 seconds in Fig. 26). However, for identical power input applied for the different bundles, a larger amount of heat remains in a FEBA rod than in the REBEKA rods during the early portion of the reflood phase as indicated already by the surface heat flux transients, plotted in Fig. 24. After the turnaround points, i.e. when the heat removal exceeds the heat input, again the stored heat transients decrease faster for the REBEKA rods than for the FEBA rods. Therefore, later quenching of the FEBA rod bundle is mainly due to the lower reflood heat transfer to the coolant.

As soon as the rod claddings are quenching the heat stored in the rods drops suddenly. The transients are similar for the FEBA rod and the REBEKA rod with helium gas filled gap. Later in time after quenching, the amount of stored heat remaining in both rods is about the same. The behavior is different for REBEKA rods with argon gas filled gap: The decrease of the stored heat is slower during quenching and, late after quenching, the amount of stored heat remaining in the rod is significantly higher than for both types of rods mentioned before. The increased heat resistance across the argon-filled gap is responsible for this phenomenon. It could be drawn a preliminary conclusion, that the higher amount of stored heat remaining after quenching in rods with argon-filled gaps is the reason for the faster quench front progression compared with rods with helium-filled gaps. However, this explana-

tion is not sufficient, because the surface heat flux transients are different for both cases. For most part of the reflood period the surface heat flux of the REBEKA rod with argon-filling is substantially higher than that of the REBEKA rod with helium-filled gap (see Fig. 24), and consequently, the heat removal is increased for increased heat resistance across the gap (compare Fig. 26, circular and triangular symbols). The effect of cladding material is excluded in this comparison, since cladding thickness and material are identical for both tests. Comparing the behavior of FEBA rod bundles with that of REBEKA rod bundles the effect of radial heat resistance as well as the effects of the physical properties and the dimensions of the rod claddings have to be considered. The quantitative separation of these effects seems not to be possible using the FEBA and SEFLEX results only. But, it can be concluded qualitatively, that both, cladding and gap effects are responsible for increased reflood heat transfer of REBEKA rod bundles compared with that of FEBA rod bundles. There is a limited number of experiments [17, 18] to examine these effects. However, for a quantitative analysis of the question whether the cladding material or the gas-filled gap is the main parameter of influence, additional experimental and analytical investigations are needed.

Further informations about the heat transfer and quench behavior of the individual rods used for the FEBA and SEFLEX tests give the following diagrams: The heat transfer coefficients evaluated for axial level 1680 from FEBA test No. 223 and SEFLEX tests No. 05 and 07 are plotted in Fig. 27. Emphasis is placed on the conditions at the time of quenching of the individual rods at the elevation indicated. Besides the fact that the quench times are different, the slopes of the transient heat transfer coefficients are different as well. For the following representations the quench times of the individual rod sections are set $t = 0$ obtaining a new time scale allowing a better comparison of the different transients. A recording window of 40 seconds, i. e. 20 seconds before through 20 seconds after the quench fronts passed the axial level 1680 mm, is used for the data plotted versus an enlarged time scale. Figure 28 shows cladding temperatures (Plot A), surface heat fluxes (Plot B), heat transfer coefficients (Plot C) and stored heat quantities (Plot D) for FEBA test No. 223 and SEFLEX test No. 05 with helium-filled gaps of the REBEKA rods. Before quenching ($t < 0$) the temperature of the REBEKA rod cladding decreases faster than that of the FEBA rod, and it drops suddenly down to saturation temperature at the moment of quenching. However, the

"quench temperatures" of both the types of rods are almost the same (see Plot A). The surface heat flux at the REBEKA rod is somewhat higher than that of the FEBA rod prior to quenching as discussed already. At the moment of quenching this trend is reversed: The peak surface heat flux at the FEBA rod then is about twice as high as that of the REBEKA rod (see Plot B). A comparison of the heat transfer coefficients (Plot C, logarithmic scale!) shows again for the REBEKA rod a somewhat higher mean value prior to quenching, significantly higher maximum at the moment of quenching and slower decrease after quenching than that of the FEBA rod. Finally, Plot D of the Fig. 28 shows that the removal of the heat stored in a REBEKA rod is increased prior to qunecheing and slightly delayed immediately after quenching compared with the heat release of a FEBA rod.

The conditions for a FEBA rod already shown are compared with those of a REBEKA rod with argon gas-filled gap in Fig. 29. Due to the increased gap heat resistance for the REBEKA rod in this case, the effects discussed before are somewhat more pronounced. Especially, the heat release is delayed significantly after quenching of a REBEKA rod with argon gas-filled gap (see Plot D of Fig. 29).

For different reflood conditions, e. g. different system pressures and flooding velocities, the trends of the quenching behavior remain the same as shown in Figs. 30, 31 and 32. The individual quantities only are different.

Analyzing the azimuthal temperatures of a REBEKA rod cladding for different reflood conditions some information is obtainable concerning the quality of the quench front progression. The transient cladding temperatures measured at bundle midplane and at four circumferential positions of a rod are plotted in Fig. 33. The data are plotted again in Fig. 34 versus an enlarged time scale for the recording windows in which quenching of the individual rods occurs.

The different times, at which the four considered positions of the rod circumference are quenching, indicate that the quench front is not strictly circular. This finding is consistent with optical observations. In some cases dryout occurs for a short period after the whole circumference was quenched already as shown in Fig. 34, Plot B.

Radial temperature profiles in gapless FEBA rods and REBEKA rod with gaps indicate the different mechanisms of heat release during the period of surface rewetting. Figure 35 shows calculated radial temperature profiles as a function of time for the axial level 1680 mm. For the suddenly increasing cooling conditions close to the quench front, the temperature of Zircaloy claddings drops fast (Plot B and Plot C) and the heat stored in the remaining portion of the rod is being removed with a certain delay after the temperature difference across the gap is established. A sudden increase of the cooling conditions or the arrival of the quench front at a FEBA rod surface has to remove more heat stored in the clad and in the filler material which are in close contact (Plot A). Therefore, the cladding temperature does not drop as fast as for a REBEKA rod or for a nuclear fuel rod. This mechanism delays the quench front progression, reduces the amount of heat released from the rods per unit of time, and lowers the effectiveness of precursory cooling.

Figure 36 shows that the quench front progression in the REBEKA rod bundle with helium-filled gaps is faster than that in the FEBA rod bundle. The plot shows also an increased quench front velocity for the upper bundle portion of REBEKA rods with argon gas filling compared with the helium-filled gaps. This is apparently due to the fact that the thermal conductivity of argon is nearly one order of magnitude lower than for helium. In both cases the internal gas pressure amounted to about 3 bar. Furthermore, it can be seen that in the REBEKA rod bundles the quench front progression is influenced by the grid spacers, especially in the upper portion of the REBEKA rod bundle with argon-gas filled gaps.

Figure 37 shows the water carry over collected downstream of the bundle exit versus reflood time. A higher amount of water entrained by the steam is being evaporated within the REBEKA rod bundle subchannels removing more heat per unit of time. Less water is carried over for identical injection rate. Less entrainment could not explain the higher rate of heat removed from the unwetted portion of the bundle (see stored heat as function of reflood time plotted in Fig. 26).

5.2 Grid Spacer Effects

The grid spacer effects on local cooling conditions influence significantly size and shape of cladding balloons. Experimental results make evident the

decrease of the cladding temperatures downstream of the individual grid spacers as well as the interaction between thermal-hydraulics and fuel clad ballooning [12, 27, 30, 31].

The transient axial profile of the cladding temperature during refill and reflood of a LOCA determines the amount of local cladding deformation along the rods. In general, clad ballooning occurs first at the axial rod section where a critical temperature level is reached. That location and the axial extension of ballooning is mainly the result of the axial cladding temperature profile between two grid spacer positions. This temperature profile is determined by the thermodynamic non-equilibrium in the two-phase flow and its interaction with the grid spacers. The presence of a grid spacer enhances substantially the heat transfer downstream.

However, this significant effect decreases on the way to the next grid spacer in flow direction and leads to the development of an axial temperature profile with a local maximum immediately upstream of the individual grid spacers. It has been found that Zircaloy claddings - separated by even a rather small gas filled gap from the internal heat source - are more sensitive to the grid spacer effects than swaged heater rods with stainless steel claddings. A typical example is shown in Fig. 38. The axial temperature profiles are recorded 30, 90 and 150 seconds after initiation of reflood. After 30 seconds the cladding temperature at and downstream of the grid spacer drops to about 30 K lower for REBEKA rods than for gapless FEBA rods. Upstream of the grid spacer the cladding temperatures of both the bundles are still at the same temperature level. After 90 and 150 seconds, respectively, the overall difference between both the temperature profiles increases. This is due to the faster overall reflood transient during the SEFLEX test with REBEKA rods. However, at and downstream of the grid spacer the differences are even more pronounced indicating again enhanced grid spacer effects in SEFLEX compared with FEBA.

Adequate fuel rod simulation is obtained using REBEKA rod bundles with helium-filled gaps. The results are still conservative concerning spent fuel rods with fission gas mixed with the helium gas as shown by the results obtained with REBEKA rods with argon-filling of the gaps. Therefore, the description of the grid spacer effects is concentrated on results obtained from SEFLEX test series 1 using undeformed REBEKA rods with helium-filled gaps.

From the sample of tests performed under different reflood conditions, Fig. 39 shows data measured at the bundle midplane. For the set of tests performed with system pressures of 2.1 and 4.1 bar and with flooding velocities of 3.8 and 5.8 cm/s, transient cladding and grid spacer temperatures are plotted. The temperatures of the grid spacers are measured near the leading edge and near the trailing edge, respectively, as described in Section 3.4.

The cladding temperatures are obtained from thermocouples embedded in the cladding of the center rod at the bundle midplane, the position of the leading edge of the grid spacer, and 12 mm downstream of the trailing edge of the grid spacer with a height of 38 mm. At initiation of reflood the temperatures of the cladding as well as of the grid spacers are close to 800 ^{o}C diverging from each other rapidly within the first 10 seconds of the reflood transient. The cladding temperatures downstream of the grid spacer then are lower than upstream by between 50 K up to 150 K depending on the reflood conditions. After the initial drop the temperatures of the grid spacer are stabilized (quasi for a certain time span) at about 200 K below the cladding temperature measured near the leading edge of the grid. The level of this temperature transient results from the radiation heat transfer from the rods to the grid, and from heat exchange with the dispersed flow, characterized by superheated steam and water droplets being at saturation temperature, which passes the grid spacer. The ratio grid quench time to cladding quench time depends on the reflood conditions. Table 4 shows a listing of the quench times of the grid spacers instrumented for the unblocked bundle SEFLEX tests.

It is important to mention that quenching is initiated at the trailing edge of a grid spacer for all cases investigated. The velocity of the downwards moving quench front between the trailing edge and the leading edge depends on the reflood conditions and the axial location of the grid spacer. The measurements do not confirm previous assumptions that the droplet impact on the grid spacer would initate quenching at the leading edge.

For many of the cases premature quenching of the rod cladding is initiated downstream of the grid spacers as well. For the bundle midplane this is shown in Fig. 39, Plot B, C and D. This leads to the conclusion that heat transfer enhancement is significant in the early portion of the dispersed flow regime. During that period the grid spacer is hot and dry. The cladding temperature

transients downstream and upstream of the grid spacer are unaltered when the grid spacer wets. Therefore, the individual droplet breakup mechanisms at a dry grid or the droplet deposition at a wet grid including re-entrainment at the trailing edge seem to lead to comparable results concerning the overall heat transfer enhancement downstream of the grids.

Heat transfer analysis from data measured confirms previous findings [1] that cooling enhancement downstream of grid spacers shows a maximum for the early portion of the transient mist flow regime. The heat flux at the rod surface 12 mm downstream of the trailing edge of the grid spacer is about 20 percent higher than at the rod surface neighboring the leading edge of the grid spacer. The enhancement disappears towards the end of the dispersed flow regime as shown in Fig. 40. There is a second maximum for the cooling enhancement at the onset of transition film boiling characterized by increased water content in the two-phase flow. The increase of the water content presumably leads to grid spacer rewetting coincidently in the case shown in Fig. 40. This coincidence is not observed in this test for the remaining grid spacers at different elevations in the bundle or for other tests performed with different reflood conditions. The cooling enhancement from the grid spacer during the transition film boiling regime is of the same order of magnitude as that during the dispersed flow regime. However, concerning clad ballooning local cooling enhancement is more important during the dispersed flow regime.

The axial extension of the grid spacer effect on the local cooling enhancement depends on the reflood conditions. Figure 41 shows surface heat fluxes and cladding temperatures upstream and further downstream of the midplane grid spacer complementing the data of the test plotted in Figs. 39 (Plot B) and 40. At axial level 1925 mm, i. e. 62 mm downstream of the trailing edge of the grid spacer, cooling enhancement can be observed only for the early portion of the dispersed flow regime compared with the cooling conditions 100 mm upstream of the grid spacer, i. e. axial level 2125 mm (Fig. 41, Plot A). Plot B and C illustrate, that 162 mm as well as 262 mm downstream of the grid spacer the cooling conditions are approximately the same as 100 mm upstream of the grid spacer during the early portion of the dispersed flow regime inspite of the increased distance from the quench front. The transients compared in Plot D indicate that 362 mm downstream of the trailing edge there is no more grid spacer effect under the reflood conditions mentioned.

It is evident from the data presented so far that a grid spacer has significant effects on the cooling conditions downstream of it. However, for a quantification of the different heat transfer mechanisms superimposed, more informations are needed about droplet size and velocity distributions as well as about local flow turbulence and steam temperature.

Figure 42 shows fluid TC signals measured upstream and downstream of the 5 x 5 rod bundle midplane complementing the data plotted in Figs. 39 (Plot B), 40 and 41. The fluid temperature signal measured 215 mm upstream of the leading edge of the grid spacer (Plot A) indicates significant steam superheat. However, liquid droplets impinging upon the TC tip lead to repeated quenching of the probe preventing the measurement of the real steam temperature. Far downstream of the grid (Plot D) steam superheat is clearly indicated lasting for the whole dispersed flow transient. Quenching of the grid spacer at t = 140 seconds does not affect the steam temperature measured 362 mm downstream of the trailing edge of the grid. The transients measured at the levels 1925 and 1825 mm (Plots B and C) give less information about the steam temperature presumably due to increased droplet impinging upon the individual probe tips by the increased number but smaller size of droplets in that portion of the rod bundle.

In Figure 43 the temperature transients, almost presented in Figs. 39 (Plot B) and 42 are plotted versus an enlarged time scale to elucidate in more detail the effects of droplets on the fluid TC signal as well as on the grid spacer temperatures. Flow pulsations of a wave period of about 4.5 seconds influence the grid spacer temperatures slightly and with some delay. The grid spacer temperature is mainly controlled by the radiation heat transfer from the rods and the droplet cooling, because the vapor temperature seems to be close to the grid temperature. High fluid TC signal indicates high vapor superheat, dry probe tip, and low cooling, presumably due to low vapor velocity and low water content in the two-phase flow. Low fluid TC signal indicates enhanced cooling especially at the grid and in the wake of it presumably due to increased vapor velocity, water entrainment, and droplet breakup leading to quenching of the fluid TC tip. The cladding temperature measured upstream of the grid is nearly unaffected by the flow pulsation.

The signals of the fluid TC probes placed immediately downstream of the grid spacer (data not shown) indicate that the probe tips stay wet inspite of the

presence of superheated steam and the flow pulsations mentioned. Higher content as well as different distribution of the water compared with the conditions upstream of the grid spacer can be assumed by the following reasons:

At a given elevation in the bundle the steam mass flux is decreasing during half a period of oscillation of the dispersed flow transient. Therefore, decreasing steam velocity may lead to fall back of a part of the water entrained before by the steam of increased velocity. Locally increased overall steam velocity within the subchannel constrictions along the individual grid spacers hinders fall back across the grids leading to somewhat increased water content immediately downstream of the grids compared with the mean water content between two grid spacer elevations.

Figure 44 shows the temperature transients later in time plotted again versus an enlarged time scale. Quenching of the grid is initiated at the trailing edge. The downwards moving quench front at the grid needs about 5 seconds to reach the leading edge in this case.

For the next grid spacer, placed 545 mm above the bundle midplane, the conditions are similar to those at the midplane grid spacer as shown in Fig. 45. However, the dispersed flow cooling is somewhat lower indicated by the longer time span until rod quenching. The fluid contains less water than upstream of the midplane grid spacer as indicated by the signal of the fluid TC placed 245 mm upstream of the leading edge of the next grid spacer. The fluid TC probe tip is quenched only once for a short time during the flow oscillation period and stays dry for the remaining - extended - dispersed flow period. Inspite of the lower water content the grid spacer effect is increased compared with the midplane grid spacer situation. This is presumably due to the increase of the steam velocity and the turbulence enhancement over the bundle length given. The peak cladding temperatures are 120 K lower at the position 17 mm downstream of the trailing edge than 45 mm upstream of the leading edge of the grid spacer. Under these reflood conditions this grid spacer is quenching when the dispersed flow turns to transition film boiling as did the midplane grid spacer.

This phenomenon has not been observed in the test run carried out with a system pressure of 2.1 bar as shown in Fig. 46. The grid spacer is quenching during the early portion of the dispersed flow regime, and the difference of

the cladding temperatures upstream/downstream of the grid spacer amounts to 220 K. The slope of the cladding temperature transient downstream of the grid spacer is somewhat affected when the grid is quenching, indicating that a wet grid spacer improves the heat removal downstream of it. However, this is not the only reason for the increase of the grid spacer effect (220 K cladding temperature difference in this test instead of 120 K for the 4.1 bar test). For the case of the low system pressure of 2.1 bar the steam velocity and hence, the water entrainment and the turbulence are higher. The signal of the fluid TC indicates that the probe tip placed 245 mm upstream of the grid spacer stays wet for a long time span of the dispersed flow period. Dryout of the probe tip and hence, measurement of steam superheat is possible during the last period of the dispersed flow regime when the steam velocity is lower. Besides the fact that the fluid flow from below is cooling the grid spacer, it is evident that the grid is cooled from above as well, since quenching is initiated at the trailing edge due to the cooling enhancement, and eventually accumulated water downstream of the grid.

The magnitude of the grid spacer effect on the cladding temperatures in this case - compared with the 4.1 bar test - results from both, the effects downstream of the grid, i.e. turbulence enhancement again increased by higher steam velocity, and the effect at the grid itself, i.e. additional steam desuperheating after grid rewetting. The ratio of the effects of the two mechanisms is still uncertain. However, turbulence enhancement seems to be dominant.

The transient cooling conditions during reflood tests make difficult the distinction whether the change of the grid spacer condition from dry to wet or the change of the arriving fluid influences the grid spacer effect.

From the transient 5 x 5 rod bundle tests boundary conditions are selected characterized by rather stable dispersed flow conditions for the time span in which a grid spacer is quenching. Furthermore, the bundle section upstream and downstream of the grid spacer selected has to be instrumented sufficiently. For the midplane grid spacer the desired flow conditions are not given during the test performed with p = 4.1 bar and v = 3.8 cm/s because of the change of the fluid conditions at quenching of the grid as shown in Fig. 40. The test performed with p = 2.1 bar and v = 3.8 cm/s provides more stable flow conditions during the period in which the midplane grid is quenching.

Figure 47 shows cladding temperatures and surface heat fluxes versus time at the leading edge and 12 mm downstream of the trailing edge of the midplane grid spacer. Quenching of the grid is initiated at the trailing edge at t = 65 seconds and terminated at the leading edge at t = 101 seconds. At t = 65 seconds the heat transfer is increasing downstream as well as upstream by about the same amount as indicated by the heat flux transients. This is presumably due to the change of the conditions of the fluid arriving at the grid spacer elevation. At t = 101 seconds the surface heat flux is increasing downstream of the grid spacer only.

The grid spacer effect may be increased at t = 101 seconds due to different droplet effects induced by the wet grid as well as due to increased droplet volume flux. However, this situation does not last for a long time. The rod surface heat flux increases then at the leading edge and decreases at the trailing edge after the peak at t = 101 seconds.

Comparing the magnitude of the grid spacer effect during the early portion of the dispersed flow regime with that evaluated for the period of grid rewetting, it becomes evident that the grid spacer effect is more important during the early portion of reflood. There is a minor effect on the cooling enhancement later in time which is not dependent on whether the grid spacer is dry or wet.

The quench front progressions in 5 x 5 REBEKA fuel rod bundles indicate more pronounced effects at the grid spacers downstream of the midplane grid as shown in Fig. 36.

In Fig. 48 rod surface heat flux transients are plotted which have been evaluated from the cladding temperatures measured close to the grid spacer above the midplane grid spacer. The cladding temperatures shown for reference are taken from the test performed with p = 4.1 bar and v = 3.8 cm/s (see Fig. 45). For a short time the heat flux at the rod surface 17 mm downstream of the trailing edge of the grid spacer is up to 60 percent higher than that at the rod surface 45 mm upstream of the leading edge of the grid spacer. The enhancement disappears towards the end of the dispersed flow regime. There is a second maximum for the cooling enhancement at the onset of transition film boiling. The cooling enhancement from the grid during the transition film boiling regime is of the same order of magnitude as that during the dispersed

flow regime. However, concerning clad ballooning local cooling enhancement is more important during the dispersed flow cooling period.

Under the reflood conditions of the test mentioned (p = 4.1 bar, v = 3.8 cm/s) grid spacer rewetting coincides with the onset of transition film boiling characterized by increased water content. The sudden rise of the water content presumably leads to grid spacer rewetting in this test. For different test conditions, e.g. higher water injection rate and/or lower system pressure, the grid spacers are quenching during dispersed flow conditions already, as shown in Figs. 46 und 47.

Figure 49 shows heat flux transients of the test performed with p = 2.1 bar, v = 3.8 cm/s. The measurement positions are the same as those chosen for Fig. 48. Downstream of the grid spacer the heat flux is up to 100 percent higher than upstream for a short time during the early portion of the dispersed flow regime. After the maximum, the heat flux is decreasing more or less steadily below the transient evaluated for the position upstream of the grid spacer.

Under identical reflood conditions except the gas filling of the rods, e.g. argon instead of helium, the ratio of the heat flux downstream/upstream of the grid spacer remains approximately the same as for helium-filled rods. However, the cladding temperatures decrease faster at all elevations, and the claddings are quenching downstream of the grid spacer earlier than upstream as shown in Fig. 50. For the sample of tests performed with unblocked bundles the main grid spacer effects are summarized in Tables 4 and 5.

The influence of fuel rod simulator geometry and physical properties on overall cooling conditions and rod quench behavior is being investigated separately. Concerning grid spacer effects the following can be summarized: For increased heat resistance between cladding and pellets the claddings intent to quench downstream of the grid spacers earlier than upstream of them. Although, the dispersed flow cooling enhancement promoted by grid spacers is rather unaffected by the conductance of a gas filled gap. The resulting difference of the cladding temperatures is e.g. about 220 K for most time of the reflood transient in both tests with either helium- or argon-filled rods. The corresponding surface heat flux transients have similar slopes and ratios (compare Figs. 49 and 50).

Table 4

Quench times of grid spacers in unblocked rod bundles as function of reflood conditions.

Grid Spacer Axial Level mm	TC Axial Level mm	Test No. Gap Gas Filling Flooding Velocity, cm/s System Pressure, bar Feedwater Temperature, °C Quench Time, s				
		05 Helium 3.8 2.1 40	03 Helium 3.8 4.1 40	06 Helium 5.8 2.1 40	04 Helium 5.8 4.1 40	07 Argon 3.8 2.1 40
3660[1]	no TC	-	-	-	-	-
3622[2]	no TC	-	-	-	-	-
3115[1]	no TC	-	-	-	-	-
3077[2]	3075[3]	7	21	18	17	27
2570[1]	2568[4]	77	78	50	51	89
2532[2]	2534[3]	73	71	36	41	68
2025[1]	2023[4]	105	145	33	67	96
1987[2]	1989[3]	65	140	12	47	66
1480[1]	1478[4]	42	202	12	59	34
1442[2]	1444[4]	28	186	12	46	25
935[1]	no TC	-	-	-	-	-
897[2]	899[3]	36	216	9	35	28
390[1]	no TC	-	-	-	-	-
352[2]	354[3]	4	57	6	17	15

[1] Leading edge of grid spacer
[2] Trailing edge of grid spacer

[3] TC placed in subchannel surrounded by rods No. 13, 18, 17, and 12.
[4] TC placed in subchannel surrounded by rods No. 13, 12, 7, and 8.

Table 5

Grid spacer effects on cladding temperature and surface heat flux in unblocked rod bundles as function of reflood conditions.

	Test No. Gap Gas Filling Flooding Velocity, cm/s System Pressure, bar Feedwater Temperature, °C				
	05 Helium 3.8 2.1 40	03 Helium 3.8 4.1 40	06 Helium 5.8 2.1 40	04 Helium 5.8 4.1 40	07 Argon 3.8 2.1 40
Maximum reduction of cladding temperature (K) comparing axial level 2125 with 1975 mm.[1]	150	60	230	120	160
Maximum heat flux enhancement (-) relating axial level 1975 mm to axial level 2025 mm.[1]	1.6	1.2	2.1	1.3	1.5
Time (s) of maximum heat flux enhancement after initiation of reflood.[1]	5	20	12	20	23
Maximum reduction of cladding temperature (K) comparing axial level 1525 with 1425 mm.[2]	220	120	230	180	220
Maximum heat flux enhancement (-) relating axial level 1425 mm to axial level 1525 mm.[2]	2.0	1.6	2.1	1.6	1.7
Time (s) of maximum heat flux enhancement after initiation of reflood.[2]	5	20	12	20	23

[1] Grid spacer at bundle midplane
(leading edge at axial level 2025 mm, trailing edge at axial level 1987 mm)

[2] Grid spacer placed 545 mm downstream of bundle midplane
(leading edge at axial level 1480 mm, trailing edge at axial level 1442 mm)

5.3 Blockage Effects

Ballooned fuel rod claddings may lead to flow blockages influencing local reflood heat transfer conditions. A blockage causes two opposite effects:

- Within and downstream of the blocked portion of the bundle, the coolant mass flux is reduced, which can lead to reduced local cooling.
- Two-phase flow passing through a blockage can lead to improved cooling due to enhancements of turbulence and water droplet dispersion.

For the coplanar 90 percent blockage formed by a 3 x 3 rod cluster with Zircaloy claddings in a corner of the 5 x 5 REBEKA rod bundle, the claddings are highly lifted from the pellets and the heat capacity of the cladding balloons is low. For the same outer shape of the blockage, investigated as part of the FEBA program, the heat capacity of the stainless steel blockage sleeves of 1 mm wall thickness, attached at the FEBA rods, is significantly higher [1] (compare Figs. 15, 16 and 17). Therefore, the two-phase flow passing through the blockage may cool down the thin Zircaloy claddings faster than the FEBA sleeves. Figure 51 shows temperature transients measured at the bundle midplane, i.e. the midplane of the 90 percent blockage as well, for a FEBA test (Plot A), for a SEFLEX test with helium-filled gaps (Plot B), and for a SEFLEX test with argon-filled gaps (Plot C). The temperatures of the sleeves and of the balloons, respectively, are lower than the cladding temperatures of the rods placed in the bypass of the blocked portion of the bundle. However, the balloons are quenching substantially earlier than the sleeves. After about 20 seconds the Zircaloy balloons, and after about 400 seconds the FEBA sleeves are quenching. After quenching the portions of the rods underneath the balloons and underneath the sleeves, respectively, remain at a high temperature level indicating the magnitude of the heat resistance between ballooned claddings and heater sheath inside the pellets as well as between FEBA rod surface and sleeve (gap of 1.0 mm width filled with stagnant steam). For the SEFLEX blockage the gap between the ballooned Zircaloy claddings and the pellets amounts to about 2.3 mm width filled with either helium or argon. The cladding temperatures measured in the bypass of the blockage are shown for reference.

For the same tests the cooling conditions downstream of the blockage are indicated by the temperature transients shown in Fig. 52. In the FEBA test

the temperatures downstream of the blockage and in the bypass are roughly the same during the early portion of reflood. The mass flux reduction in the blockage is approximately compensated by the cooling enhancement effect of the blockage. However, quenching is delayed compared with the bypass conditions. For the Zircaloy cladding the cooling enhancement, prevailing at beginning of reflood mainly, is sufficient to quench the thin Zircaloy claddings rapidly. The quench front initiated within the SEFLEX blockage moves fast through the whole blockage increasing the precursory cooling immediately downstream of the blockage. Both effects, low heat capacity of the Zircaloy claddings and high heat resistance between the heat source and the lifted clad within the blockage are responsible for the quick cooling of the rod claddings. Most part of the heat stored in the portions of the rods with nominal gap width of 0.05 mm is being removed after quenching of the claddings as indicated by the heater sheath temperatures shown in Fig. 52, Plot B and Plot C. Due to the low heat conductivity of argon the heater sheath temperature remains at a higher level for the quasi steady state conditions late after quenching (Plot C) compared with the temperature level measured in the test with helium-filled gaps (Plot B). Again, the cladding temperatures measured in the bypass of the blockage are shown for reference.

The instrumentation of some of the heater rods in the center of the alumina pellet column of the REBEKA rods used in SEFLEX test series 3 and 4 provides information about the real temperature distribution in the rod cross sections. For the calculation of the temperature distribution concentric arrangement of the cladding, the alumina pellets and the heater rod has been assumed. However, it is more probable that the arrangement is non-concentric for a given measurement position. For analysis of data measured this fact has to be taken into account.

Figure 53 shows a comparison of measured and calculated heater sheath temperatures and corresponding cladding temperatures measured at the bundle midplane in the blockage bypass. In the individual plots data obtained from different tests are plotted versus time. For each plot identical locations in rod No. 4 of the 5 x 5 REBEKA rod bundle have been chosen. Across the gap of 0.05 mm nominal width between cladding and pellet significantly different temperature differences are calculated depending on the filling of either argon or helium gas. The temperature difference across the pellet is unaffected by the physical properties of the gases.

The temperature transients shown in Plot A of Fig. 53 indicate (1) large temperature difference across the argon-filled gap and (2) rather good agreement between measured and calculated heater sheath temperatures. For the helium-filled gap (Plot B) the temperature drop across the gap is small. The comparison of the heater sheath temperatures measured and calculated seems to indicate a bad agreement. However, there is no information about pellet excentricity at that location. Furthermore, there is an axial displacement between heater rod and Zircaloy cladding. This is due to different thermal extensions of the heater rod and the cladding during the tests. Therefore, with respect to uncertainties of the geometrical conditions, the data comparison shows a satisfactory matching.

Plot C shows the conditions for a argon-filled gap again. However, the system pressure applied in the corresponding test is 2.1 bar instead of 4.1 bar comparing Plot C with Plot A. For lower system pressure the reflood heat transfer and hence, the heat flux across the gap are lower. Therefore, the temperature difference between rod cladding and heater sheath is somewhat smaller in Plot C than in Plot A. The same trend is true comparing the data of Plot B with those of Plot D.

In Fig. 54 the temperatures measured at various locations within the blocked portion of the REBEKA rod bundle are shown. Upstream of the blockage the temperature difference between cladding and heater sheath is the same as in a rod placed in the bypass as shown comparing Plot A of Fig. 54 with Plot D of Fig. 53. At the axial level 2075 mm, i.e. at the lower conical end of a rod balloon, the temperature difference between balloon surface and heater sheath is substantially larger and the quench time for the cladding is shorter than for the axial level upstream with nominal rod geometry (compare Plot B with Plot A of Fig. 54). At the axial level 2025 mm, i.e. the blockage midplane, the balloon is quenching rapidly as shown in Plot C of the Fig. 54. The cooling conditions within the fully blocked subchannels seem to be rather unstable as indicated by the peak of the balloon temperature after quenching due to a short dryout period in a subchannel.

The upper conical end of a rod balloon, i.e. downstream of the blockage midplane, is quenching earlier than the lower conical end as shown in Plot D of Fig. 55 compared with Plot B of Fig. 54. Even downstream of the blockage the quench times are substantially shorter for rod sections of nominal geo-

metry compared with the conditions in the bypass (compare Plots E and F of Fig. 55 with Plot B of Fig. 52). It has to be mentioned that the corner rod of the blocked rod cluster, rod No. 13 (Plot F), is surrounded by one fully blocked and three partly blocked subchannels whilst rod No. 17 (Plot E) is surrounded by four fully blocked subchannels. Therefore, the cooling conditions for these two rods are different within as well as downstream of the blockage. May be that water accumulation and enhanced turbulence downstream of the blockage, as assumed previously [1], are responsible for increased heat transfer at that location. The temperature transient measured at the heater sheath of rod No. 17 at the axial level 1925 mm indicates rapid removal of the heat stored in that section of the rod as shown in Fig. 55 Plot E. For the sections of the rods underneath the clad balloons, most part of the heat stored remains in the pellets and the heater rod as indicated by the temperature transients plotted in Plots B and C of Fig. 54 and Plot D in Fig. 55. Therefore, early quenching of the balloons is possible inspite of reduced coolant flow through the blocked bundle subchannels. Poor heat transmission from the pellets through a large gas-filled gap to the thin Zircaloy cladding balloons having small heat capacity are responsible for rapid quenching of the blocked bundle portion. In contrast to that behavior the FEBA blockage array, characterized by substantial larger amount of stored heat and smaller heat resistances in radial direction of the rods and the blockages, leads to conservative results concerning the behavior of blocked fuel rod clusters. Investigating the coolability of blocked fuel elements the simulation of a 90 percent blockage applied in the SEFLEX tests leads to rather realistic results.

6. ANALYTICAL SIMULATION OF REFLOOD EXPERIMENTS

The reflood behavior of both the unblocked bundles consisting of either 5 x 5-FEBA and 5 x 5 REBEKA rods were calculated using the COBRA-TF (Coolant Boiling in Rod Arrays - Two Fluid) computer code developed at the Pacific Northwest Laboratory (PNL) as part of the cooperative USNRC, Electric Power Research Institute (EPRI), and Westinghouse (W) FLECHT-SEASET program.

6.1 COBRA-TF, A "Best-Estimate" Computer Program

The COBRA-TF code was developed to predict the thermal-hydraulic response of a LWR rod bundle during LOCA reflood. The computer code [37] provides a two-fluid, three-field representation of the two-phase flow. The two fluids are: Water and its vapor. The three field are: Continuous vapor, continuous liquid, and entrained liquid droplets. In addition, COBRA-TF allows for the transport of a non-condensible gas mixture with the vapor field.

This two-fluid, three-field description of the two-phase flow results in a set of nine conservation equations. Four continuity equations are required for the vapor, continuous liquid, entrained liquid, and non-condensible gas mixture. Three momentum equations are solved, allowing the liquid and entrained liquid fields to flow with different velocities relative to the vapor phase. Two energy equations are specified for the vapor-gas mixture and the combined liquid fields. The liquid and entrained liquid fields are assumed to be in thermal equilibrium.

These conservation equations and the equations for heat transfer from and within the solid structures in contact with the two fluids are solved using a semi-implicit, finite-difference numerical technique on an Eulerian mesh. The selection of either rectangular Cartesian or subchannel coordinates is provided. This allows a fully three-dimensional treatment in geometries amenable to description in a Cartesian coordinate system. The constitutive relations include state-of-art physical models for the interfacial mass transfer, the interfacial drag forces, the liquid and vapor wall drag, the wall and interfacial heat transfer, the rate of liquid entrainment and de-entrainment, and the thermodynamic properties of the fluid. A mixing length turbulence model is included as an option.

A consistent set of heat transfer models was implemented. It consists of five components:

a) A conduction model specifies the conductor geometry (fuel rods, electrically heated rods, tubes, and walls) and material properties, and solves the heat conduction equations.
b) A heat transfer package selects and evaluates the appropriate heat transfer correlations.
c) A quench front model employs a fine mesh rezoning technique in which fine mesh heat transfer cells with axial and radial conduction are superimposed upon the coarse hydrodynamic mesh spacing. The quench front propagation is calculated by applying a boiling heat transfer package to each node, so that the resulting quench front velocity is a function of the axial conduction, the boiling curve shape, the prequench heat transfer, and the internal heat conduction within the structure.
d) A dynamic gap conduction model evaluates the fuel pellet to clad heat conduction for a nuclear fuel rod.
e) A subchannel-based radiation model determines the rod to rod, rod to vapor, and rod to droplet radiation heat transfer.

Physical models [38], [39] were implemented into the code to describe, as realistic as possible,

a) the two-phase enhancement of convective heat transfer in the dispersed flow,
b) the subchannel thermal radiation,
c) the effects of grid spacers, i.e. single-phase convective heat transfer enhancement, droplet impact heat transfer, droplet breakup, droplet entrainment and de-entrainment, micro-droplet evaporation, and grid spacer rewetting,
d) the effects of blockages, i.e. flow redistribution, single- phase convective heat transfer enhancement, droplet impact heat transfer on the blockage, droplet breakup due to the blockage.

6.2 Simulation of FEBA and SEFLEX tests

For the calculation with COBRA-TF, the FEBA test section was modeled by using two representative fluid channels, one center channel, and one peripheral channel. The 5 x 5 heater rods were simulated by two rods, one center rod and one peripheral rod. The test section housing was described by a wall with an inside heat transfer surface and an insulated outer surface. Figure 56 shows the radial noding scheme of the bundle. Transverse connections were specified between the coolant subchannels to complete the multidimensional mesh for the region taken into consideration. The flow area between the channels was given by the width and the vertical length increment for the mesh. Form drag loss coefficients and wall friction factors were additional informations required as input data for the transverse momentum equations. Figure 57 shows the axial noding scheme of the FEBA test section. For the simulation of the heated length of 3900 mm, 18 vertical mesh cells were chosen. The vertical location of the faces of the individual cells are indicated correspondingly to the input data for COBRA-TF (reference level or zero level at the coolant inlet) as well as with respect to the experiments to be simulated (reference level or zero level at the upper end of the housing). The latter informations are written in the brackets. The numbers of these mesh cells depend on the degree of detail required to resolve the fluid field, the phenomena being modeled, and practical restrictions such as computing time and computer storage limitations. To capture the dominant physical phenomena and to coincide with selected measurement locations, a variable node length was provided. At the mesh cell faces, the fluid velocities are computed. Local pressure losses in the vertical flow due to grid spacers, orifice plates or other obstructions in the flow field are modeled in the code as a velocity head loss. On the other hand, the state variables, e.g., pressure, density, enthalpy, and phasic volume fractions are computed at the mesh cell center. This means the three field conservation equations for multidimensional flow are solved using a standard "staggared" differencing scheme for the convected quantities (donar cell differencing). Both fluid and rod temperatures are also calculated at the centers of the fluid continuity cell. Wen the axial temperature differences between adjacent axial nodes exceed maximum surface temperature differences, an additional node row is inserted halfway between the two original nodes. This splitting process continues until the mesh is fine enough to resolve the surface temperature adequately, when the temperature is near the critical heat flux temperature. Conversely, fine mesh nodes coalesce when the

quench front has propagated downstream and the criterion based on minimum temperature differences between adjacent nodes indicates coalescense of finer nodes. The axial noding scheme was bounded by phantom bottom and top nodes which contained the known boundary conditions. The data comparison was carried out for the axial locations (2225, 1975, 1875, 1675, and 1125 mm referred to the zero level of the experiments) marked by dots.

For the description of the conduction models, the characteristics of the heater rods (referred to as solid cylinders) and housing (referred to as flat plate) were specified. The modeling requirements included the following features: Unequal mesh spacing, internal resistance due to gaps, radial heat generating profiles, and temperature- and space-dependent material properties.

A maximum of five different material tables can be used by the code data input. The FEBA and REBEKA rods consist of concentric rings of material regions, as shown in Figs. 11 and 12, respectively. In each region, the number of radial nodes, width, and power factor as well as the material type were specified by the data input. Contact resistances were not calculated between material regions but were modeled by including a region, one node wide, with material properties which gave them the appropriate thermal resistances. The FEBA and REBEKA rod geometries were defined by eight and nine radial nodes, respectively. With respect to the maximum of five different material tables, the material properties of the heater rod with 6.02 mm o.d., which is placed in the center of the REBEKA rod, were described by those of a pseudomaterial. The averaged thermophysical properties of that pseudomaterial took into account the densities, heat capacities, and heat conductivities (including heat resistances at the interfaces) of the filler material (magnesium oxide), heating element (Inconel), electrical insulator material (boron nitride) and sheath material (Inconel). This approach seemed to be adequate since calculations [40] have shown that the dimensions of the alumina pellets and of the encapsulated heater rod have in comparison with the gas filled gaps a minor influence on the thermal behavior of the REBEKA fuel rod simulator during the reflood phase.

The thick-walled housing, shown in Figure 56, was modeled by four radial nodes to account for conduction and heat transfer from and to the inner surface. The outer surface was assumed to be insulated.

All thermophysical material properties as function of temperature were taken from Refs. 42 and 43. The initial axial temperature profiles of the center rods, peripheral rods, and the housing as well as the flooding parameters, i.e. flooding velocity, system pressure, and feedwater temperature, were specified corresponding to the individual test runs. The actual power profile was slightly modified to fit the fluid cell boundaries with reference to the actual power profile step changes. The total power of the rod bundle was conserved in the input data.

6.3 Comparison of Test Data with COBRA-TF Calculations

A total of four computer runs were made to simulate forced flow bottom reflood tests of the FEBA and SEFLEX-program, respectively. The comparison of code predictions against the experimental data for such main informations as cladding temperatures and quench front velocities are described in detail in Refs. 34 and 36. Therefore, the data comparisons presented in this report document only the results for SEFLEX test No. 03 obtained on the latest version of the COBRA-TF computer code available to EPRI in fall 1984.

This SEFLEX test is a run of test series 1 carried out with an unblocked bundle geometry containing seven grid spacers. The 5 x 5 rod bundle consisted of REBEKA fuel rod simulators with helium-filled gaps between the alumina pellets and the Zircaloy claddings.

For the calculations measured initial and boundary conditions were used as input data. Figure 58 shows the initial axial temperature profiles of the center rods, the peripheral rods, and housing, obtained by averaging all initial thermocouple readings of the instrumented axial levels. The temperature profiles are roughly symmetric about the bundle midplane (axial level 2025 mm). Figure 59 shows the boundary conditions plotted as function of reflood time. The flooding velocity (3.8 cm/s in the cold bundle), the system pressure (4.1 bar), and the feedwater temperature (40 ^{o}C) were kept constant during the test. For about two hours prior to reflood, the bundle and the housing were heated in an essentially stagnant steam environment to the desired initial temperatures using a low bundle power. The power input was stepped up, when the rising water level reached the bottom end of the heated bundle length, to about 200 kW followed by a decay heat transient corresponding to 120 percent ANS standard 40 seconds after scram.

COBRA-TF was run from the start of reflooding, with the initial and boundary conditions already described. The simulation continued until about 75 percent of the heated bundle length was quenched, in view of the computing time.

Figure 60 shows the measured and calculated cladding temperatures for three axial positions in the rod bundle, always approximately 300 mm downstream of the trailing edge of a grid spacer. Plot A represents a fairly good agreement between the measured and calculated data for the axial level 2225 mm, just upstream of the bundle midplane, a position characterized by the maximum rod power. The measured data (solid line) are taken from rod No. 18 (TC-position 18a1, see Fig. 20). The diamonds represent the results of COBRA-TF calculation for a simulated center rod. The time interval of the symbols is every 5 seconds (the print interval). It can be seen that for the early portion of the dispersed flow, the code overpredicts slightly the measured data. Later in time, the cladding temperature is underpredicted. The quench time is reached slightly earlier than in the experiment; the quench temperature is well predicted. Plot B represents a similar comparison for the axial level of 1680 mm, just downstream of the bundle midplane, again a region of maximum rod power. The measured data are taken from rod No. 12 (TC-position 12b4, see Fig. 20). The diagram indicates a good matching of the temperature transient; and it is noticeable that the small divergences between the compared data decrease with increasing distance from the bottom end of the heated bundle length. Plot C illustrates the comparison for the axial level 1135 mm, the beginning of the last quarter of heated bundle length. The peak-to-average rod power amounts to 1.06 at this position. The measured data are taken again from rod No. 12 (TC-position 12b3, see Fig. 20). A comparison of the measured data against COBRA-TF calculation indicates an excellent agreement for temperature rise, turnaround time, quench temperature, and quench time.

Figure 61 shows a comparison of the observed and computed cladding temperature immediately downstream of the trailing edge of the grid spacer at the bundle midplane, i.e. for axial levels at 1975 and 1875 mm, respectively. The measurements were recorded from the center rod (rod No. 13; i.e. TC-position 13i3 at axial level 1975 mm and TC-position 13i1 at axial level 1875 mm, respectively, see Fig. 20).

The grid spacer effects modeled in COBRA-TF predict well the trends observed at these axial positions of the simulated SEFLEX test run.

The quench times of the grid spacers located just upstream of the bundle midplane (No. 3), at the midplane (No. 4), and just downstream of it (No. 5) show an excellent agreement as plotted on an enlarged time scale in Fig. 62, Plot A through C. Only the characteristic temperature drops within the first 10 seconds of the reflood time are not very well predicted by the computer code. Figure 63 shows a comparison of measured housing data against COBRA-TF calculation for the axial positions 2225 mm (Plot A), 1680 mm (Plot B), and 1135 mm (Plot C). These axial positions correspond to the data comparison for the rod surface temperatures, plotted in Fig. 60. The COBRA-TF simulations show again a reasonable agreement with the reflood data, even if the quench times are predicted slightly earlier (< 20 %) than observed in the experiment.

Figure 64 shows a comparison of the measured and calculated quench front progression, which indicates an excellent matching of the data for the most part of the heated bundle length. Only for the upper most portion of the rod bundle, the differences increase and the quench times are slightly underpredicted.

Figure 65 shows a comparison of the measured and calculated quench front progressions for four simulated test runs. All experiments were carried out under identical initial and boundary conditions, as far as experimentally possible; in particular, same axial temperature profiles at initiation of reflood, same flooding velocities of the rising water levels in the cold bundles (3.8 cm/s), and same feedwater temperatures (40 ^{o}C). However, the reflood experiments were carried out with different system pressures of 4.1 and 2.1 bar, respectively, using rod bundles which have fuel rod simulators of different design and in case of gapped rods with helium- or argon-filled gaps. For the FEBA "solid-type" rod bundle (Plot A) flooded at a system pressure of 4.1 bar, the calculated quench time becomes slightly shorter than the experimental as the axial elevation increases. As discussed earlier, a remarkably good agreement is obtained for the REBEKA rod bundle with helium-filled gaps (Plot B) under identical flooding conditions. For flooding experiments performed at a system pressure of 2.1 bar using REBEKA rod bundles with helium- (Plot C) and argon-filled gaps (Plot D), respectively, the computed quench times are slightly higher than the measured. The overprediction of the quench times is presumed to be due to an underprediction of the liquid content of the flow and hence, heat transfer at lower system pressure.

Finally should be mentioned that COBRA-TF does a remarkably good job of predicting peak cladding temperatures and quench times of forced reflood tests, though the code has undergone only a limited assessment since the completion of its development. To define remaining deficiencies in the physical models the COBRA-TF code should run against data from the SEFLEX experiments, since a source version of the program was not available and hence no modifications or enhancements were made to the code during the course of this study.

7. CONCLUSIONS

Fuel rod simulators with Zircaloy claddings and a gas filled gap beetween claddings and pellets (REBEKA rods) exhibit lower peak cladding temperatures and shorter quench times during reflood than gapless heater rods with stainless steel claddings (FEBA rods).

Due to earlier quenching of the claddings the removal of the heat stored in the pellets is accelerated for increasing gap heat resistance and nominal rod geometry.

Grid spacers cause significant cooling enhancement downstream during the time span at which maximum cladding temperatures occur. The effect is more pronounced for REBEKA rods than for FEBA rods.

Ballooned Zircaloy claddings, forming e.g. a coplanar 90 percent blockage, are quenched substantially earlier than thickwall stainless steel blockage sleeves, and even earlier than undeformed rod claddings.

The most recent version of COBRA-TF, "a best-estimate" computer code, developed as part of the FLECHT-SEASET program, has been used to simulate selected test data. The comparison of measured and calculated data demonstrates the capability of the code for reflood applications.

The results obtained comparing FEBA and SEFLEX data suggest a higher safety margin than evaluated from gapless heater rods for the coolability of blocked as well as unblocked PWR cores under LOCA conditions.

8. REFERENCES

[1] P. Ihle and K. Rust:
"FEBA - Flooding Experiments With Blocked Arrays."
a) Evaluation Report, KfK 3657, March 1984,
b) Data Report 1, Test Series I Through IV, KfK 3658, March 1984,
c) Data Report 2, Test Series V Through VIII, KfK 3659, March 1984.

[2] M. J. Loftus et al.:
"PWR FLECHT-SEASET, 21-Rod Bundle Flow Blockage Task,
Data and Analysis Report."
NUREG/CR-2444, EPRI NP-2014, WCAP-9992, Vol. 1 and 2, September 1982.

[3] C. A. Cooper, K. G. Pearson and D. Jowitt:
"The THETIS 80% Blocked Cluster Experiment,
Part 3: Forced Reflood Experiments."
AEEW - R 1765, September 1984.

[4] S. A. Fairbairn and P. D. G. Piggott:
"Flow and Heat Transfer in PWR Rod Bundles in the Presence of Blockage due to Clad Ballooning."
a) Experimental Data Report, Part 1, TPRD/B/0458/N84, May 1984,
b) Experimental Data Report, Part 2, TPRD/B/0511/N84, November 1984,
c) Experimental Data Report, Part 3, TPRD/B/0512/N84, November 1984.

[5] H. Adachi et al.:
"SCTF Core I Reflooding Test Results."
NUREG/CP-0041, Vol. 1, January 1983, p. 287.

[6] Y. Murao et al.:
"Findings in CCTF Core I Test."
NUREG/CP-0041, Vol. 1, January 1983, p. 275.

[7] C. Vitanza et al.:
"Blowdown/Reflood Tests With Nuclear Heated Rods,
(IFA-511.2)."
OECD Halden Reactor Project, HPR 248, May 1980.

[8] T. Johnsen and C. Vitanza:
"Blowdown/Reflood Tests With SEMISCALE Heaters,
(IFA-511.3, Data Collection)."
OECD Halden Reactor Project, HWR 17, May 1981.

[9] T. Johnsen and C. Vitanza:
"Results of LOCA Tests With SEMISCALE Heaters,
(IFA-511.5)."
OECD Halden Reactor Project, HPR 313, May 1984.

[10] C. Vitanza and T. Johnsen:
"Results of Blowdown/Reflood Tests With REBEKA Electric Simulators,
(IFA-511.4, Cycle 2)."
OECD Halden Reactor Project, HWR 85, May 1983.

[11] C. L. Mohr et al.:
"LOCA Simulation in National Research Universal Reactor Program."
NUREG/CR-2528, PNL-4166, April 1983.

[12] F. J. Erbacher:
"Interaction Between Fuel Clad Ballooning and Thermal-Hydraulics in a LOCA."
KfK 3880, Vol. 1, December 1984, pp. 299-310.

[13] R. C. Gottula:
"Effects of Cladding Surface Thermocouples and Electrical Heater Rod Design on Quench Behavior."
NUREG/CR-2691, EGG-2186, February 1984.

[14] B. D. G. Pigott and R. B. Duffey:
"The Quenching of Irradiated Fuel Pins."
Nuclear Engineering and Design, Vol. 32, 1975, pp. 182-190.

[15] V. K. Dhir and I. Catton:
"Reflood Experiments With a 4-Rod Bundle."
EPRI NP-1277, December 1979.

[16] V. K. Dhir, R. B. Duffey and I. Catton:
"Quenching Studies on a Zircaloy Rod Bundle."
Journal of Heat Transfer, Vol. 103, No. 2, May 1981, pp. 293-299.

[17] N. E. Kaiser and O. Rathmann:
"Study of Rewetting and Quench Phenomena by Single Pin Out-of-Pile Experiments, With Special Emphasis on the Effect of the Fuel Pin Composition."
Commission of the European Communities: Seminar on the Results of the Indirect Action Research Programme, Safety of Thermal Water Reactors (1979 - 1983),
Brussels, Belgium, October 1-3, 1984.

[18] T. C. de Boer and S. B. van der Molen:
"Heat Transfer to a Dispersed Two-Phase Flow and Detailed Quench Front Velocity Research."
Commission of the European Communities: Seminar on the Results of the Indirect Action Research Programme, Safety of Thermal Water Reactors (1979 - 1983),
Brussels, Belgium, October 1-3, 1984.

[19] M. K. Denham and D. Blackburn:
"A Study of Rewetting Propagation Over Zircaloy Under Bottom Flooding Conditions."
Commission of the European Communities: Seminar on the Results of the Indirect Action Research Programme, Safety of Thermal Water Reactors (1979 - 1983),
Brussels, Belgium, October 1-3, 1984.

[20] P. Ihle and K. Rust:
"SEFLEX - Fuel Rod Simulator Effects in Flooding Experiments, Part 2: Unblocked Bundle Data."
KfK 4025, March 1986.

[21] P. Ihle and K. Rust:
"SEFLEX - Fuel Rod Simulator Effects in Flooding Experiments, Part 3: Blocked Bundle Data."
KfK 4026, March 1986.

[22] P. Ihle, K. Rust und H. Schneider:
"Brennstab-Simulator-Effekte in Flutexperimenten, (SEFLEX-Programm)."
In: Projekt Nukleare Sicherheit, Jahresbericht 1983,
KfK 3450, Juni 1984, S. 4200/97-111.

[23] P. Ihle, K. Rust und F. J. Erbacher:
"Temperatur- und Wiederbenetzungsverhalten von Brennstäben beim Kühlmittelverluststörfall: Einfluß des Spaltes zwischen Pellet und Hüllrohr."
Jahrestagung Kerntechnik '84, Frankfurt, 22.-24. Mai 1984, S. 65-68.

[24] P. Ihle:
"Vergleich des thermischen Verhaltens verschiedener Brennstab-Simulatoren unter DWR-Notkühlbedingungen."
Commission of the European Communities: 7th Project Review Meeting in Area A on LOCA-ECCS (Loss-of-Coolant Accident - Emergency Core Cooling Systems),
Risø National Laboratory, Denmark, June 13-15, 1984.

[25] P. Ihle, K. Rust and F. J. Erbacher:
"Dispersed Flow Reflood Heat Transfer in Rod Bundles of Different Fuel Rod Simulator Design."
NUREG/CP-0060, December 1984, pp. 575-582.

[26] P. Ihle, K. Rust and F. J. Erbacher:
"Quenching of Rod Bundles of Different Fuel Rod Simulator Design."
NUREG/CP-0060, December 1984, pp. 171-178.

[27] P. Ihle, K. Rust and F. J. Erbacher:
"Grid Spacer Effects in Reflooding Experiments Using Rod Bundles of Different Fuel Rod Simulator Design."
NUREG/CP-0060, December 1984, pp. 673-681.

[28] M. Nishida:
"Fuel Rod Simulator Effects in Flooding Experiments, Single Rod Tests (Zry-Cladding)."
KfK 3786 B, September 1984.

[29] F. J. Erbacher, P. Ihle, K. Rust and K. Wiehr:
"Temperature and Quenching Behavior of Undeformed, Ballooned and Burst Fuel Rods in a LOCA."
KfK 3880, Vol. 1, December 1984, pp. 516-524.

[30] S. L. Lee and P. Ihle:
"A Study of Mist Cooling Enhancement from Grid Spacers in LOCA Reflood of a PWR Combined Gross Heat Transfer and Local Temperature and LDA Droplet Sizing Analysis."
NUREG/CP-0058, Vol. 1, January 1985, pp. 286-306.

[31] P. Ihle and K. Rust:
"Grid Spacer Effects on PWR Reflood Heat Transfer Measured in Bundles of 5 x 5 Rods With Zircaloy Claddings and Pellets."
Proceedings of 23rd ASME, AIChE, ANS National Heat Transfer Conference, Denver, CO, U.S.A., August 6-9, 1985.

[32] K. Rust, A. Singh, R. B. Duffey and P. Ihle:
"Effects of Fuel Rod Simulator Geometry on Reflood Behavior Following a LOCA."
Proceedings of 23rd ASME, AIChE, ANS National Heat Transfer Conference, Denver, CO, U.S.A., August 6-9, 1985.

[33] P. Ihle, K. Rust und H. Schneider:
"Fuel Rod Simulator Effects in Flooding Experiments (SEFLEX)."
In: Projekt Nukleare Sicherheit, Jahresbericht 1984,
KfK 3550, Juni 1984, S. 15-16.

[34] K. Rust:
"Reflood Behavior of Rod Bundles Having Fuel Rod Simulators of Different Design."
EPRI NP-4103-SR, July 1985.

[35] P. Ihle and K. Rust:
"PWR Reflood Experiments Using Full-Length Bundles of Rods With Zircaloy Claddings and Alumina Pellets, (Results of the SEFLEX Program)."
Proceedings of Third International Topical Meeting on Reactor Thermal Hydraulics, Vol. 2, Session 13, Paper 13.H,
Newport, RI, U.S.A., October 15-18, 1985.

[36] A. Singh, K. Rust, R. B. Duffey and P. Ihle:
"The Effects of Thermal Diffussion and Gap Conductance on Quench Velocity During Bottom Reflooding of Rod Bundles."
Proceedings of Third International Topical Meeting on Reactor Thermal Hydraulics, Vol. 2, Session 13, Paper 13.G,
Newport, RI, U.S.A., October 15-18, 1985.

[37] "COBRA/TRAC - A Thermal-Hydraulics Code for Transient Analysis of Nuclear Reactor Vessels and Primary Coolant Systems."
NUREG/CR-3046, PNL-4385, March 1983.
a) M. J. Thurgood et al.:
Vol. 1: "Equations and Constitutive Models."
b) M. J. Thurgood and T. L. George:
Vol. 2: "COBRA/TRAC Nummerical Solution Methods."
c) M. J. Thurgood et al.:
Vol. 3: "Users' Manual."
d) M. J. Thurgood et al.:
Vol. 4: "Developmental Assessment and Data Comparison."
e) A. S. Koontz and J. M. Cuta:
Vol. 5: "Programmers' Manual."

[38] J. M. Kelly and R. J. Kohrt:
"COBRA-TF: Flow Blockage Heat Transfer Program."
NUREG/CP-0048, Vol. 1, January 1984, pp. 209-232.

[39] J. M. Kelly, C. Y. Paik and L. E. Hochreiter:
"The Analysis of the FLECHT-SEASET Flow Blockage Data With COBRA-TF."
NUREG/CP-0057, Vol. 1, October 1984, p. 324.

[40] V. Casal, S. Malang and K. Rust:
"Thermal and Mechanical Behaviour of PWR Fuel Rod Simulators for LOCA-Experiments."
KfK 3331, May 1982.

[41] S. Malang:
"HETRAP - A Heat Transfer Analysis Program."
ORNL-TM-4555, September 1974.

[42] K. Rust, S. Malang und W. Götzmann:
"PEW - Ein FORTRAN IV-Rechenprogramm zur Bereitstellung physikalischer Eigenschaften von Werkstoffen für LWR-Brennstäbe und deren Simulatoren."
KfK-Ext. 7/76-1, Dezember 1976.

[43] N. B. Vargaftik:
"Tables on the Thermophysical Properties of Liquids and Gases."
John Wiley & Sons, Inc., New York 1975.

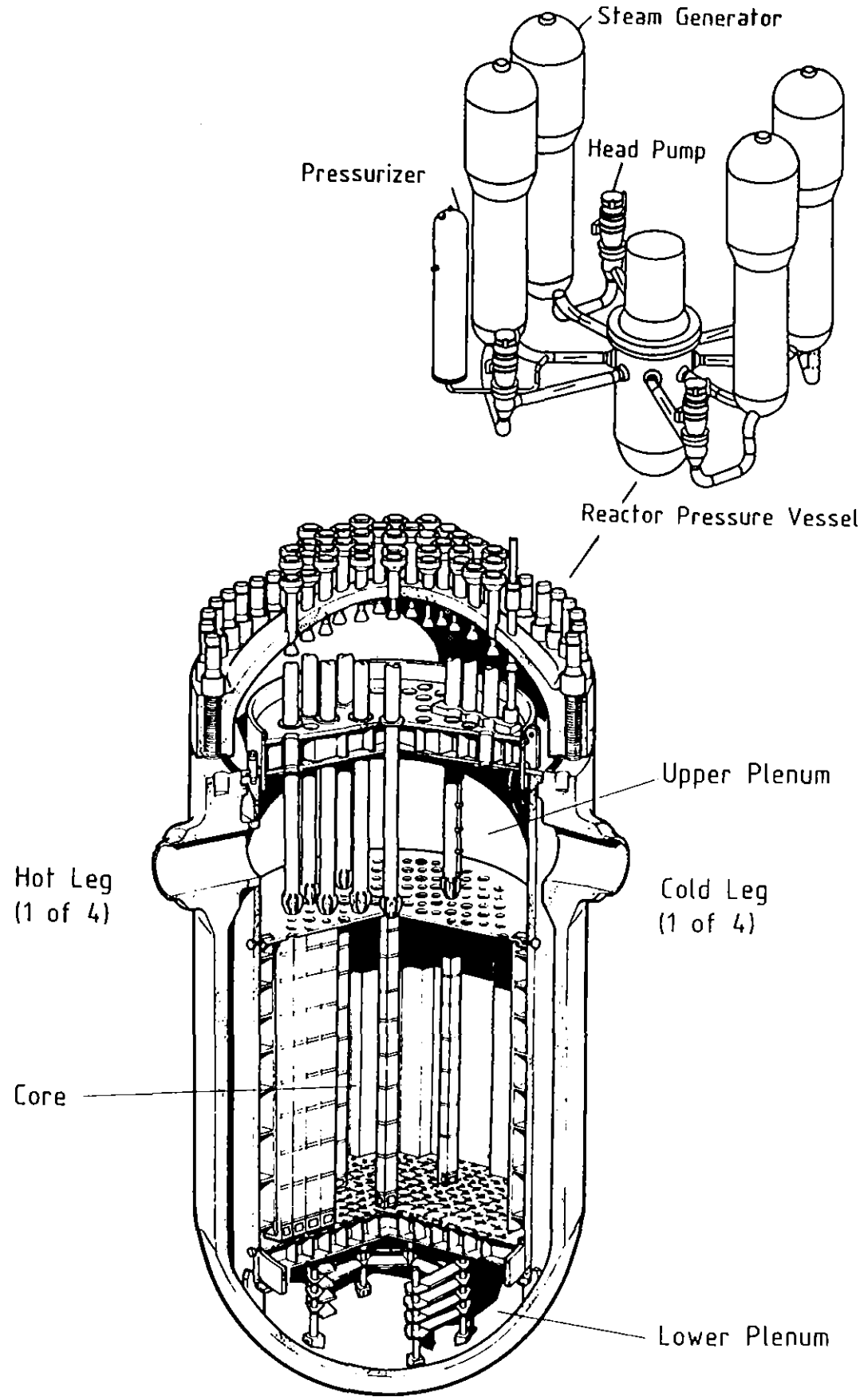

Figure 1. 4-loop steam generator system and pressure vessel with installations of a pressurized water reactor.

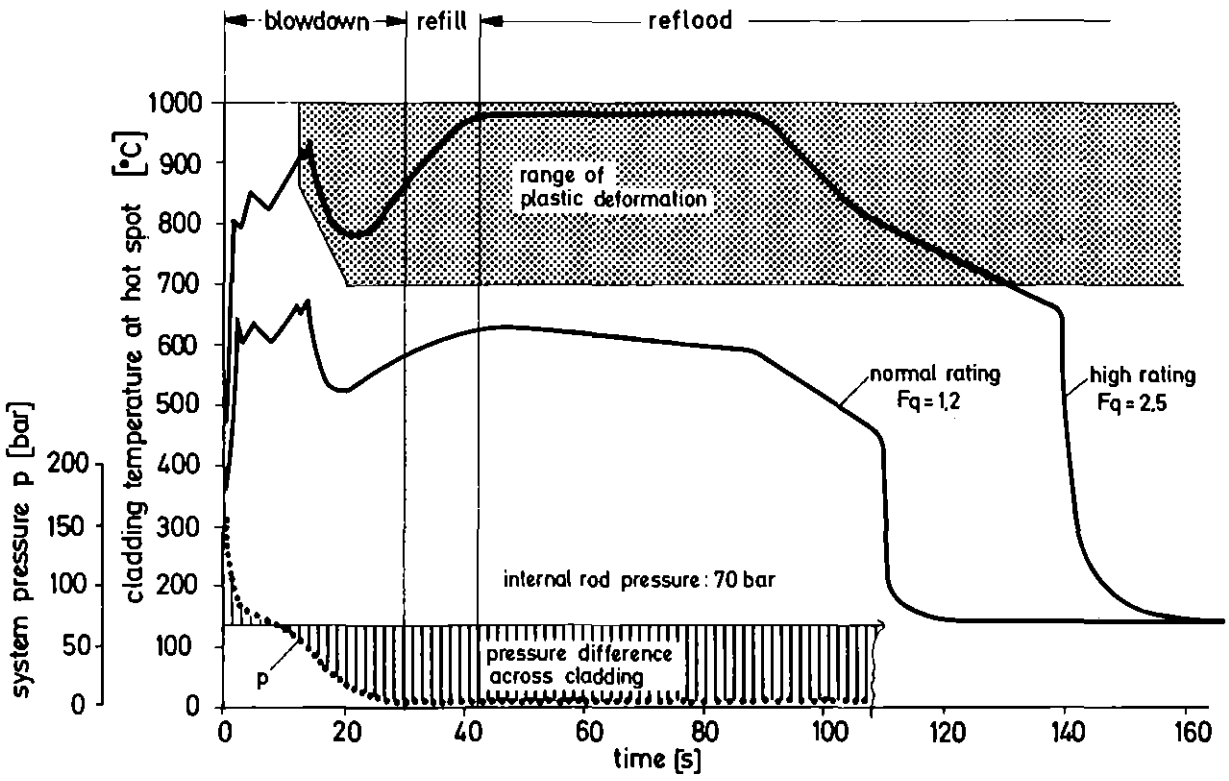

Figure 2. Fuel rod cladding loading in a 2F-cold leg break LOCA.

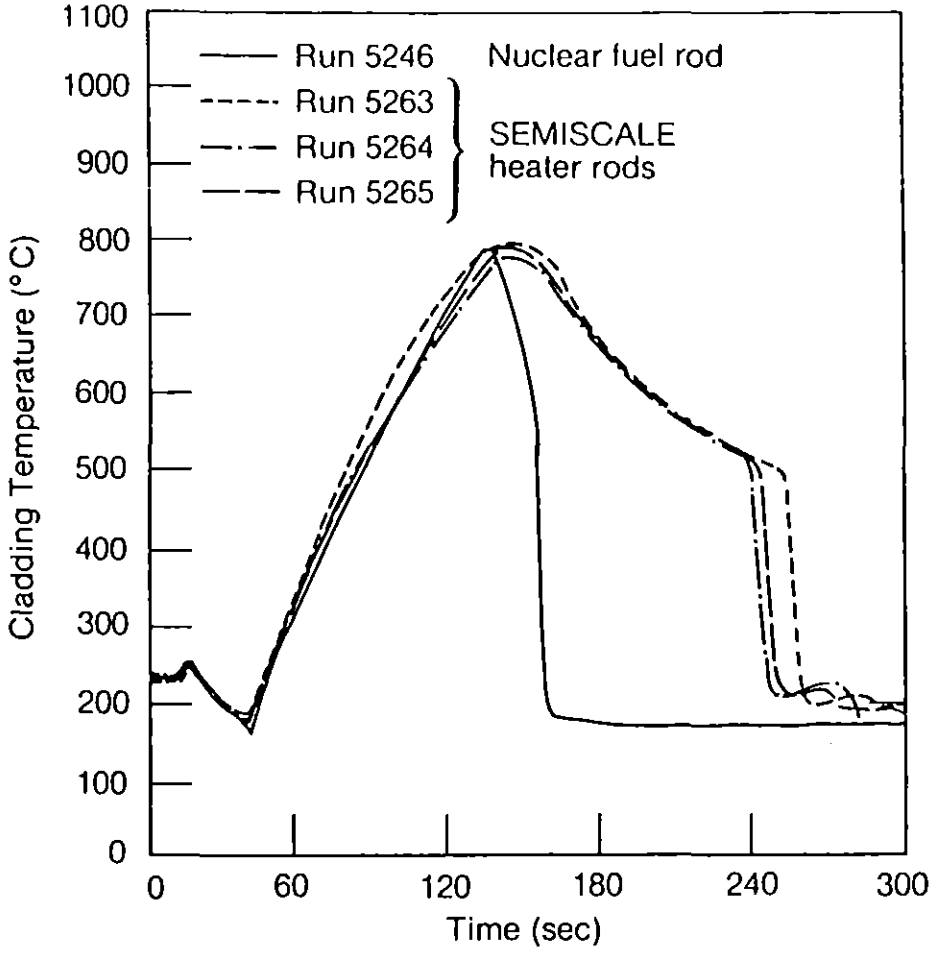

Figure 3. OECD Halden Reactor Project: Comparison of nuclear fuel rod and SEMISCALE heater rod responses.

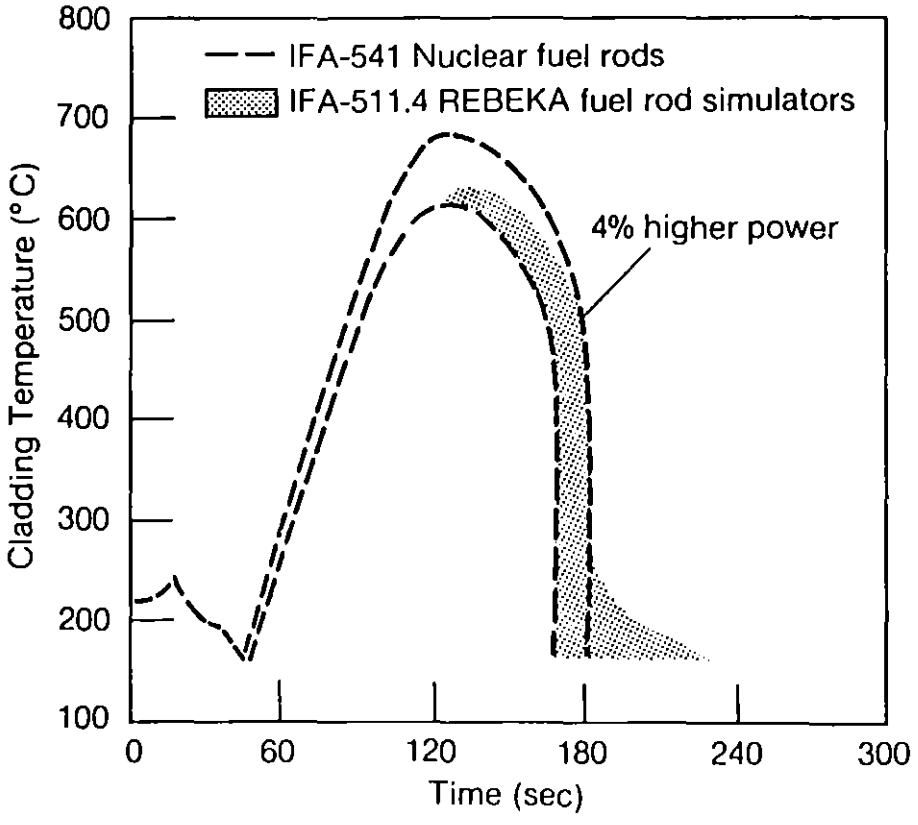

Figure 4. OECD Halden Reactor Project: Comparison of nuclear fuel rod and REBEKA fuel rod simulator responses.

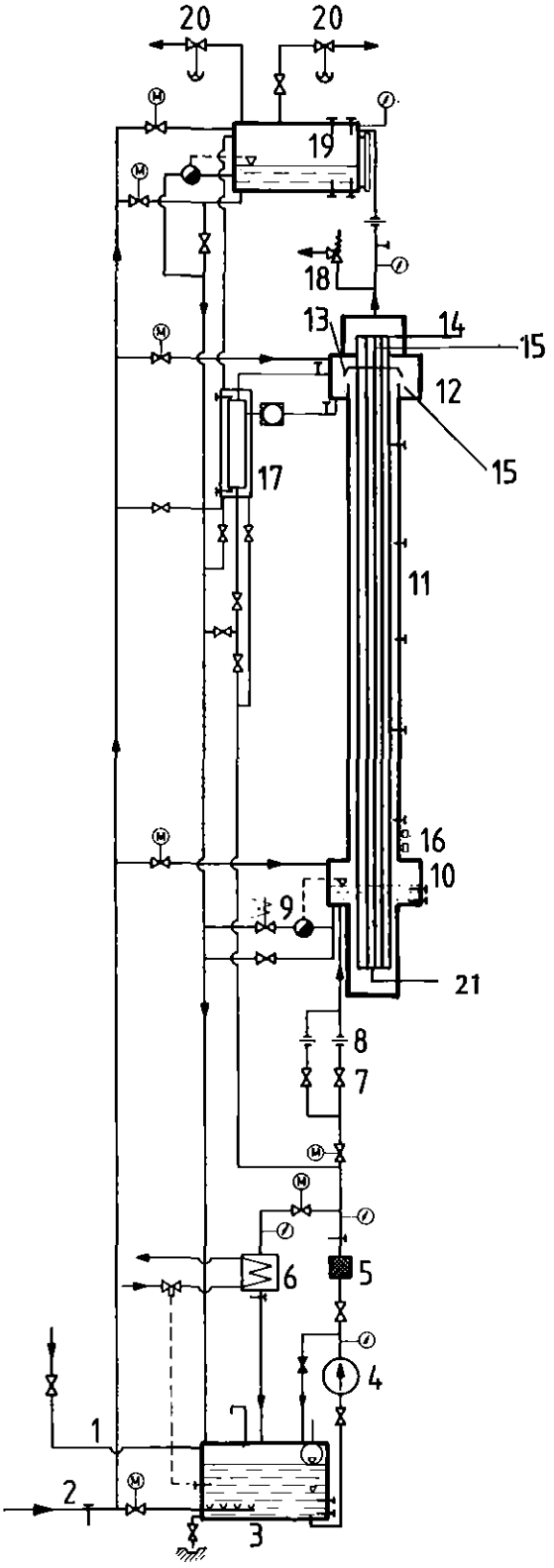

LEGEND

1 Water Supply
2 Steam Supply
3 Storage Tank
4 Water Pump
5 Filter
6 Heat Exchanger
7 Throttle Valve
8 Turbine Meter
9 Water Level Regulation Valve

10 Lower Plenum
11 Test Section
12 Upper Plenum
13 Water Separator

14 Power Supply
15 Rod Instrumentation Exits
16 Water Level Detector
17 Water Collecting Tank
18 Outlet Valve
19 Buffer
20 Pressure Regulator
21 Filling Gas Supply

Figure 5. FEBA test loop used for SEFLEX tests.

Legend

3 Storage Tank
4 Water Pump
9 Water Level Regulation Valve
10 Lower Plenum
11 Test Section
12 Upper Plenum
14 Power Supply
15 Rod Instrumentation Exits
17 Water Collecting Tank
18 Outlet Valve
19 Buffer
21 Filling Gas Supply

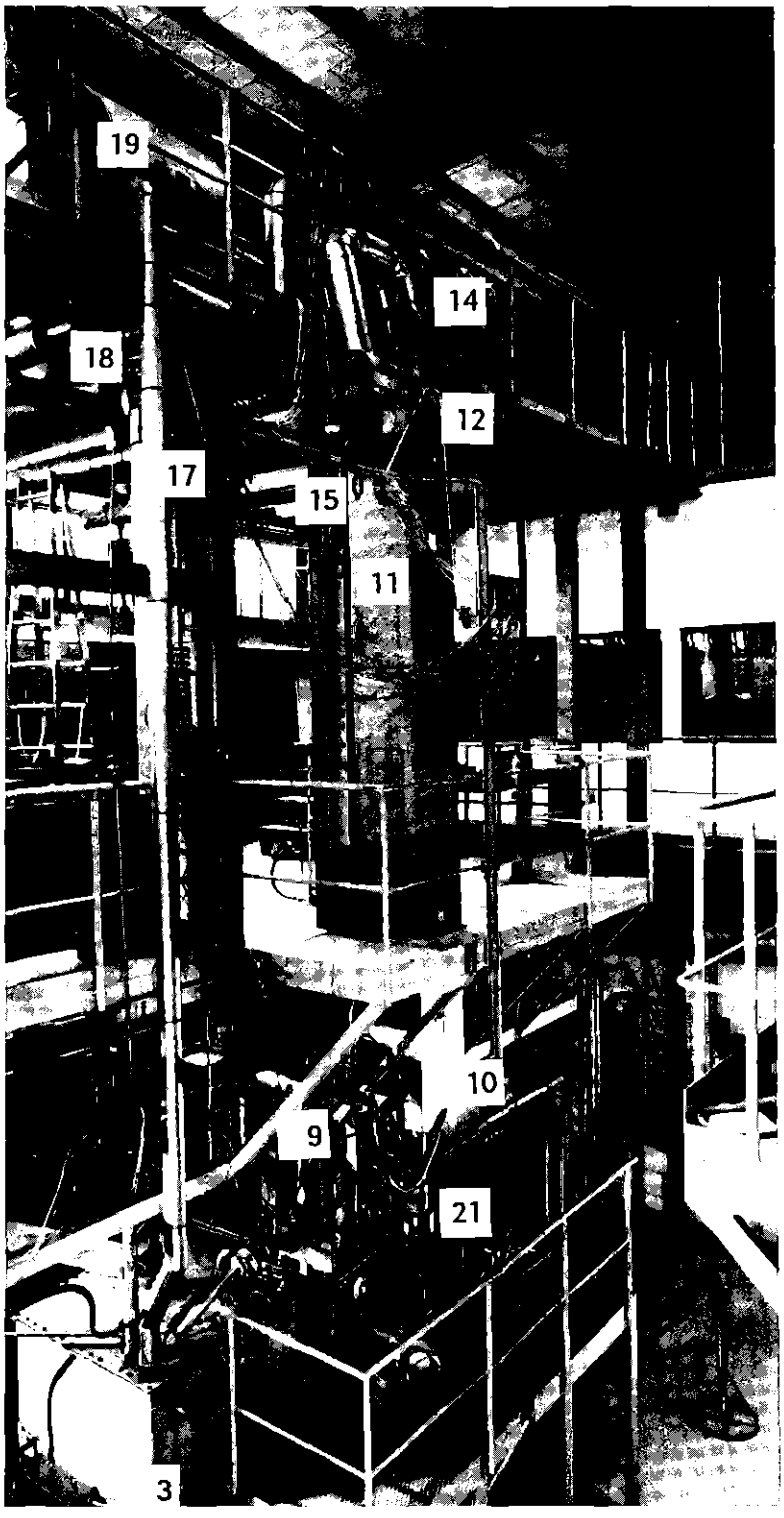

Figure 6. Photograph of FEBA/SEFLEX test rig.

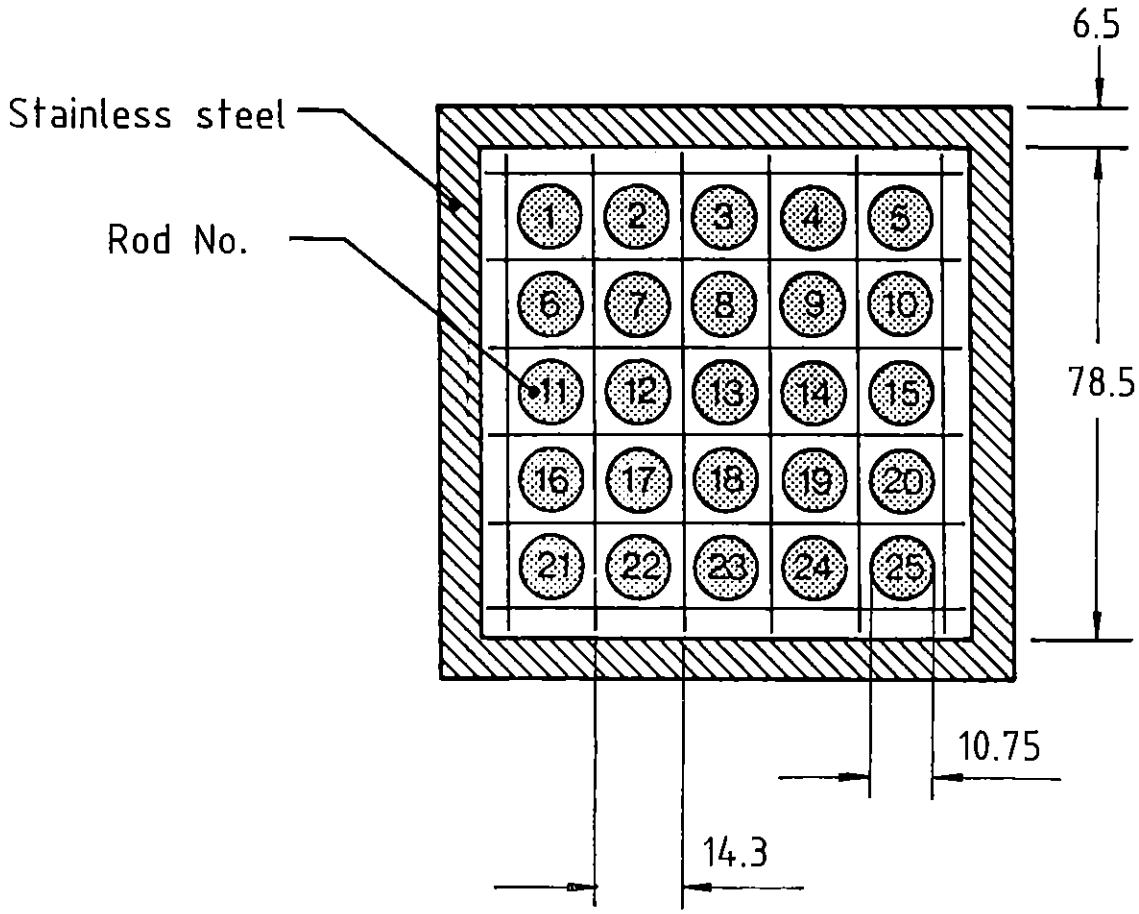

Figure 7. Cross-sectional view of a 5 x 5 rod bundle.

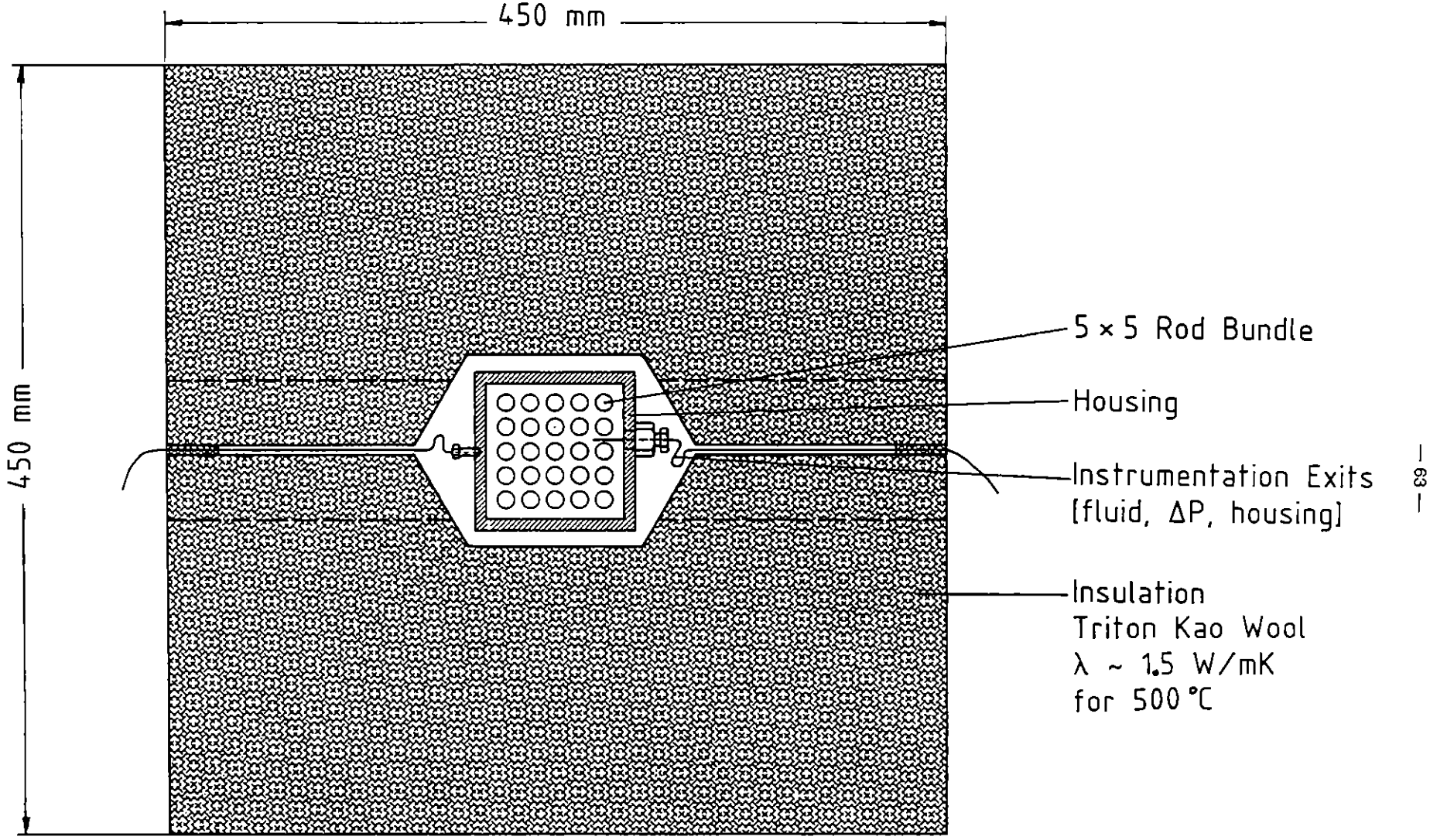

Figure 8. Cross-sectional view of FEBA/SEFLEX test section.

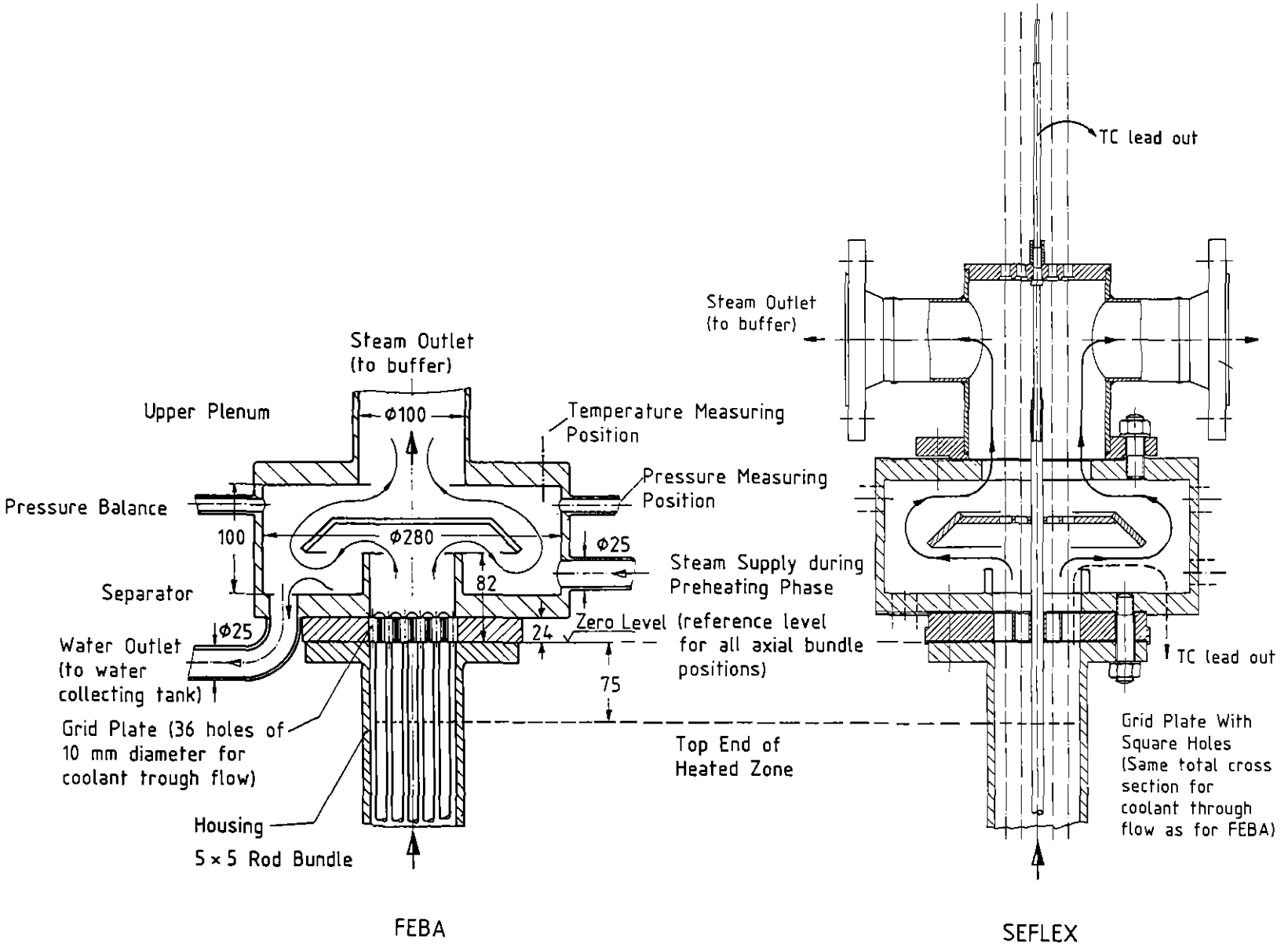

Figure 9. Original and modified upper bundle end and plenum of FEBA/SEFLEX test section.

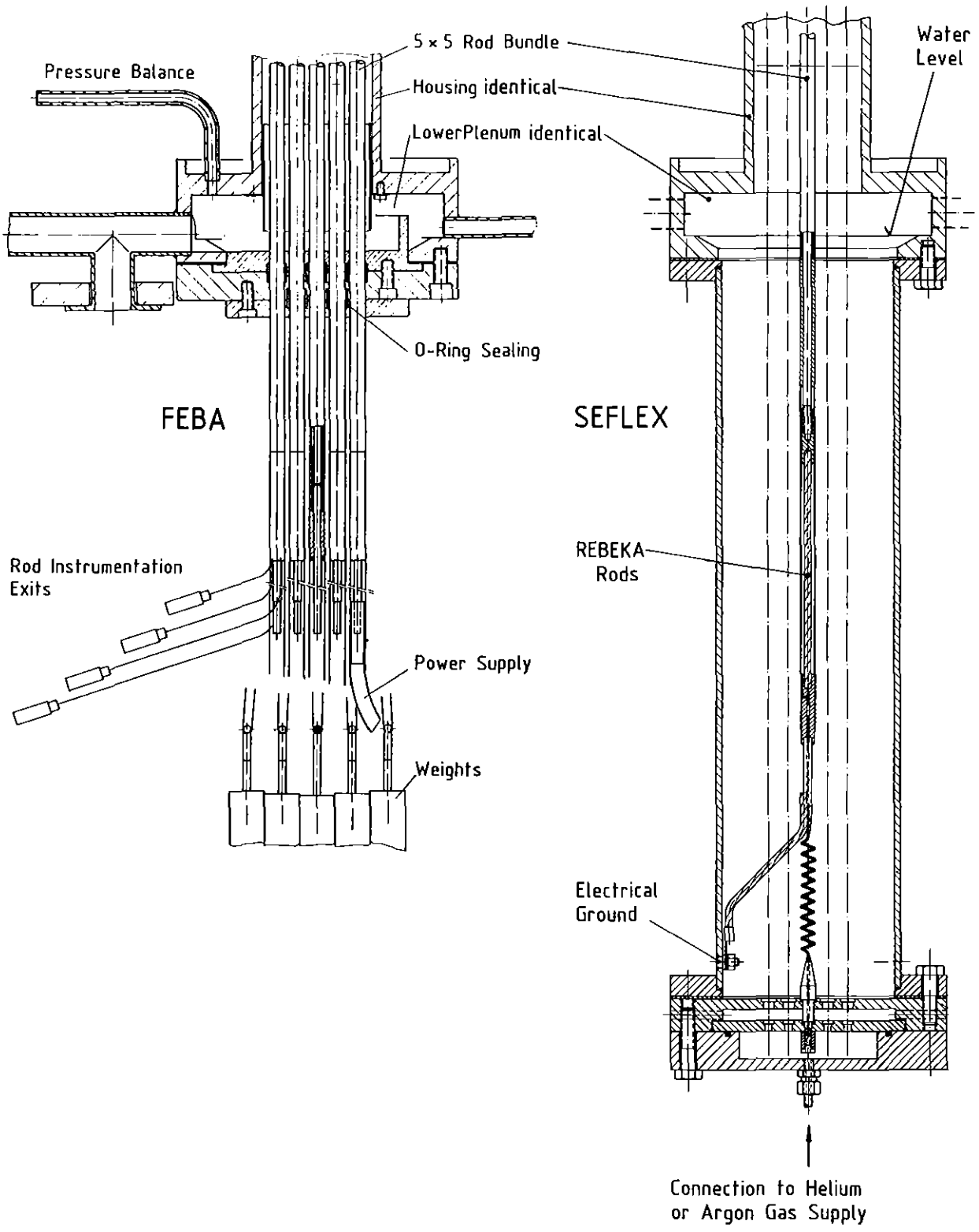

Figure 10. Original and modified lower bundle end and plenum of FEBA/SEFLEX test section

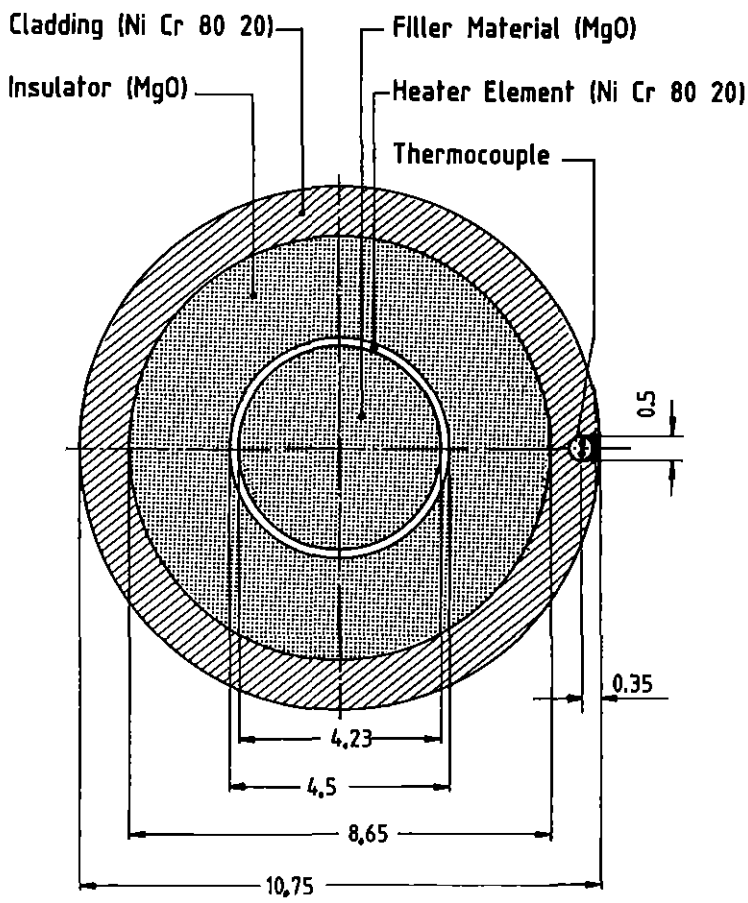

Figure 11. Cross section of a FEBA heater rod.

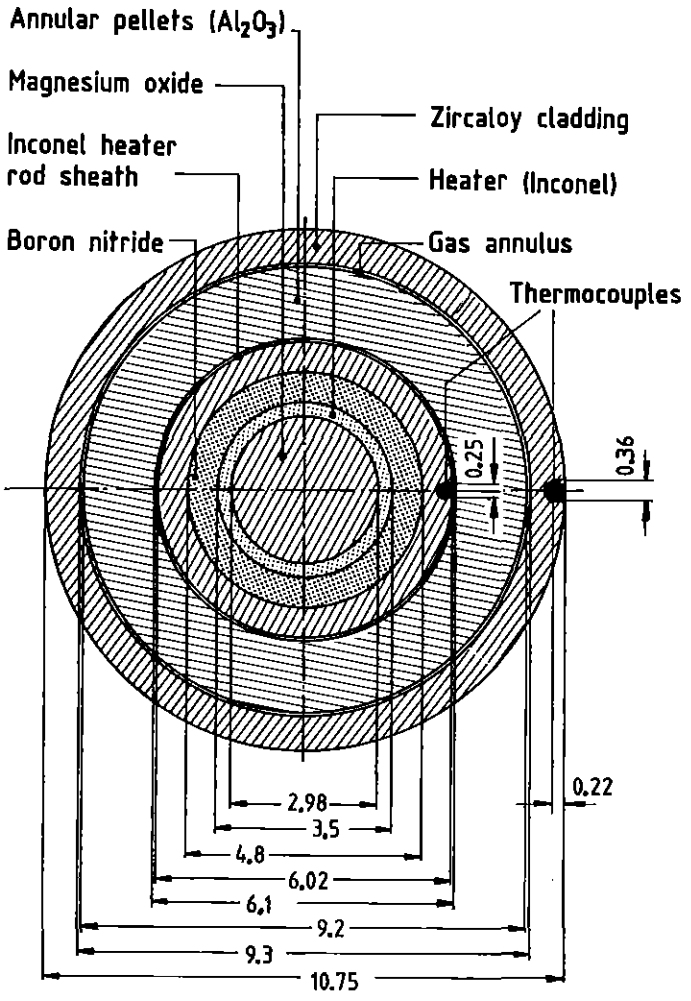

Figure 12. Cross section of a REBEKA fuel rod simulator.

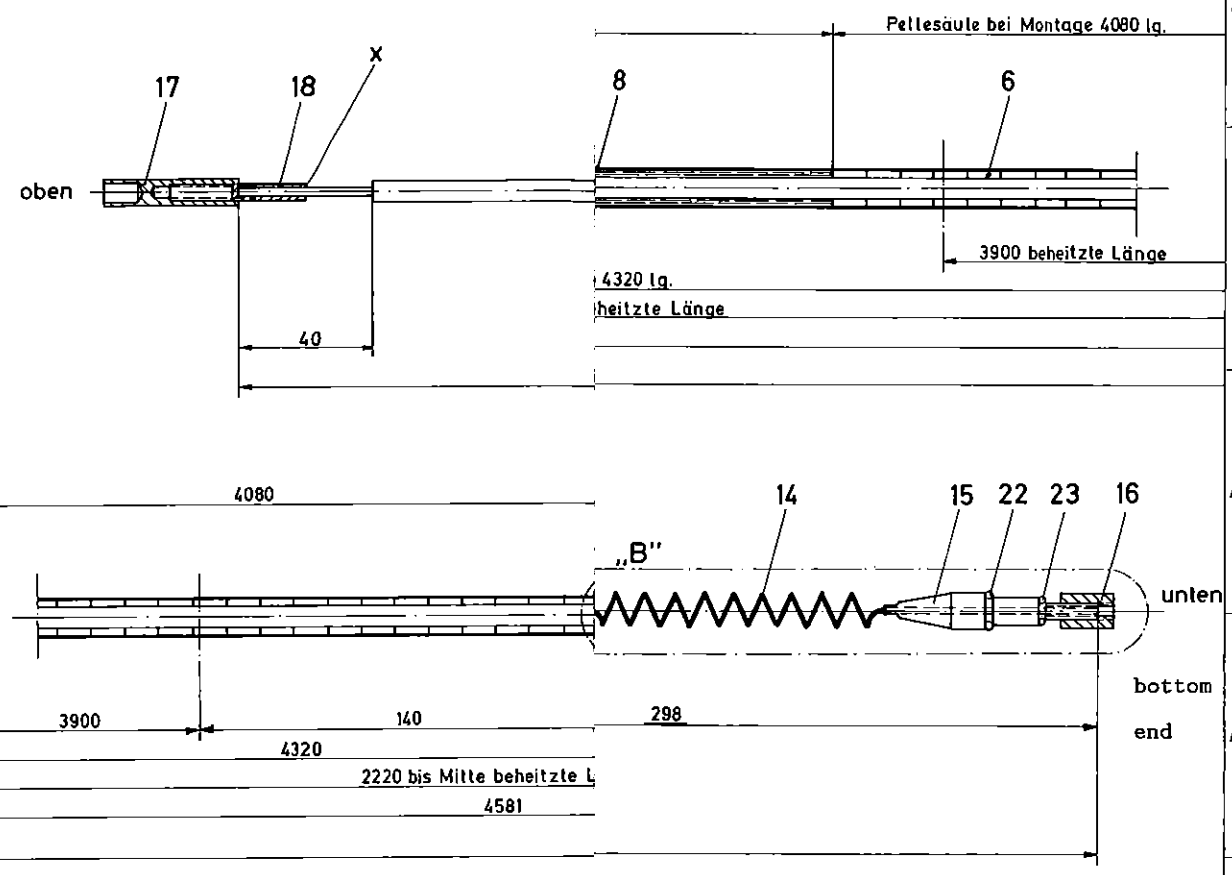

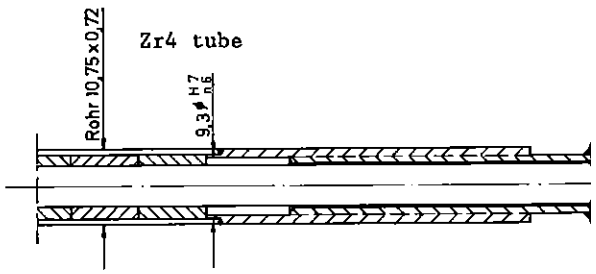

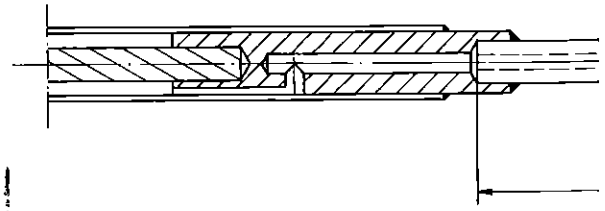

Figure 13. Worki

Legend

1 Heater Rod
2 Soldering Tube
3 Cold Welding (SS - Zr4)
4 Spring
5 Connection
6 Alumina Pellets
7 Tube Plug
8 Zircaloy-4 Tube
9 Flexible Copper Tape
10 Connection
11 Check Nut
12 Stainless Steel Tube
13 Tube
14 Spiral Coil
15 Screw Cap
16 Nut
17 Top Cap
18 Screw
19 Nut
20 Screw
21 Sealing
22 Sealing
23 Sealing

Kernforschungszentrum Karlsruhe GmbH

Maßstab 1 : 1 | Gewicht | Werkstoff

Bearb. 18. 1. 83

Benennung: BE-Simulator (Seflex)

Vorhaben: PNS 4260

Zeichnungs-Nr.: R2.39-1-03a

Blatt 81

Spirale 6.6.84

Zust. | Änderung | Datum | Name | Ursp. | Ersatz für: | Ersetzt durch:

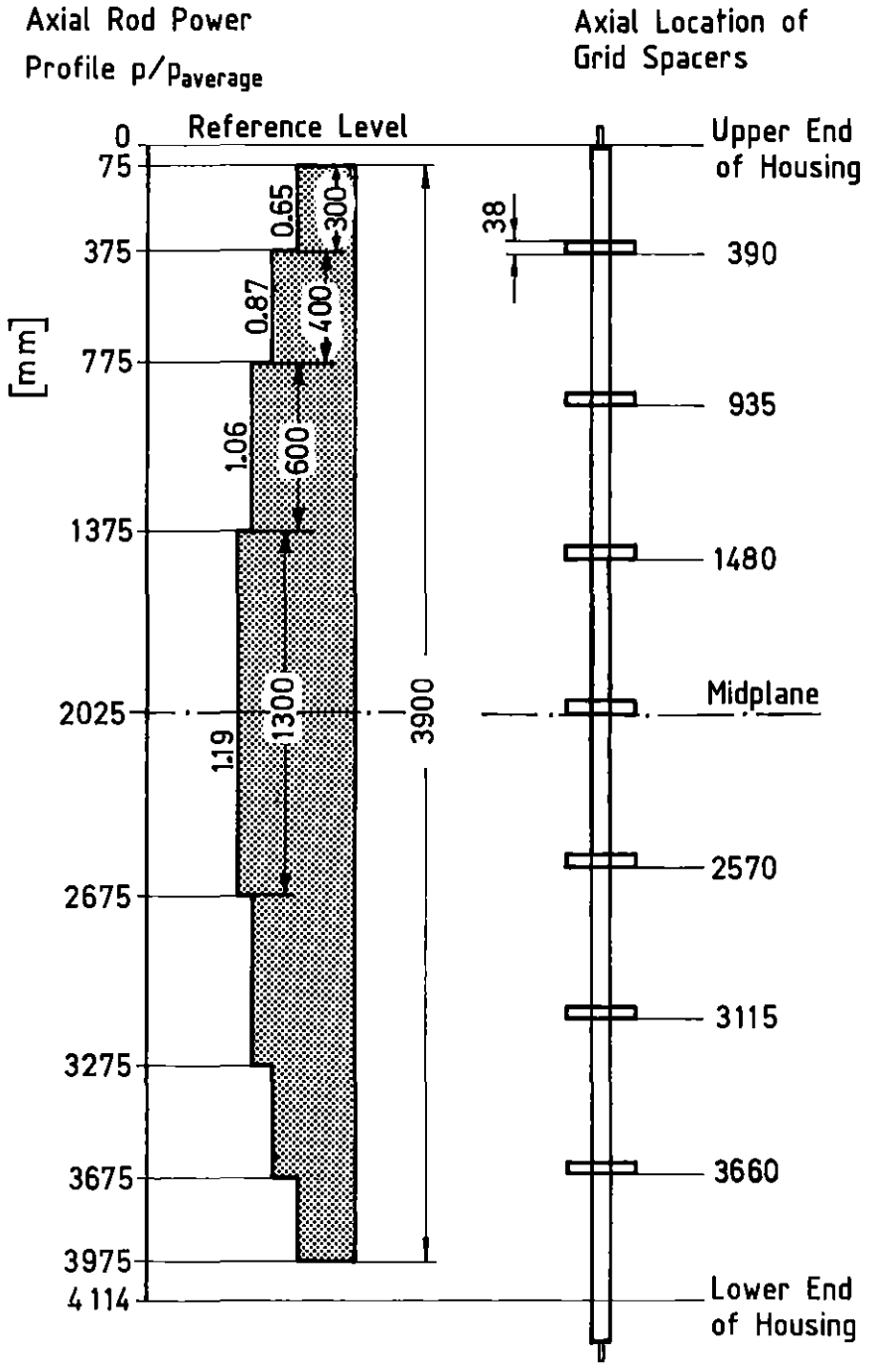

Figure 14. Axial power profile and location of grid spacers of FEBA and REBEKA rod bundles in SEFLEX tests.

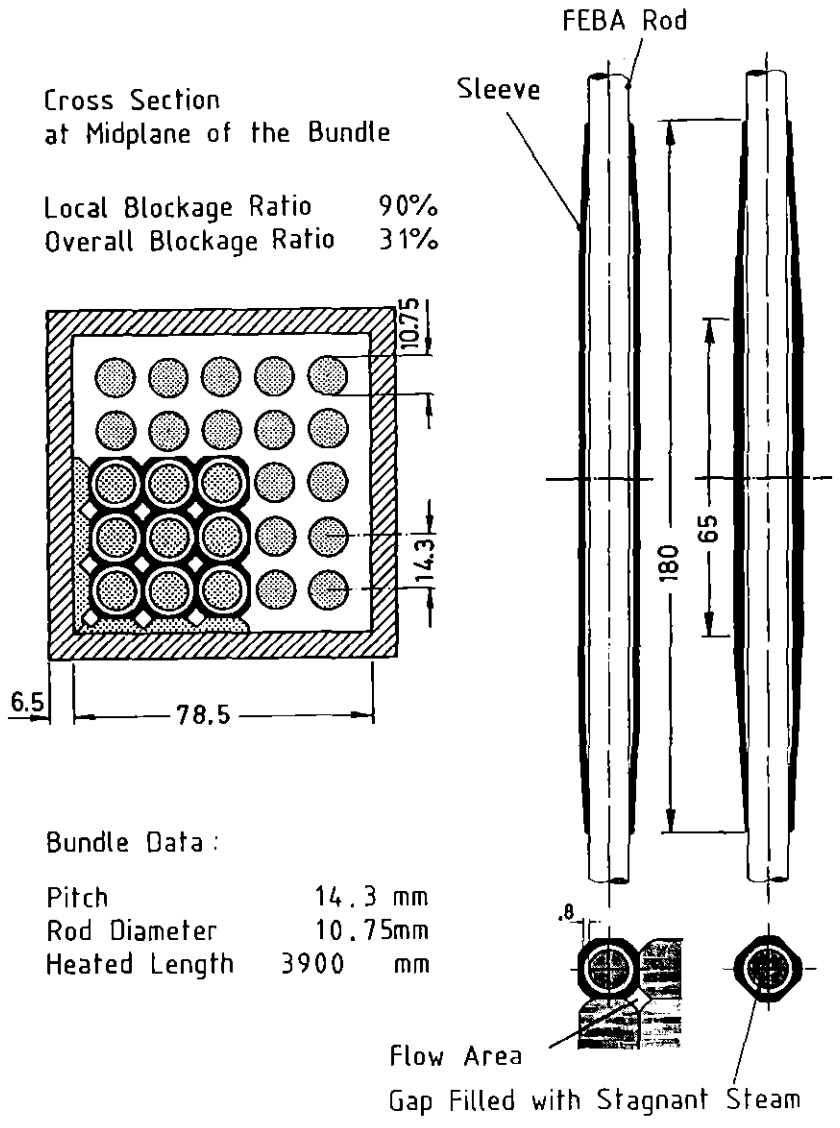

Figure 15. Sectional view of the 90 percent blockage with bypass realized for FEBA tests.

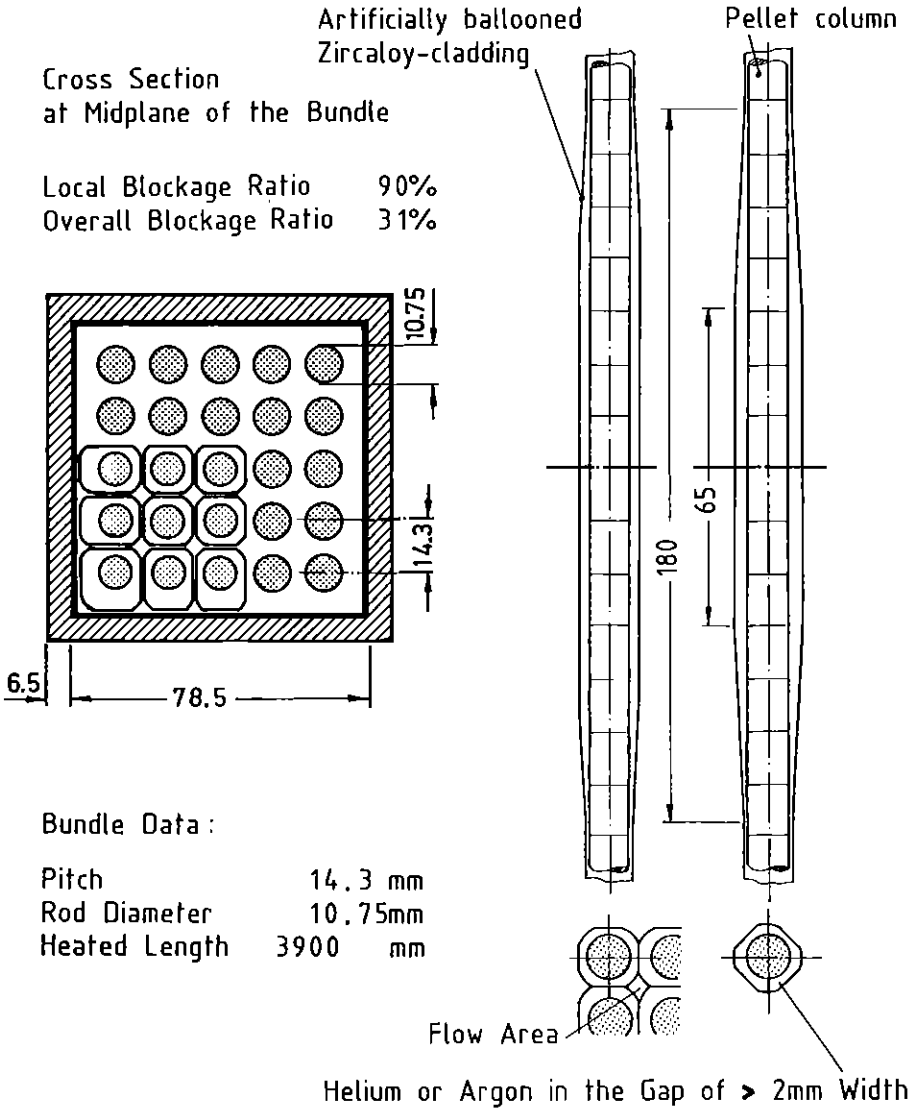

Figure 16. Sectional view of the 90 percent blockage with bypass realized for SEFLEX tests.

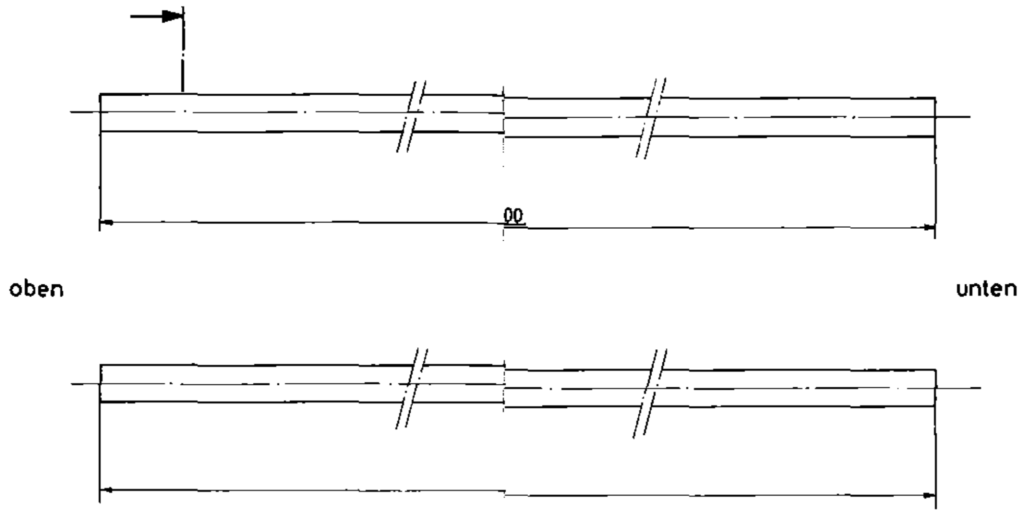

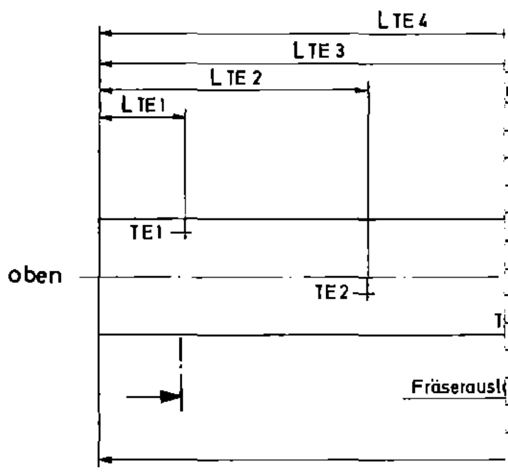

mulator Typ	L TE 1	L TE 2	L TE 3	L TE 4	Blockade	Heizleiter Typ
a	2430	2975	3520	4065	——	
a	2430	2975	3520	4065	R2.39-2-23	a
b	250	795	1340	1885	——	
b	250	795	1340	1885	R2.39-2-23	b
f	2330	2430	2530	2630	——	
f	2330	2430	2530	2630	R2.39-2-24	
g	1830	1930	2030	2130	——	
g	1830	[1930]	[2030]	[2130]	R2.39-2-24	
j	1430	1530	1630	1730	——	
k	305	405	505	605	——	
l	2130	2180	2230	2280	——	l
l	[2130]	2180	2230	2280	R2.39-2-23	l

[ ] nicht fräsen, nur anreißen

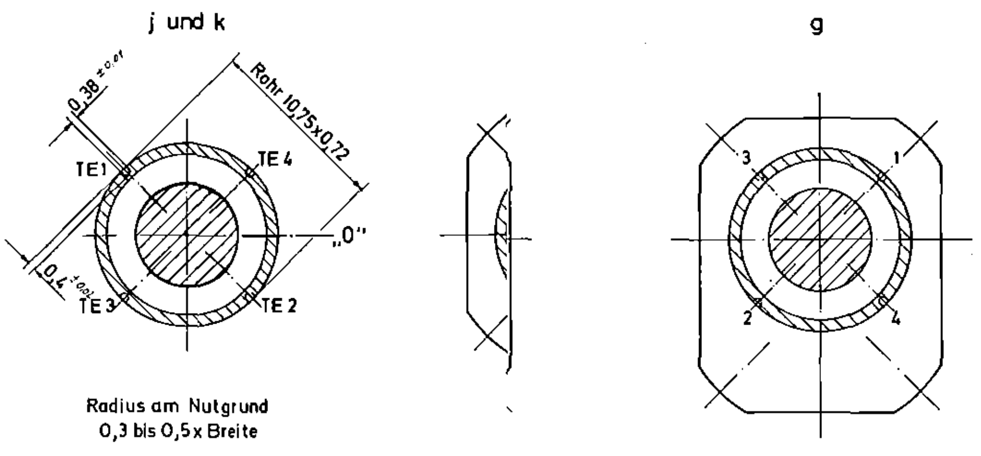

Radius am Nutgrund
0,3 bis 0,5 x Breite

Kernforschungszentrum Karlsruhe GmbH

Maßstab 1 : 1 | Gewicht | Werkstoff

1984 | Tag | Name
Bearb. 8. 8. Schneider
Gepr.
Gen.
P.

Benennung: Blockaden und TE Anordnung

Vorhaben: PNS 4260

Zeichnungs-Nr.: R 2.39 - 1 - 31

Blatt 01

Zust. | Änderung | Datum | Name | Urspr. | Ersatz für: | Ersetzt durch:

Figure 17. Working drawin

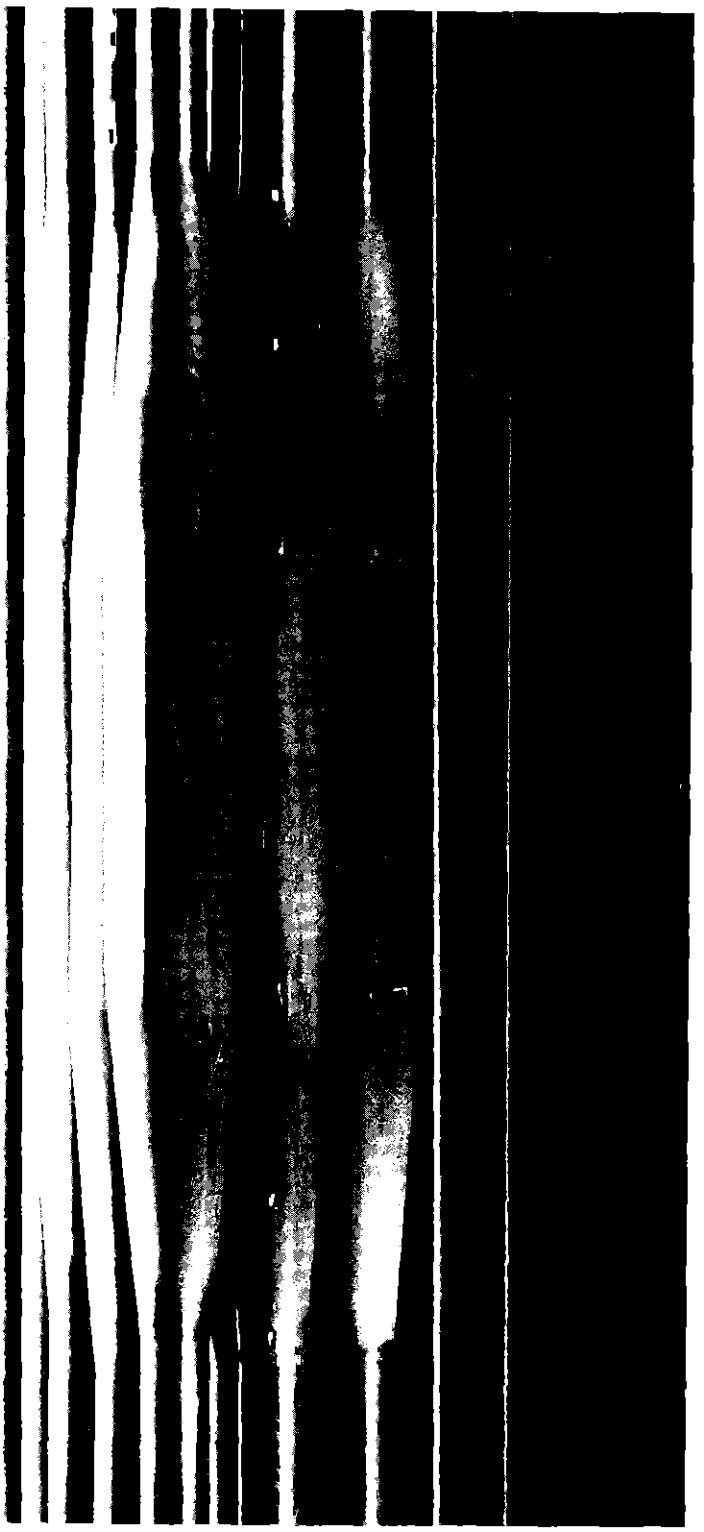

Figure 18. Photograph of the SEFLEX 90 percent blockage after the tests.

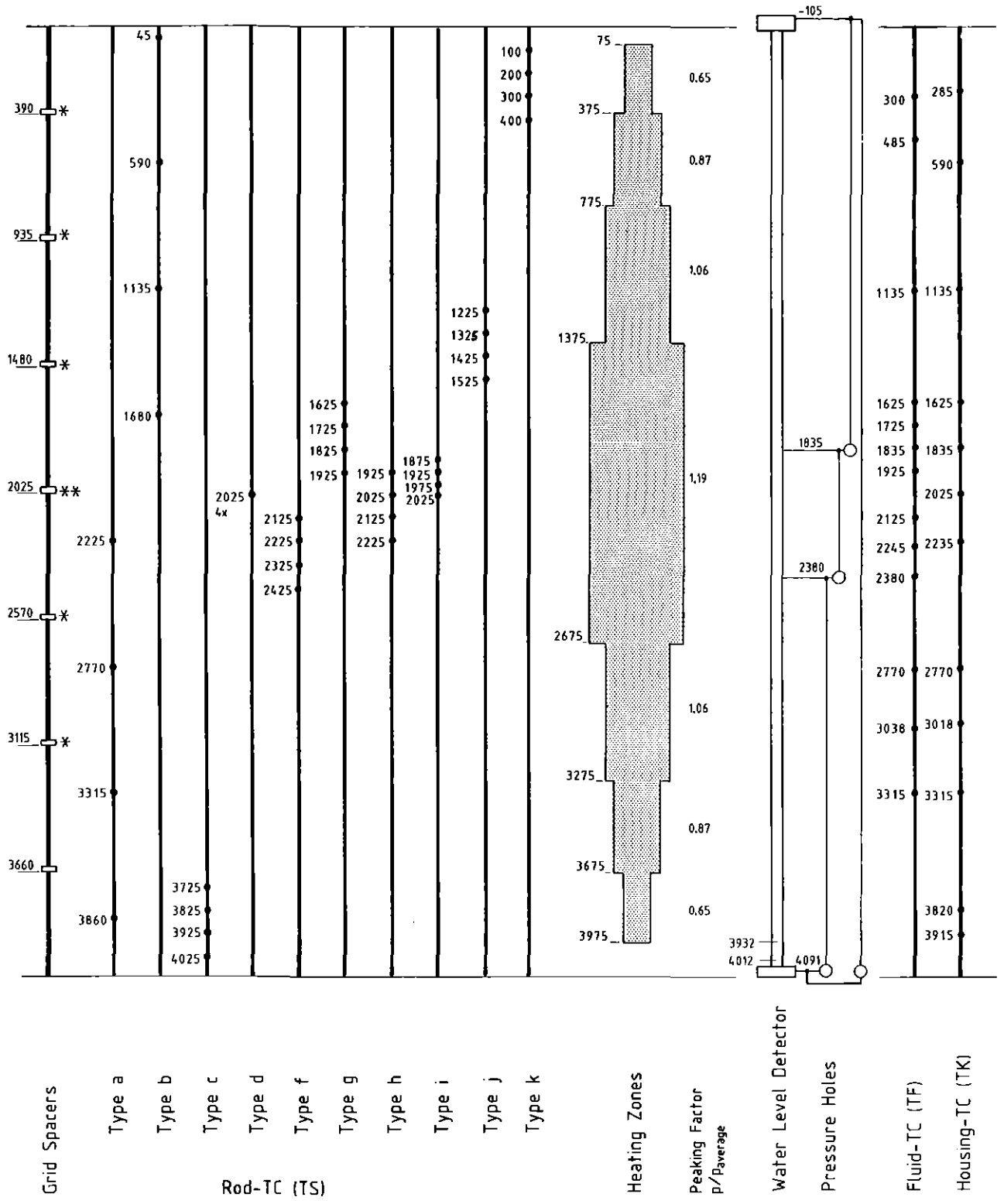

* Grid spacer instrumented

** Location of 90% blockage in series 3 and 4

Figure 19. Schematic diagram of SEFLEX instrumentation for unblocked and blocked rod bundle tests.

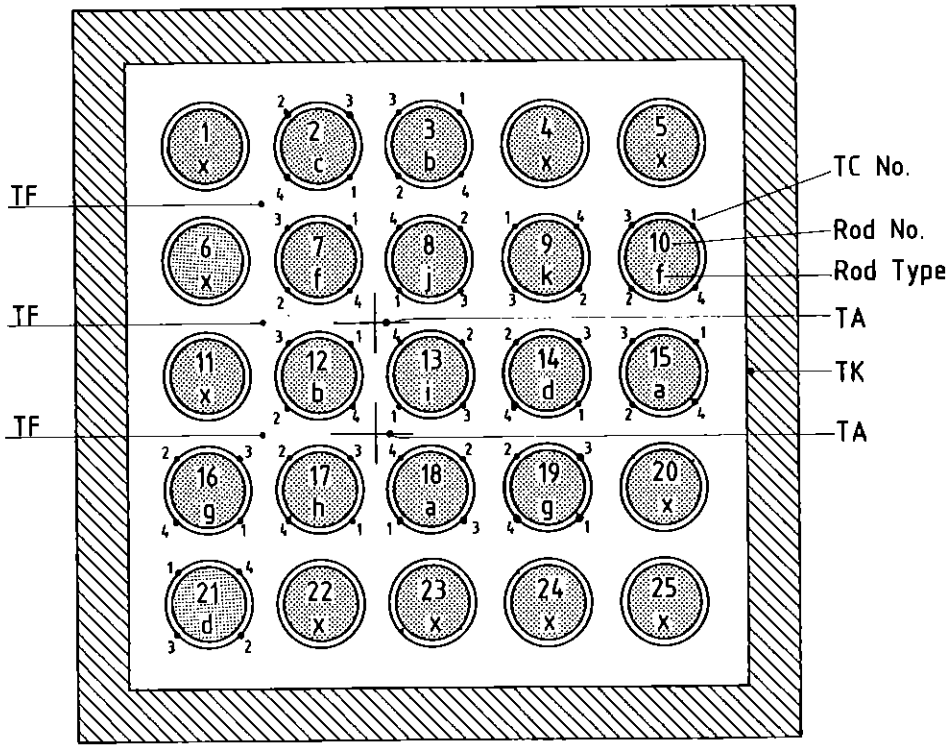

Rod Type	TC No.	Axial Level mm
a	1	2225
	2	2770
	3	3315
	4	3860
b	1	45
	2	590
	3	1135
	4	1680
c	1	3725
	2	3825
	3	3925
	4	4025
d	1	2025
	2	2025
	3	2025
	4	2025

Rod Type	TC No.	Axial Level mm
f	1	2125
	2	2225
	3	2325
	4	2425
g	1	1625
	2	1725
	3	1825
	4	1925
h	1	1925
	2	2025
	3	2125
	4	2225
i	1	1875
	2	1925
	3	1975
	4	2025

Rod Type	TC No.	Axial Level mm
j	1	1225
	2	1325
	3	1425
	4	1525
k	1	100
	2	200
	3	300
	4	400
x	without TC's	

Figure 20. Radial and axial positions of cladding, grid spacer, fluid, and housing TC's for unblocked rod bundle tests.

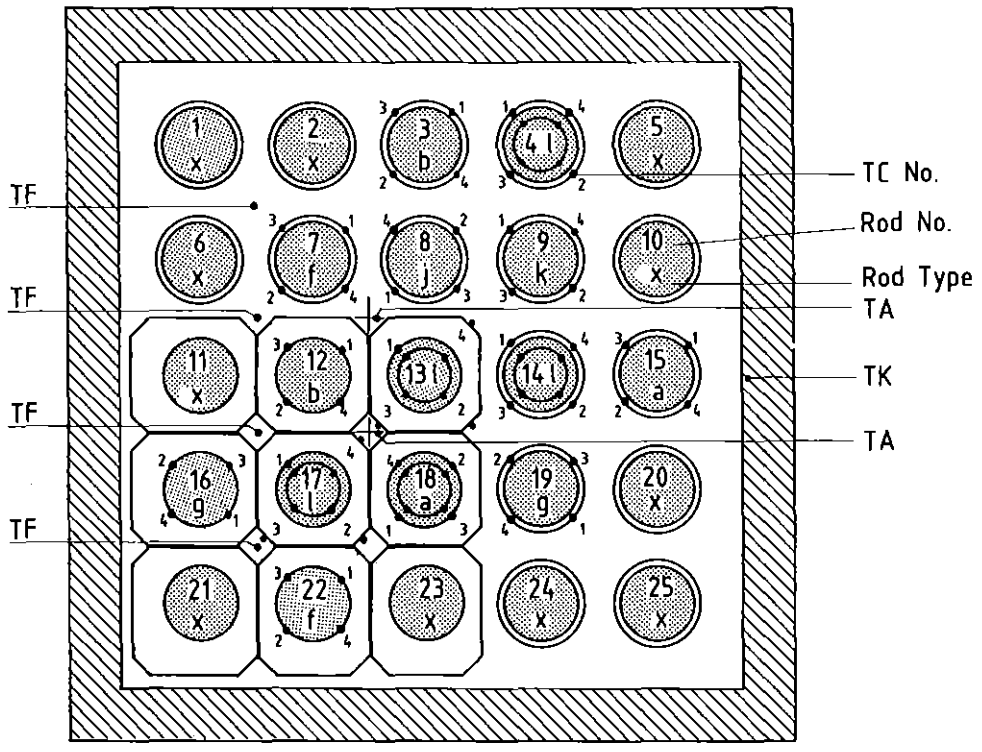

Rod Type	TC No.	Axial Level mm
a	1	2225
	2	2770
	3	3315
	4	3860
b	1	45
	2	590
	3	1135
	4	1680
f	1	2125
	2	2225
	3	2325
	4	2425

Rod Type	TC No.	Axial Level mm
g	1	1625
	2	1725
	3	1825
	4	1925
j	1	1225
	2	1325
	3	1425
	4	1525
k	1	100
	2	200
	3	300
	4	400

Rod Type	TC No.	Axial Level mm
l	1	1925
	2	1975
	3	2025
	4	2075
x	without TC's	

Figure 21. Radial and axial positions of cladding, heater sheath, grid spacer, fluid, and housing TC's for blocked rod bundle tests.

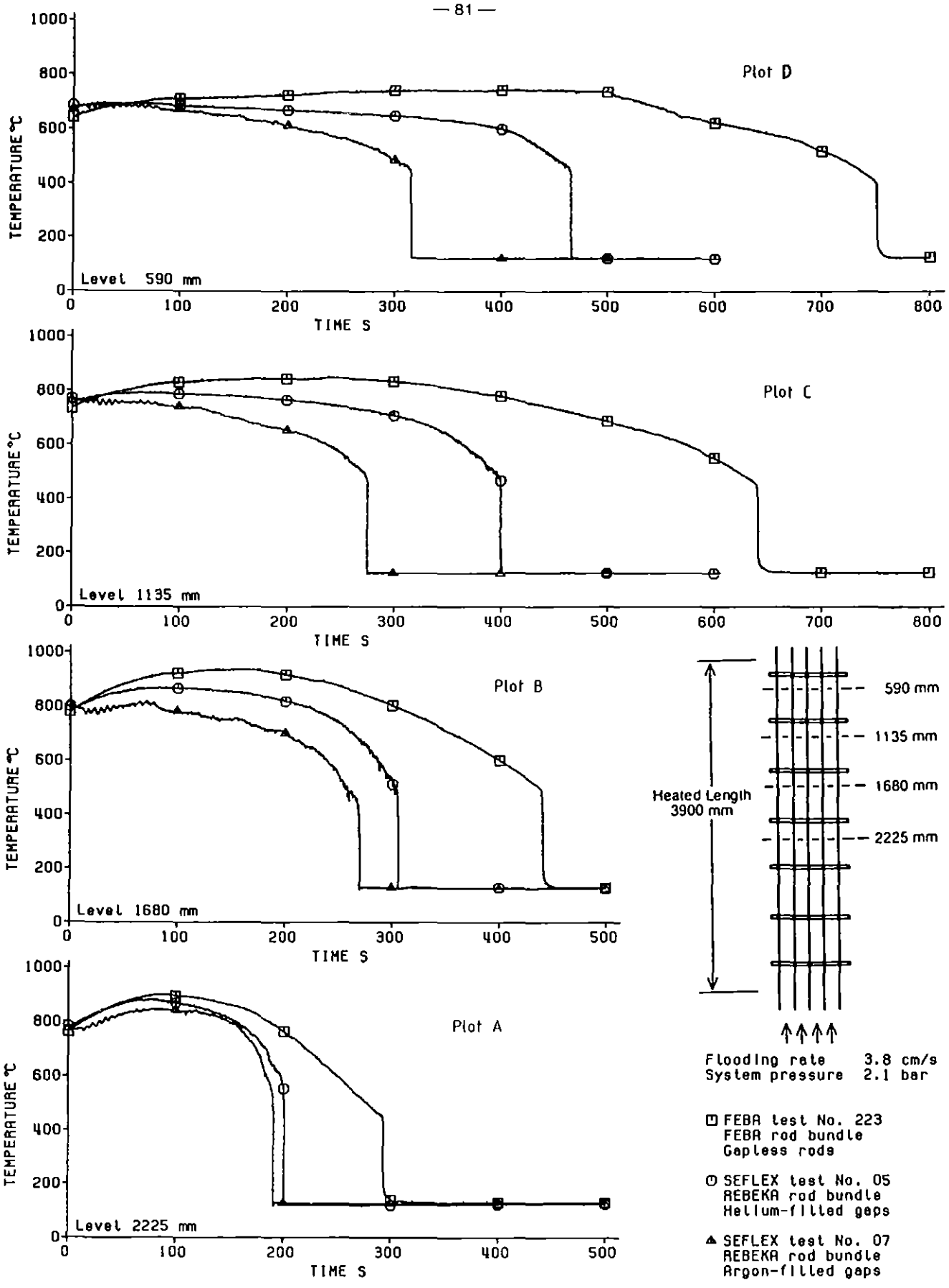

Figure 22. Cladding temperatures measured at four different axial levels in FEBA and REBEKA rod bundles.

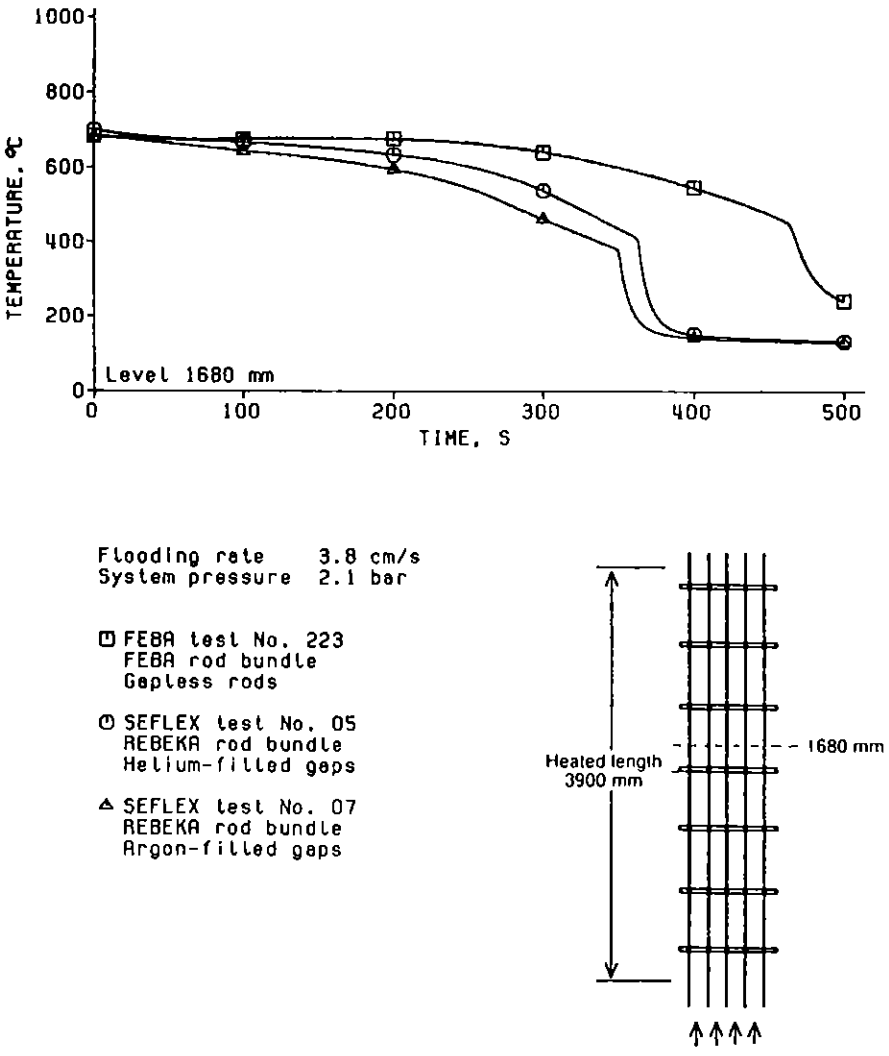

Figure 23. Housing temperatures in FEBA and REBEKA rod bundles.

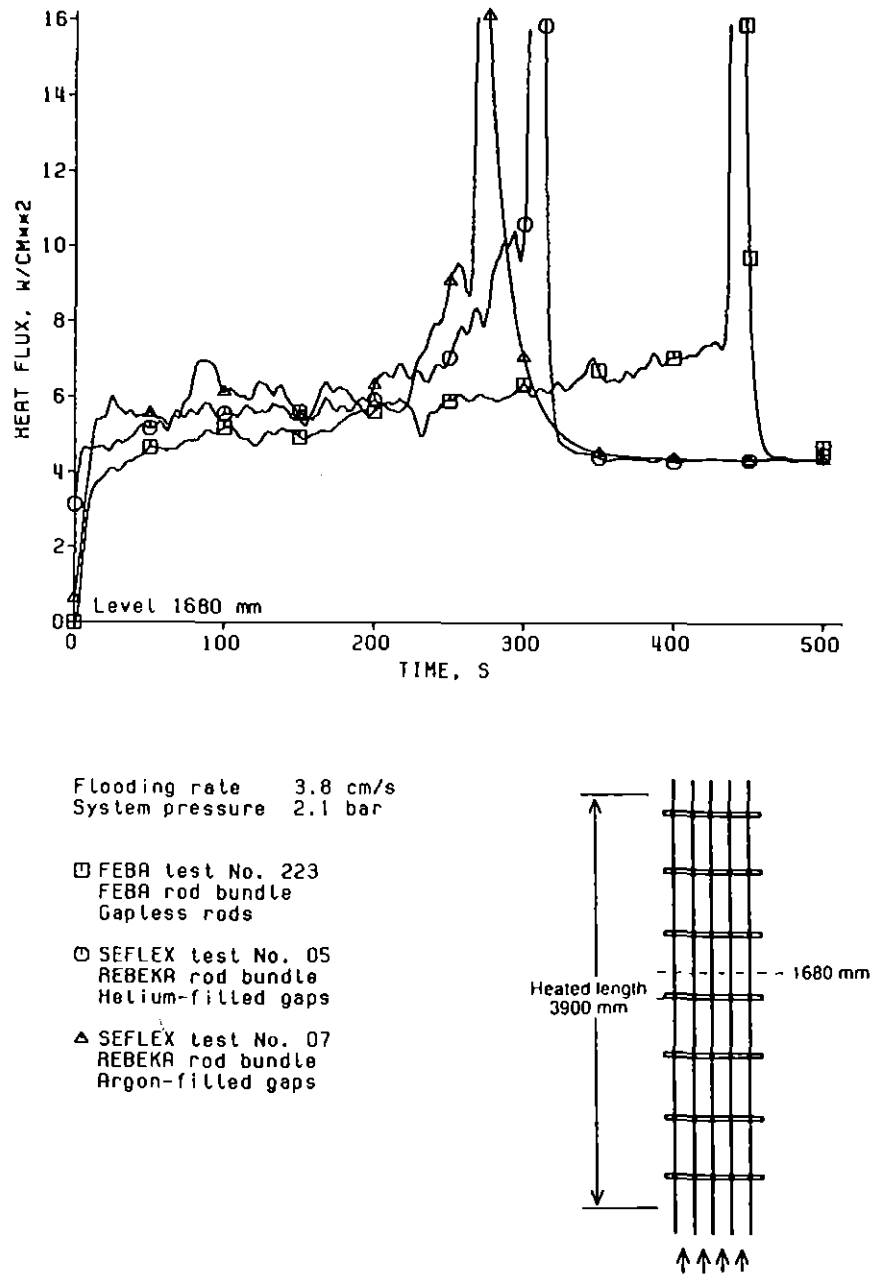

Figure 24. Surface heat fluxes of FEBA and REBEKA rods.

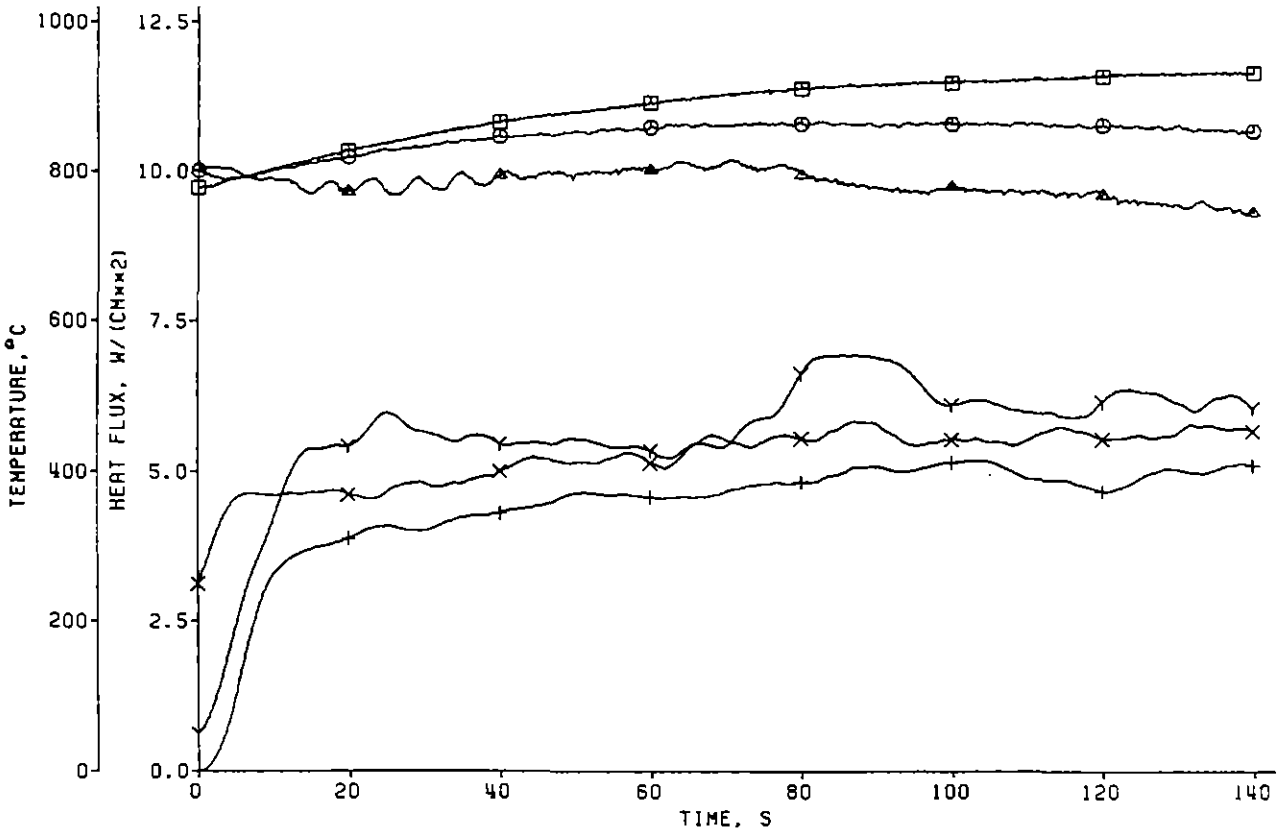

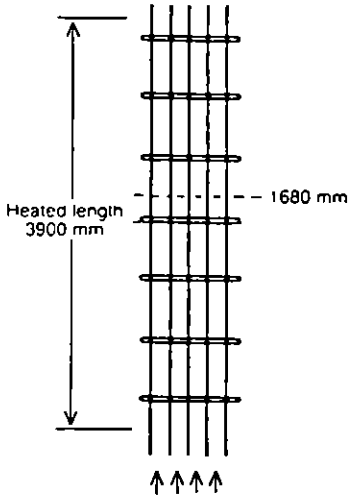

Flooding rate 3.8 cm/s
System pressure 2.1 bar

Axial level 1680 mm
TC 12.b.4

FEBA test No. 223	SEFLEX test No. 05	SEFLEX test No. 07
FEBA rod bundle	REBEKA rod bundle	REBEKA rod bundle
Gapless rods	Helium-filled gaps	Argon-filled gaps
□ Cladding temperature	⊙ Cladding temperature	△ Cladding temperature
+ Surface heat flux	X Surface heat flux	Y Surface heat flux

Figure 25. Cladding temperatures and surface heat fluxes of FEBA and REBEKA rods during the early portion of reflooding.

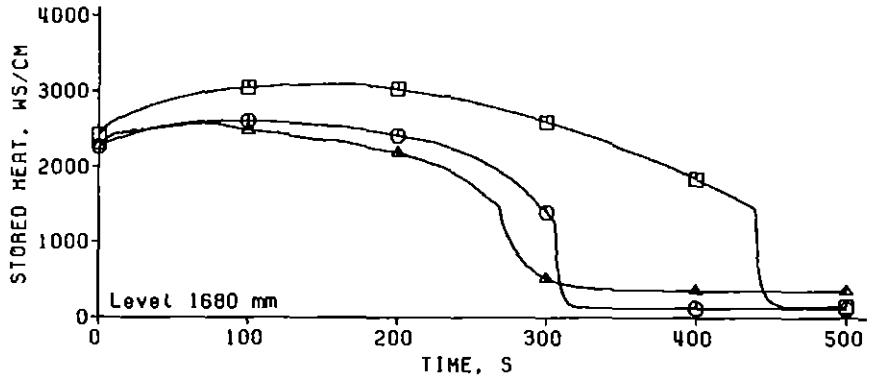

Flooding rate 3.8 cm/s
System pressure 2.1 bar

□ FEBA test No. 223
FEBA rod bundle
Gapless rods

○ SEFLEX test No. 05
REBEKA rod bundle
Helium-filled gaps

△ SEFLEX test No. 07
REBEKA rod bundle
Argon-filled gaps

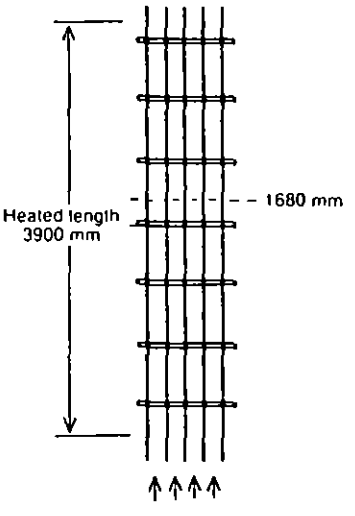

Figure 26. Release of stored heat from FEBA and REBEKA rods.

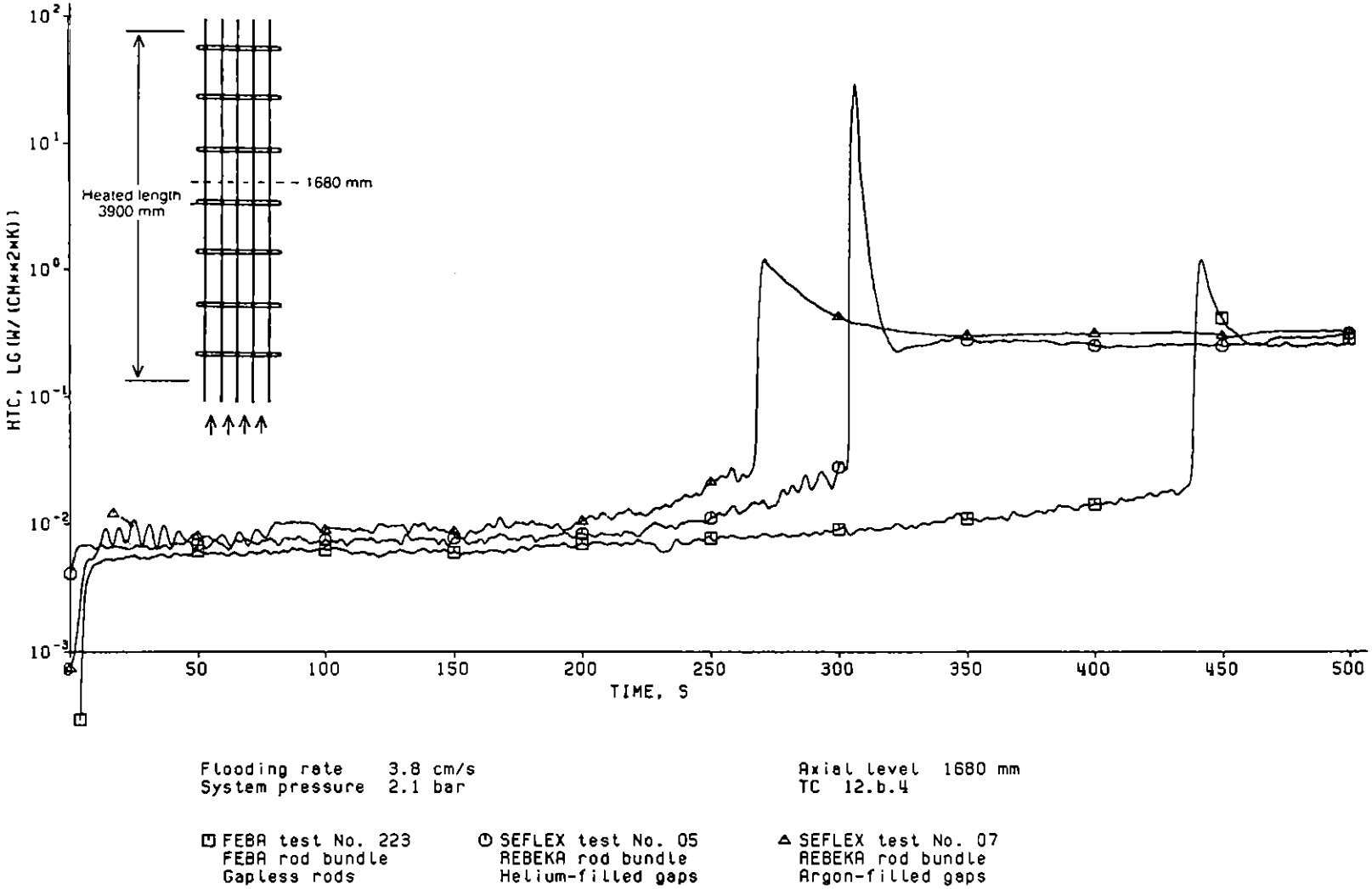

Figure 27. Heat transfer from FEBA and REBEKA rods (related to coolant saturation temperature).

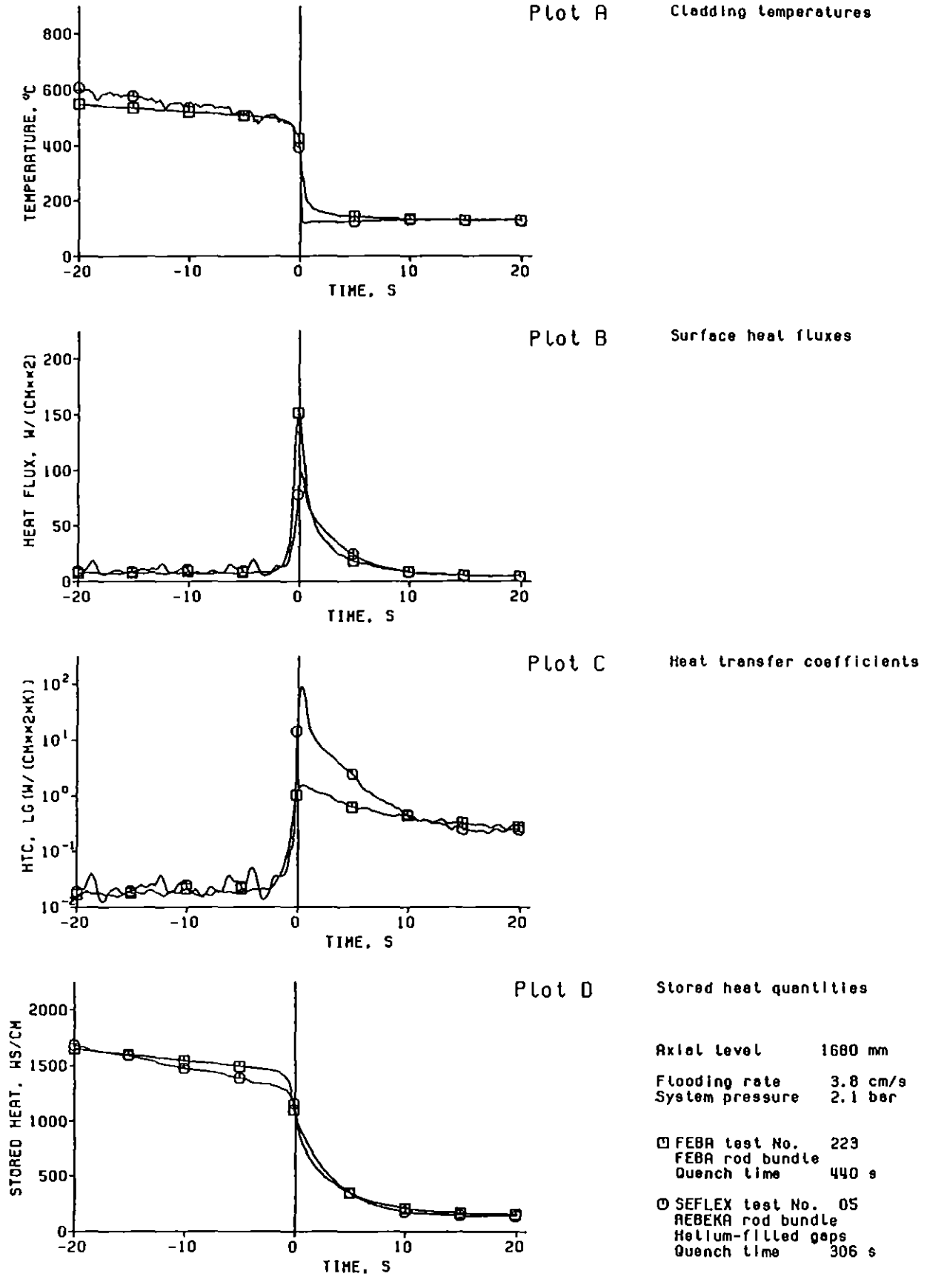

Figure 28. Cladding temperatures, surface heat fluxes, heat transfer, and heat release during quenching of FEBA and REBEKA rods (FEBA test No. 223, SEFLEX test No. 05).

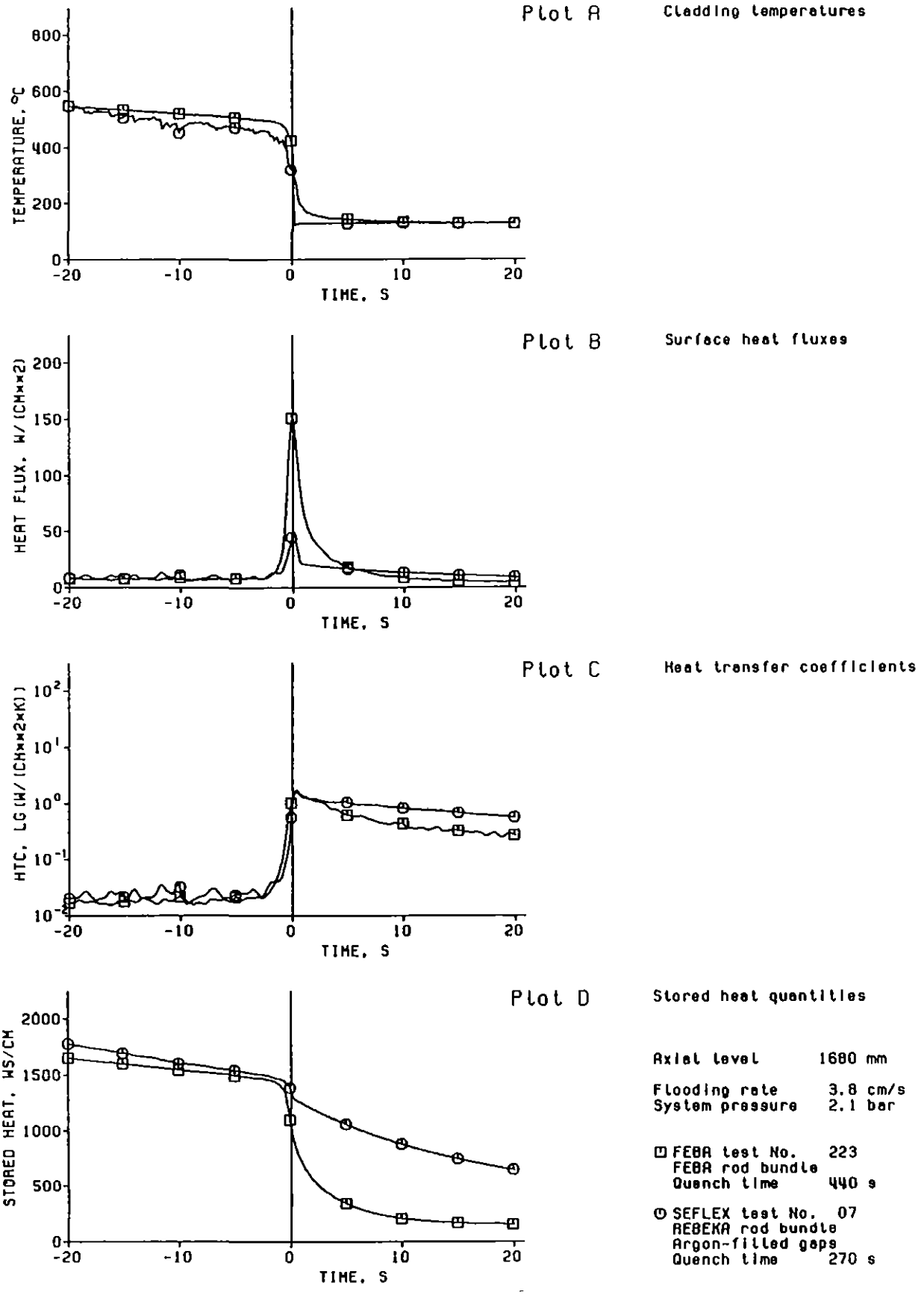

Figure 29. Cladding temperatures, surface heat fluxes, heat transfer, and heat release during quenching of FEBA and REBEKA rods (FEBA test No. 223, SEFLEX test No. 07).

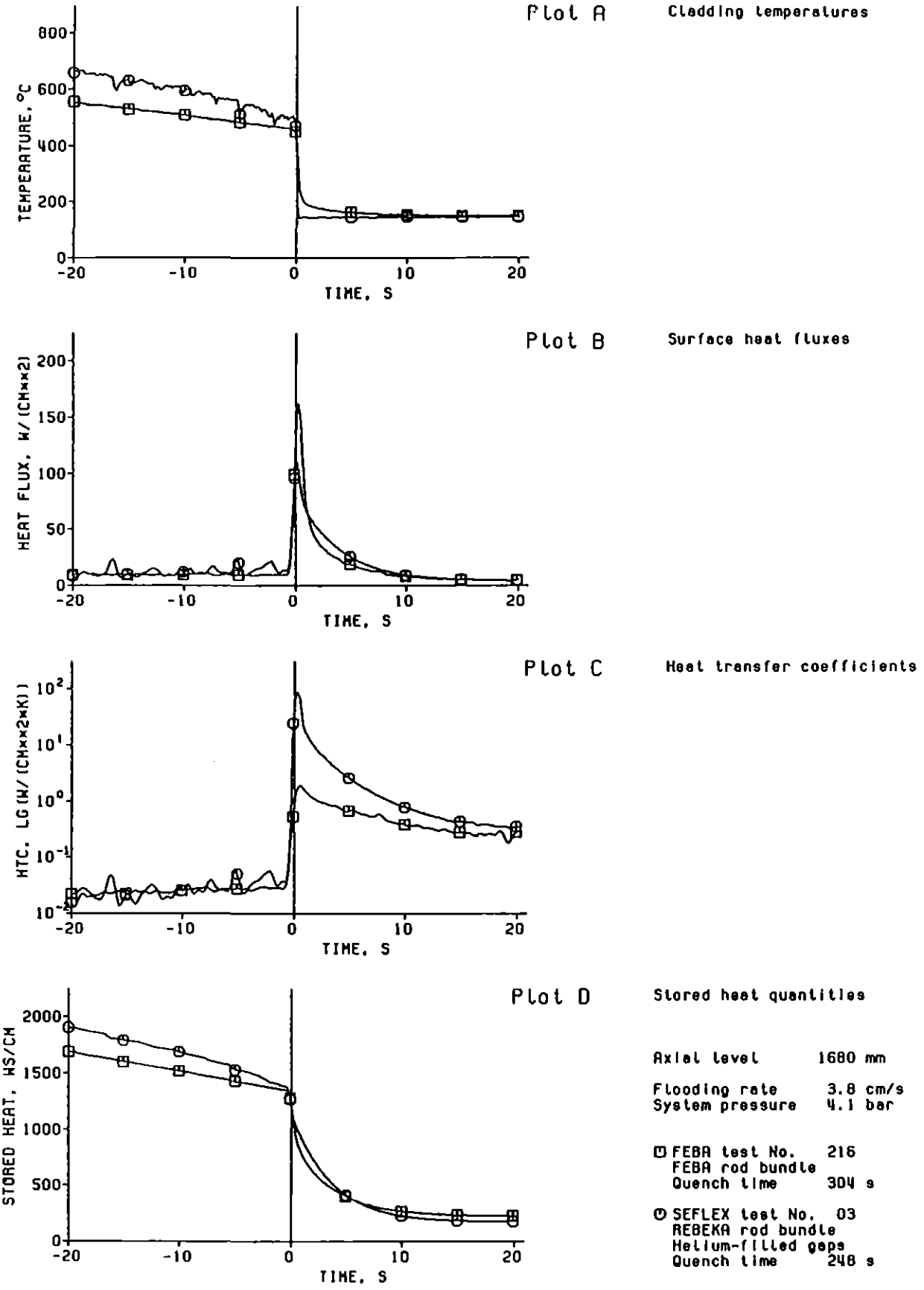

Figure 30. Cladding temperatures, surface heat fluxes, heat transfer, and heat release during quenching of FEBA and REBEKA rods (FEBA test No. 216, SEFLEX test No. 03).

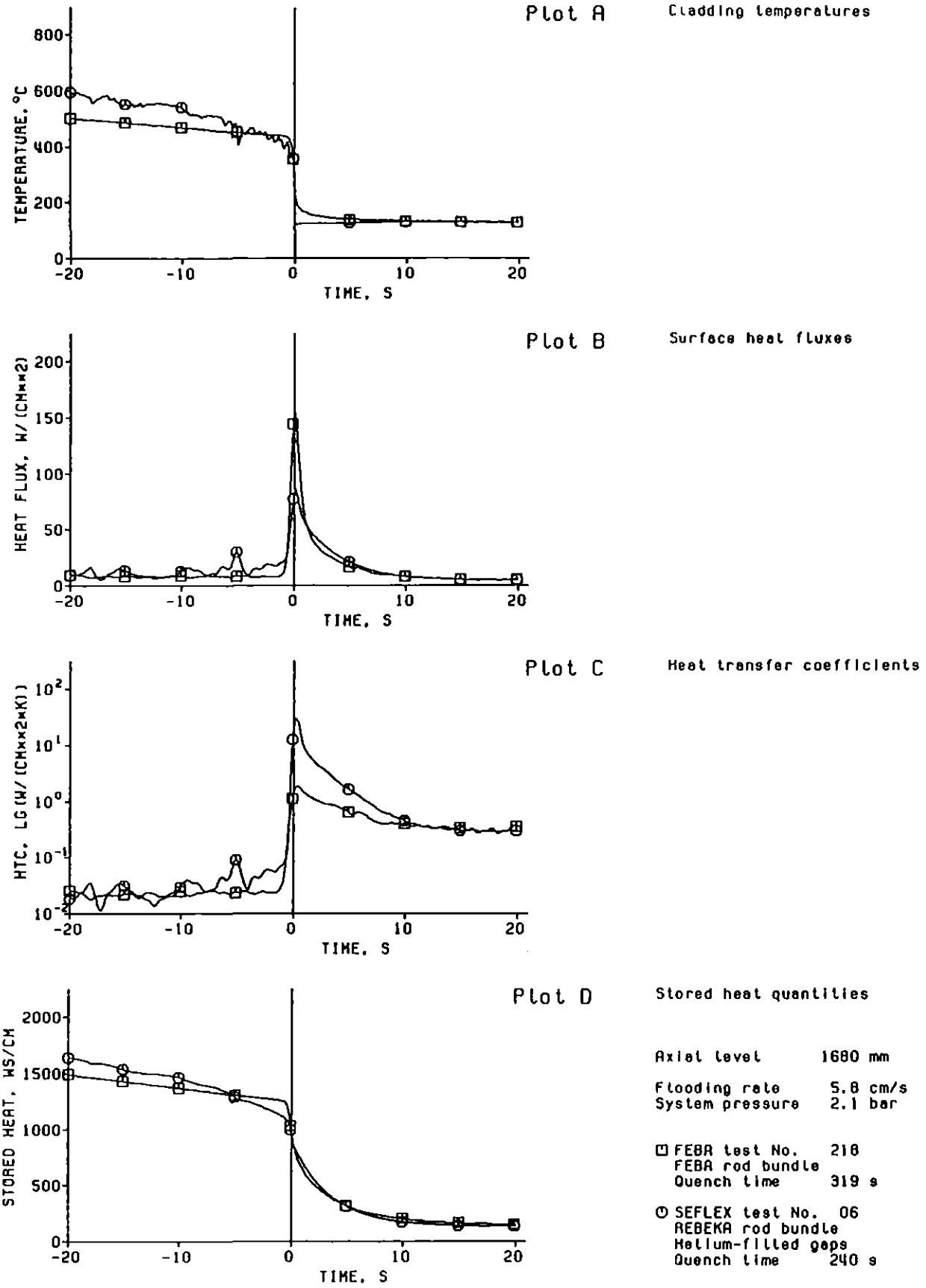

Figure 31. Cladding temperatures, surface heat fluxes, heat transfer, and heat release during quenching of FEBA and REBEKA rods (FEBA test No. 218, SEFLEX test No. 06).

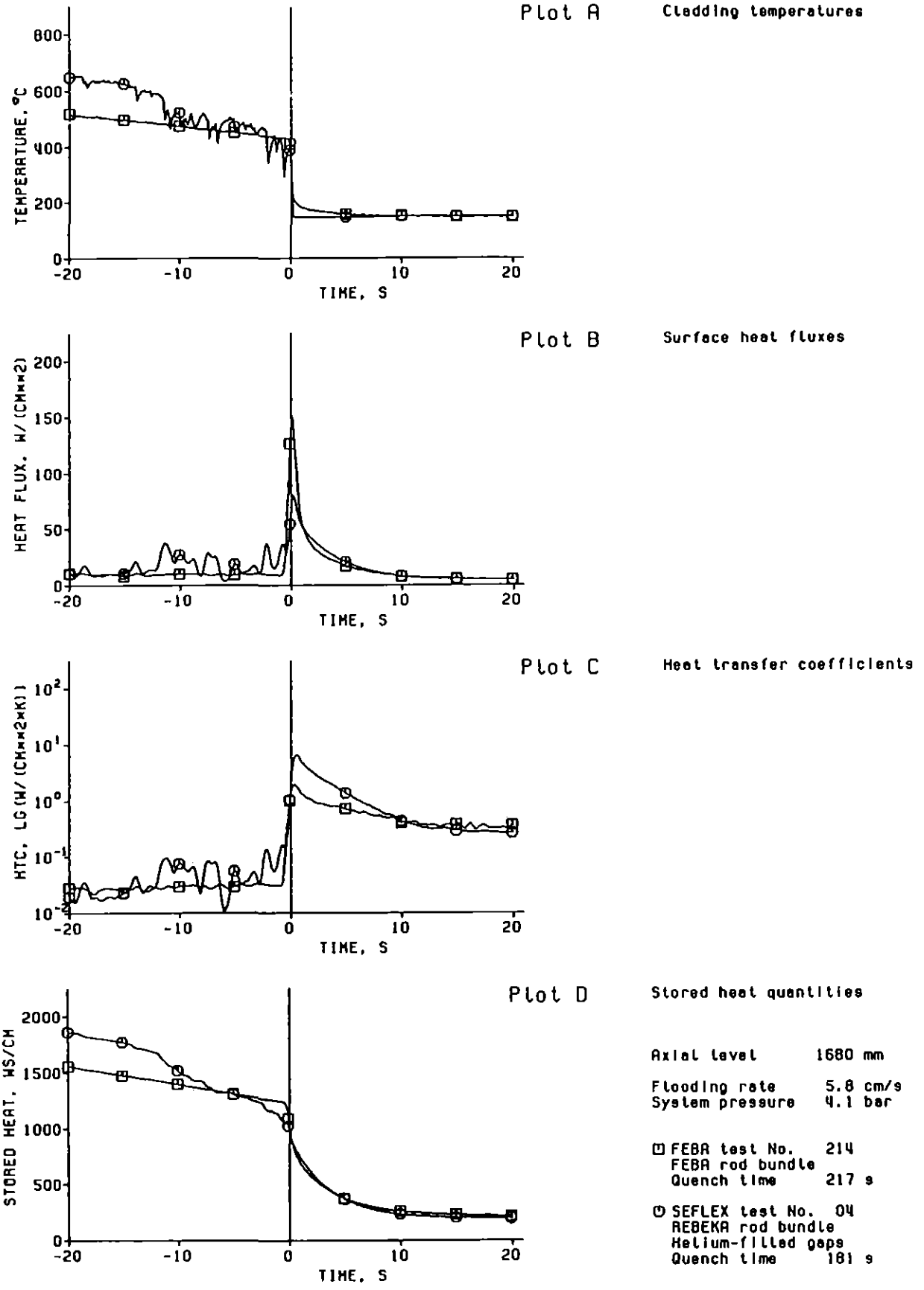

Figure 32. Cladding temperatures, surface heat fluxes, heat transfer, and heat release during quenching of FEBA and REBEKA rods (FEBA test No. 214, SEFLEX test No. 04).

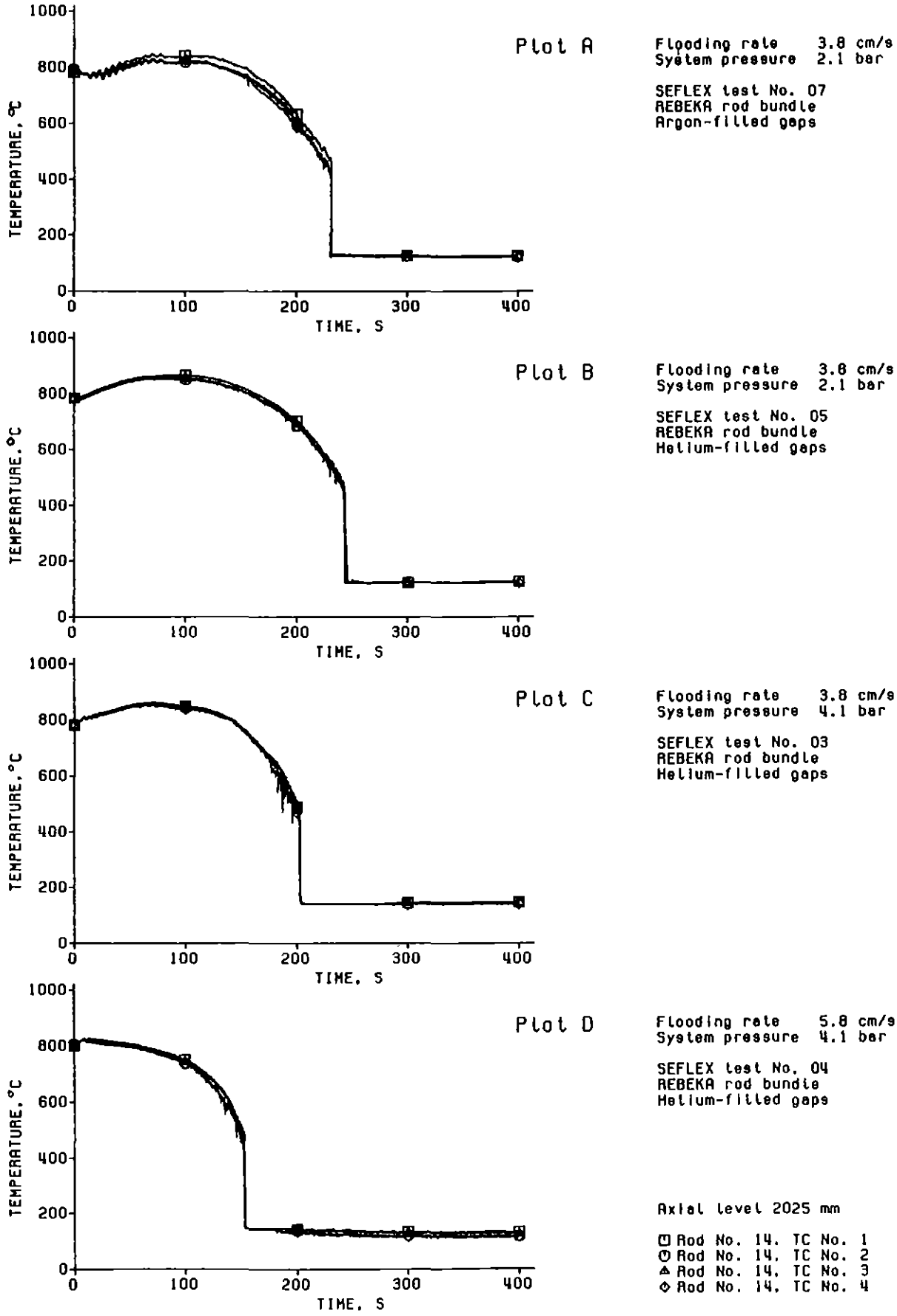

Figure 33. Azimuthal cladding temperatures of a REBEKA rod measured at the bundle midplane.

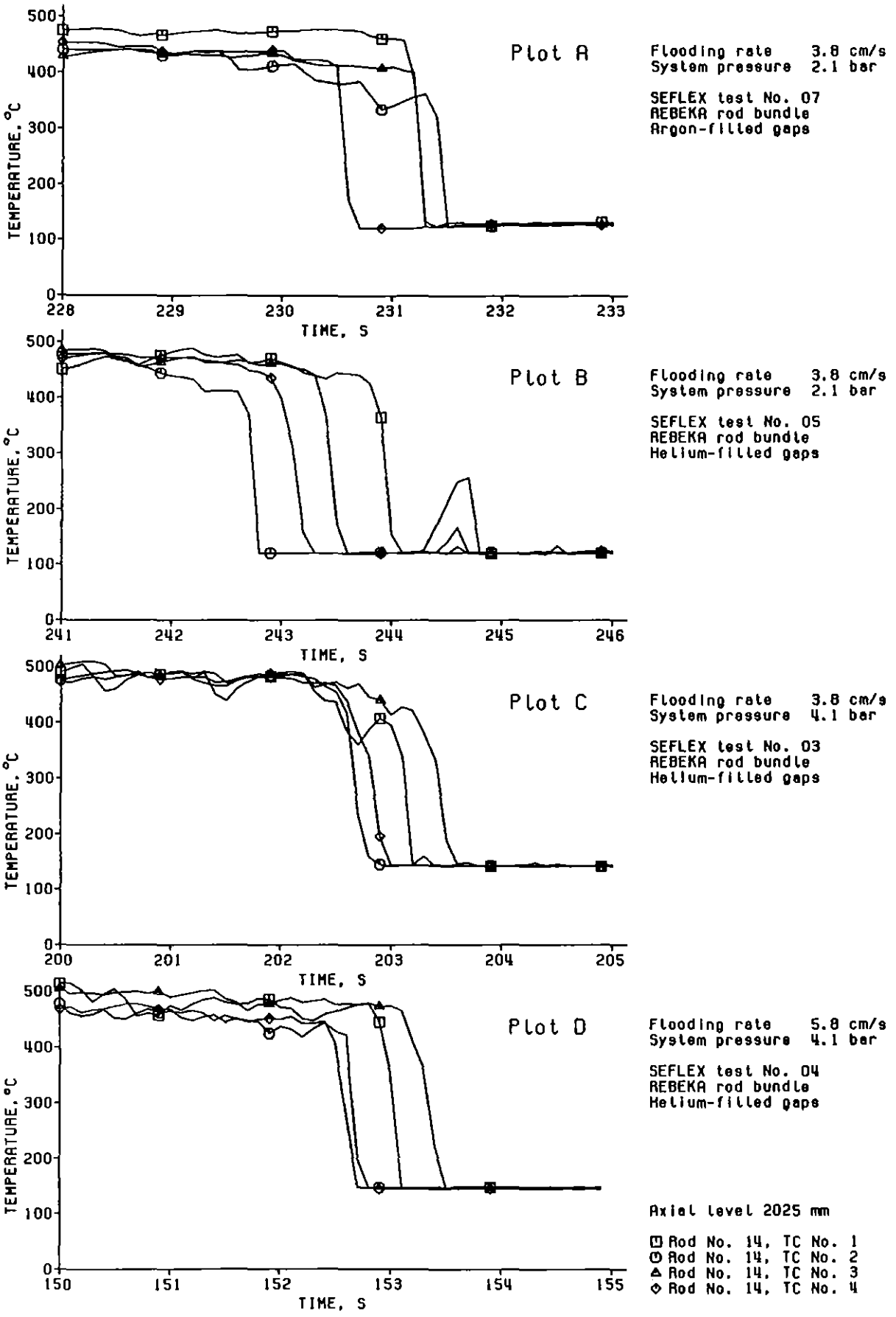

Figure 34. Azimuthal cladding temperatures of a REBEKA rod during quenching measured at the bundle midplane.

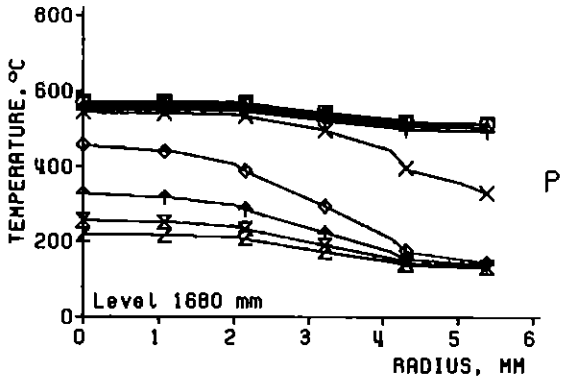

Plot A

Flooding rate 3.8 cm/s
System pressure 2.1 bar

FEBA test No. 223
FEBA rod bundle
Gapless rods

Quench time 440 s

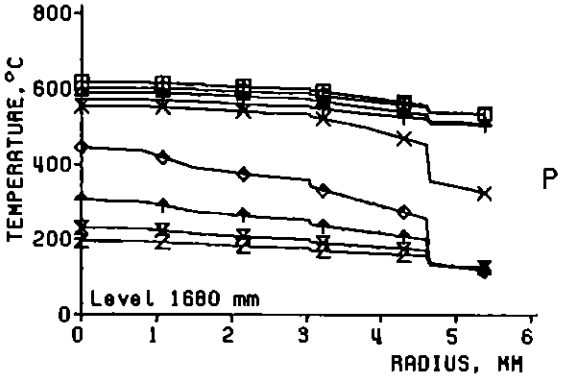

Plot B

Flooding rate 3.8 cm/s
System pressure 2.1 bar

SEFLEX test No. 05
REBEKA rod bundle
Helium-filled gaps

Quench time 306 s

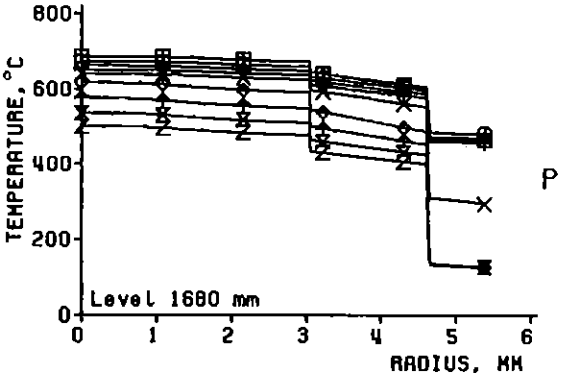

Plot C

Flooding rate 3.8 cm/s
System pressure 2.1 bar

SEFLEX test No. 07
REBEKA rod bundle
Argon-filled gaps

Quench time 270 s

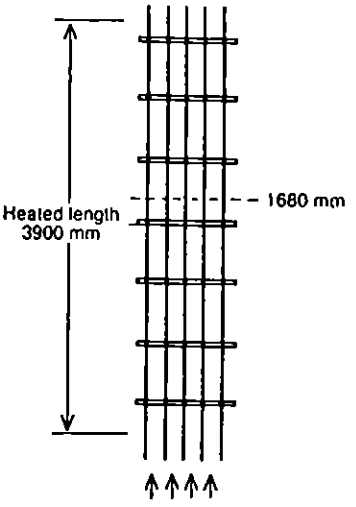

Shifted time scale

□ -10.0 s
○ -7.5 s
△ -5.0 s
\+ -2.5 s
× 0.0 s (surface rewetting)
◇ 2.5 s
↑ 5.0 s
⋈ 7.5 s
Z 10.0 s

Analysis:

One-dimensional inverse heat conduction problem

Finite-difference method

Explicit time integration

Temperature-dependent material properties

Figure 35. Radial temperature profiles as function of time during quenching of FEBA and REBEKA rods.

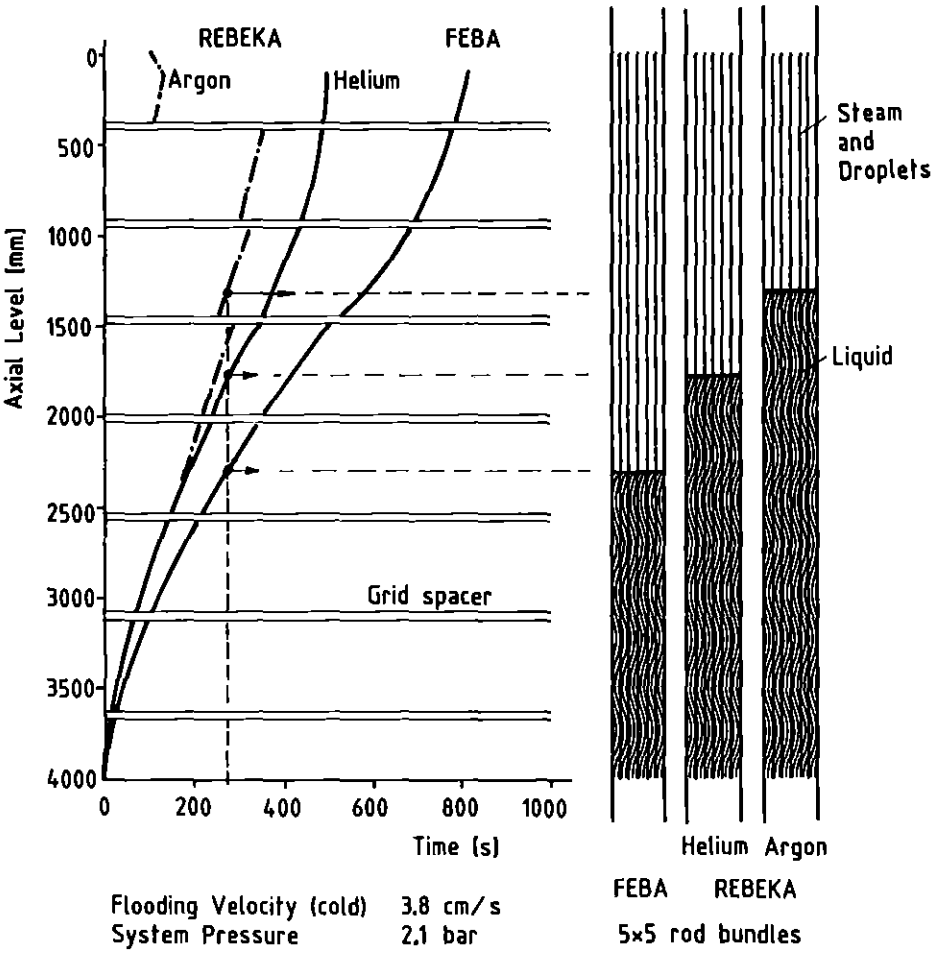

Figure 36. Quench front progression and liquid inventory after 275 seconds in FEBA and REBEKA rod bundles.

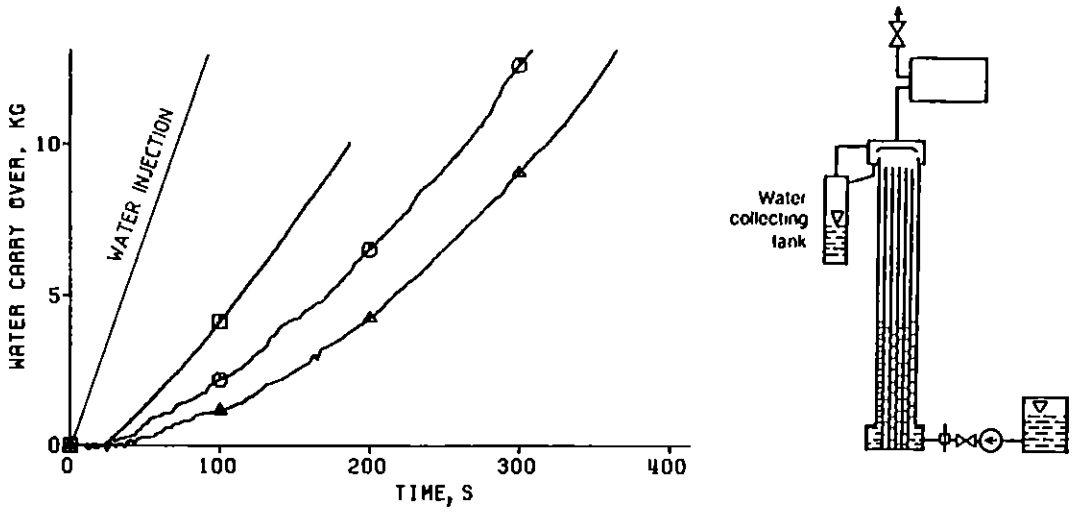

Flooding rate 3.8 cm/s
System pressure 2.1 bar

□ FEBA test No. 223
FEBA rod bundle
Gapless rods

○ SEFLEX test No. 05
REBEKA rod bundle
Helium-filled gaps

△ SEFLEX test No. 07
REBEKA rod bundle
Argon-filled gaps

Figure 37. Water carry over from FEBA and REBEKA rod bundles.

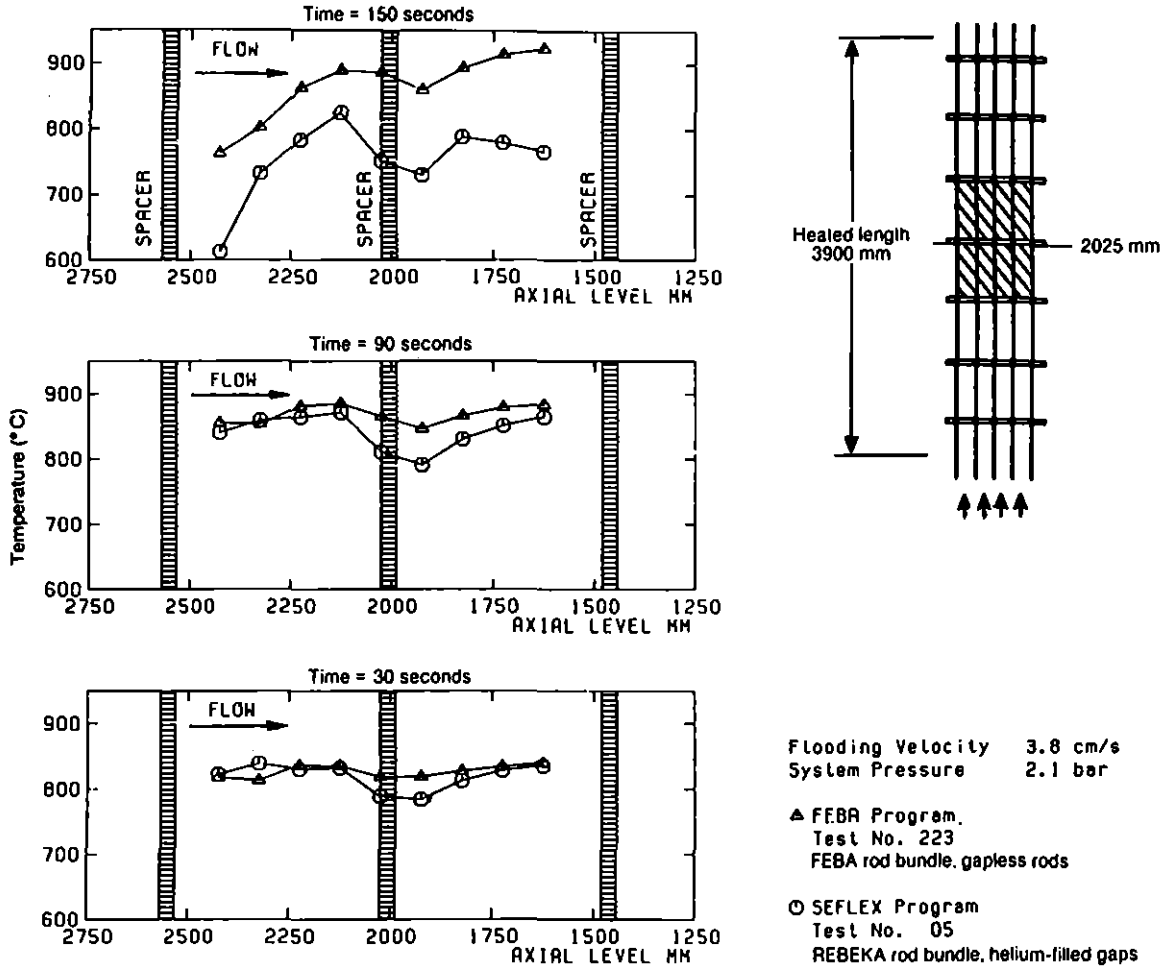

Figure 38. Influence of the grid spacer at the bundle midplane on the axial temperature profiles in FEBA and REBEKA rod bundles.

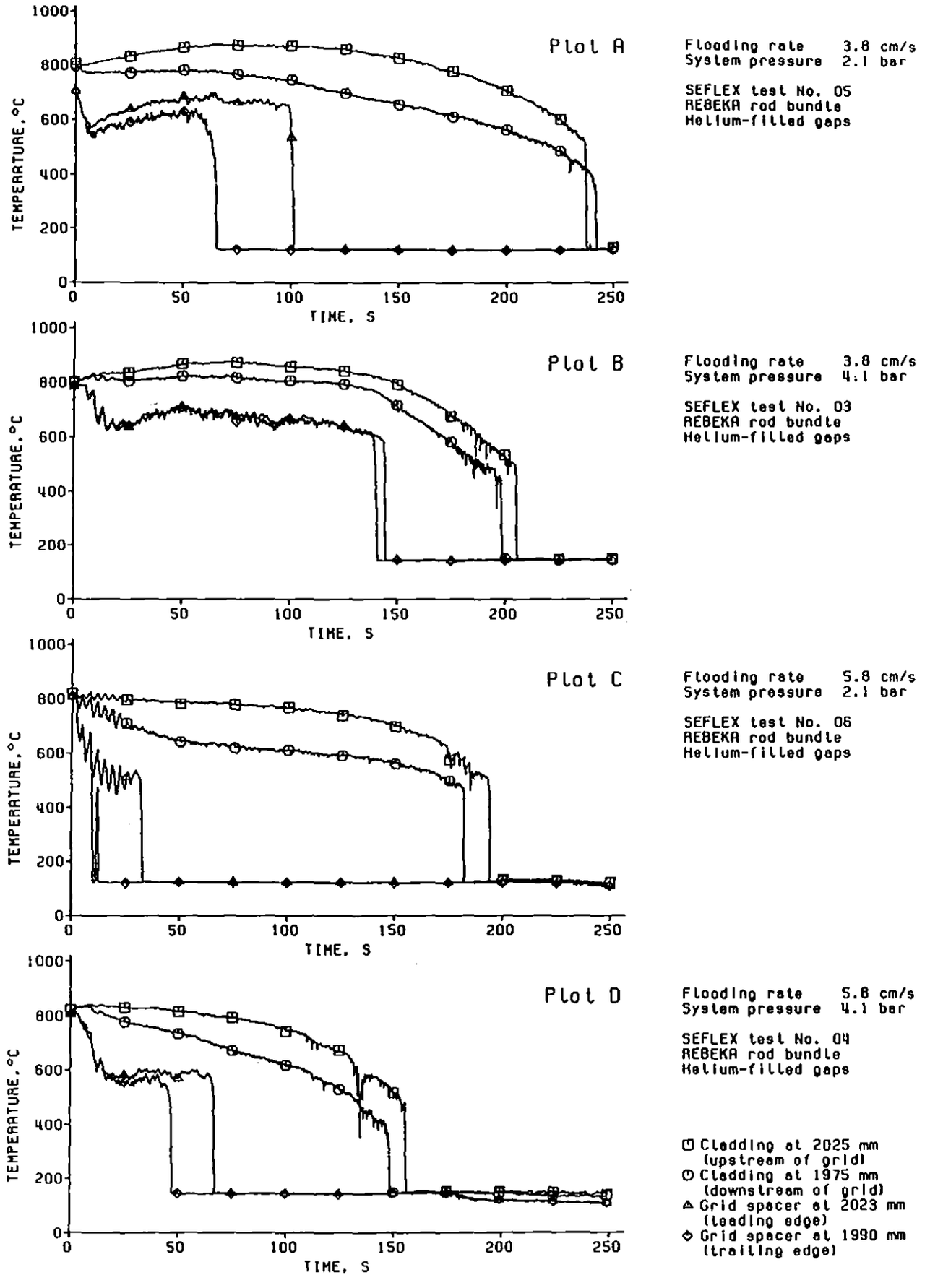

Figure 39. Influence of reflood conditions on cladding and grid spacer temperatures at the bundle midplane.

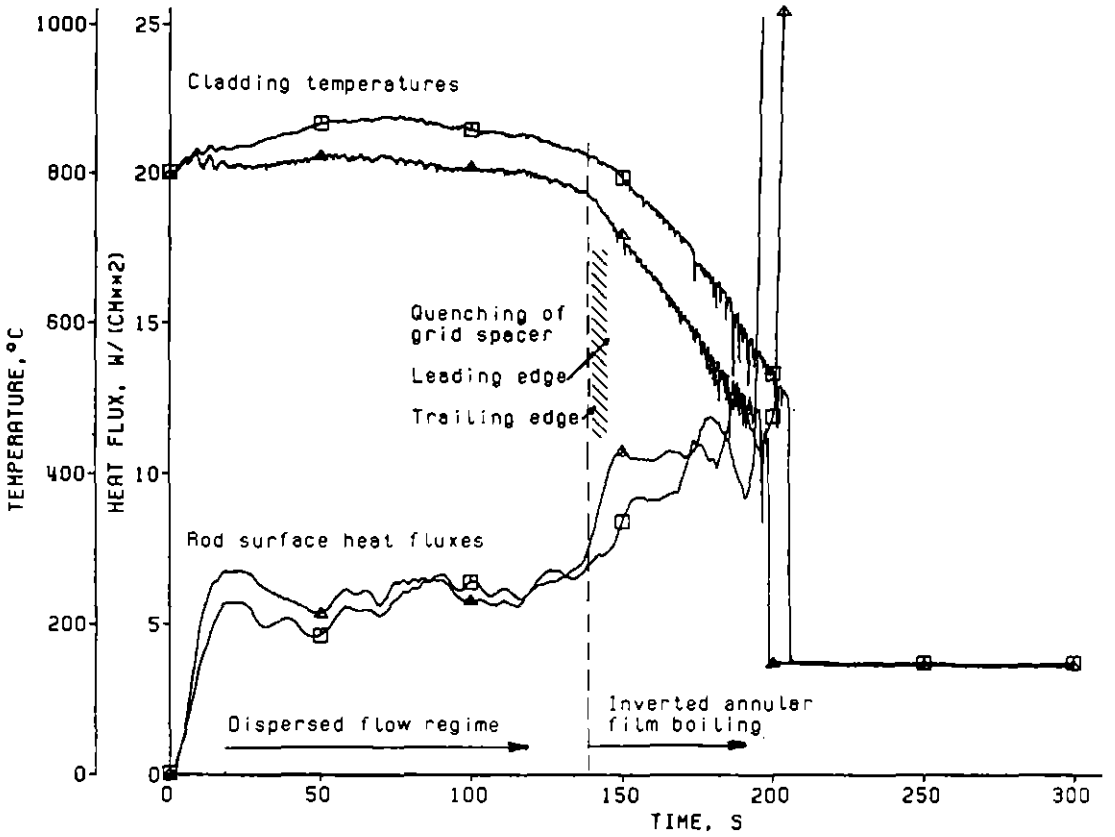

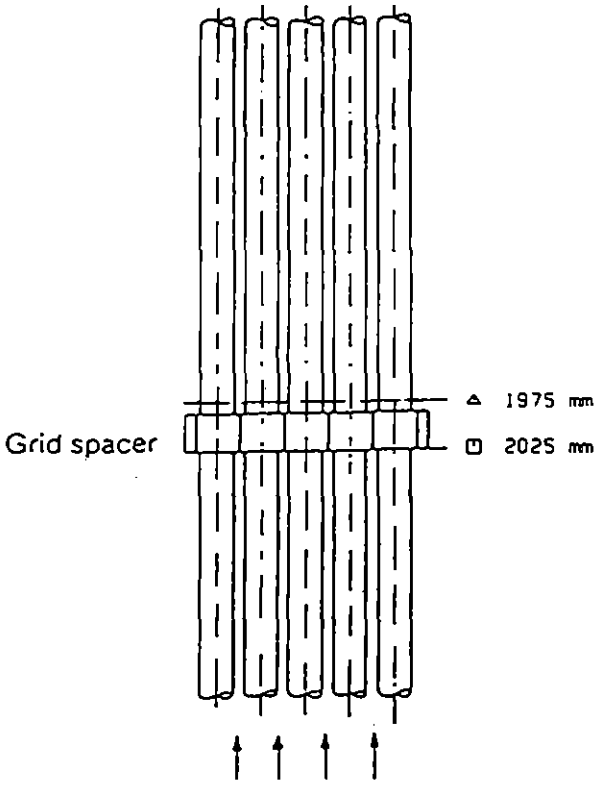

Flooding rate 3.8 cm/s
System pressure 4.1 bar

SEFLEX test No. 03
REBEKA rod bundle
Helium-filled gaps

Axial levels:
□ At leading edge of grid spacer (2025 mm)
△ 12 mm downstream of trailing edge of grid spacer (1975 mm)

Figure 40. Cladding temperatures and surface heat fluxes at leading edge and 12 mm downstream of bundle midplane grid spacer (test No. 03).

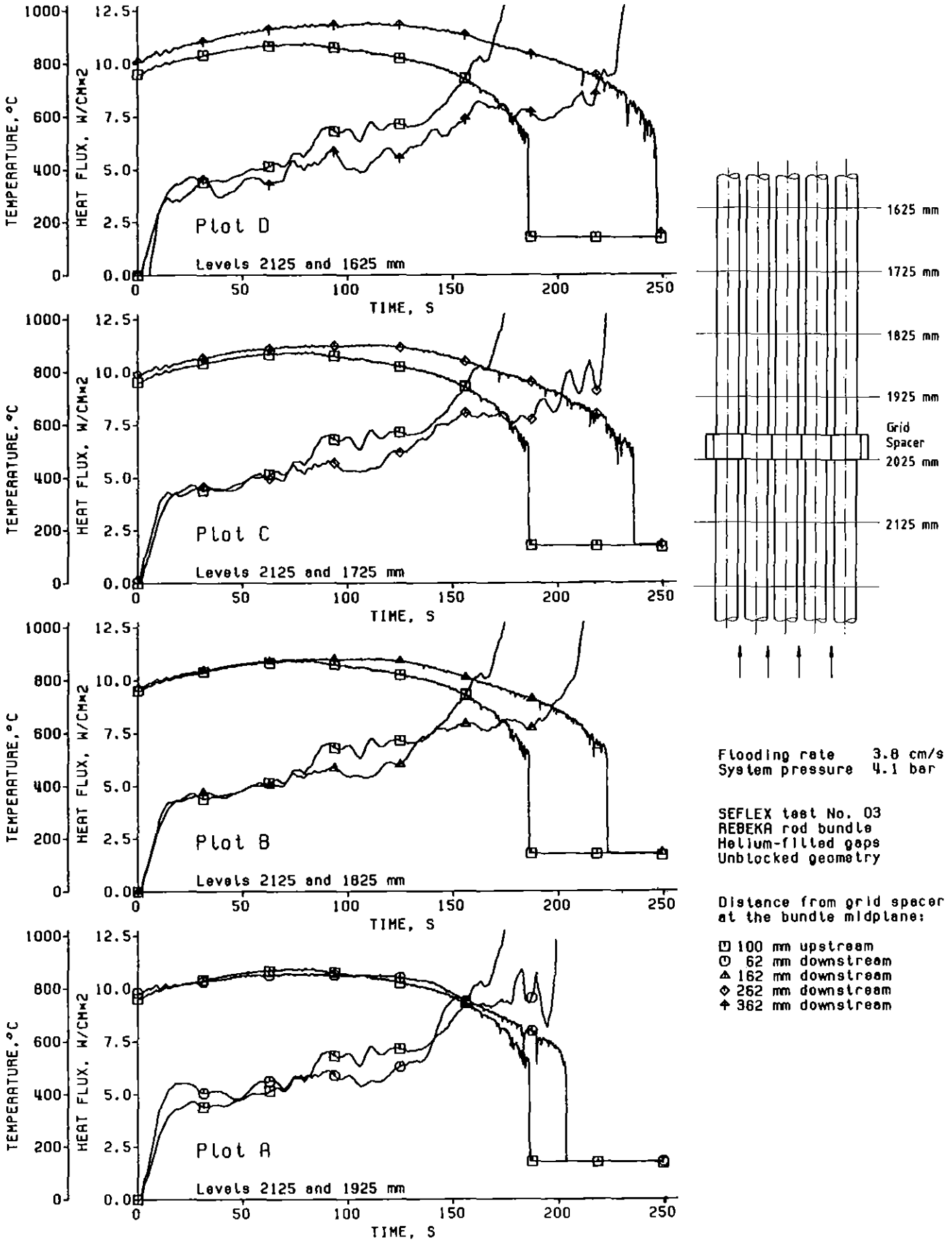

Figure 41. Cladding temperatures and surface heat fluxes upstream and downstream of bundle midplane grid spacer (test No. 03).

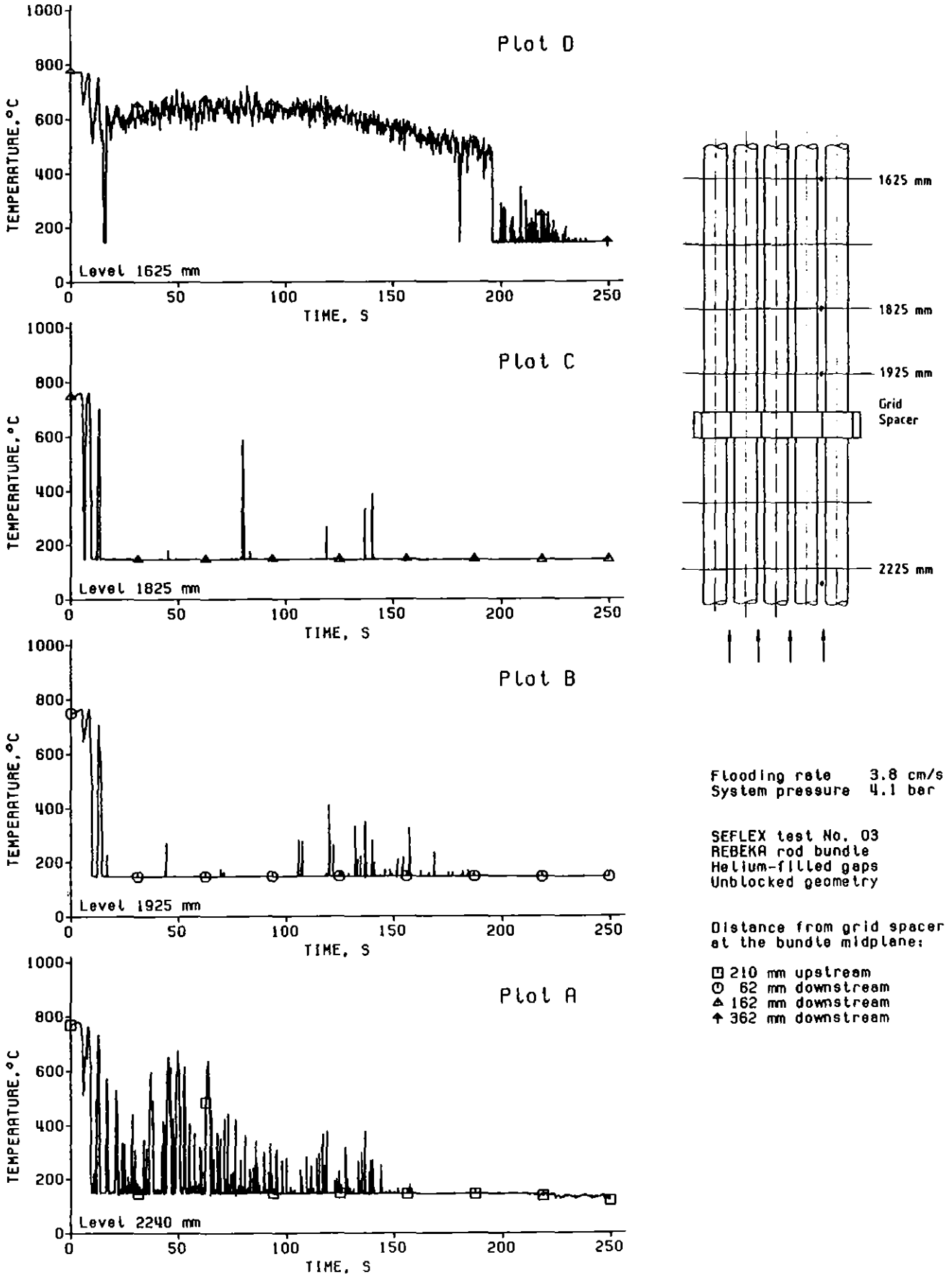

Figure 42. Fluid TC signals upstream and downstream of bundle midplane grid spacer (test No. 03).

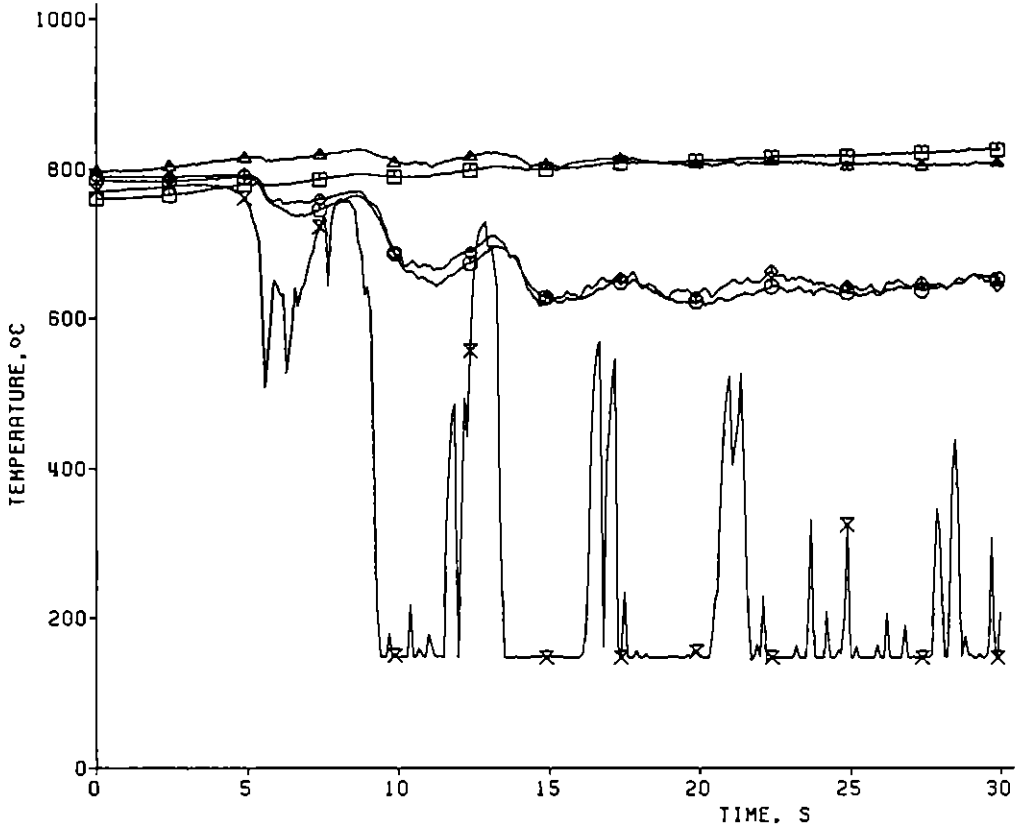

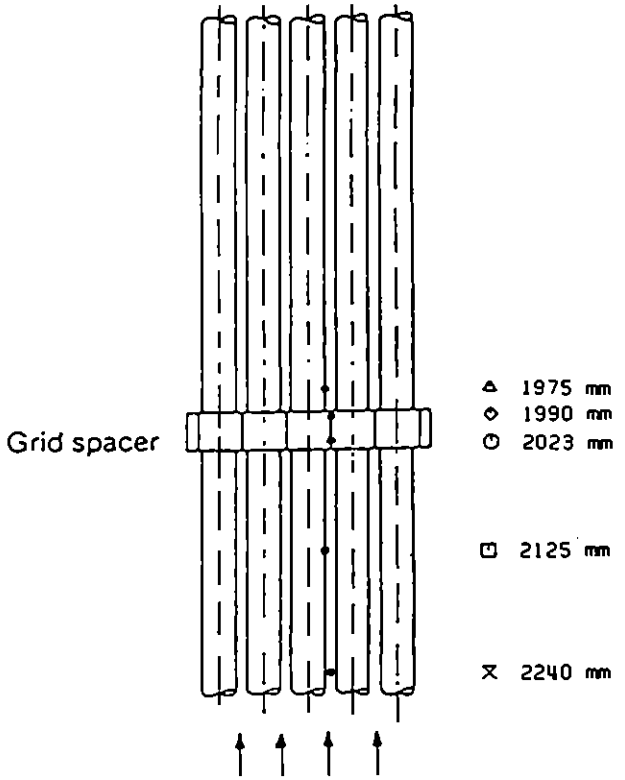

Flooding rate 3.8 cm/s
System pressure 4.1 bar

SEFLEX test No. 03
REBEKA rod bundle
Helium-filled gaps

Axial levels:
Cladding, 2125 mm
Cladding, 1975 mm
Grid spacer, leading edge, 2023 mm
Grid spacer, trailing edge, 1990 mm
Fluid TC signal, 2240 mm

Figure 43. Cladding and grid spacer temperatures, and fluid TC signal on enlarged time scale at beginning of reflood (test No. 03).

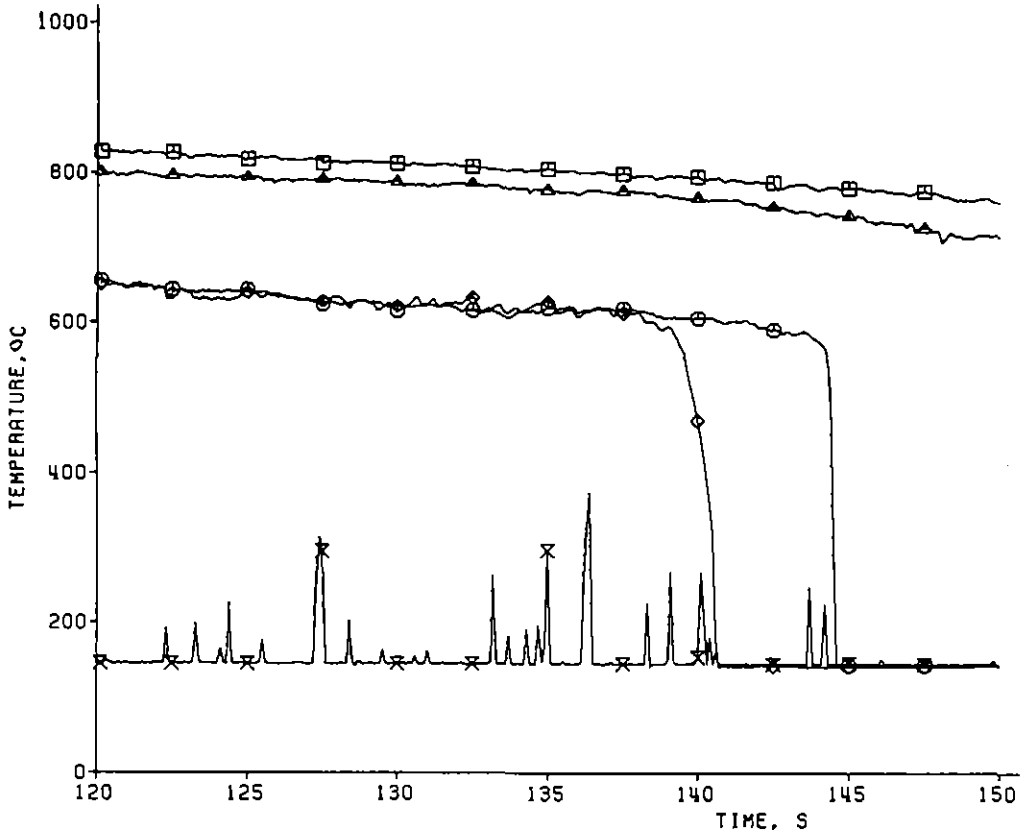

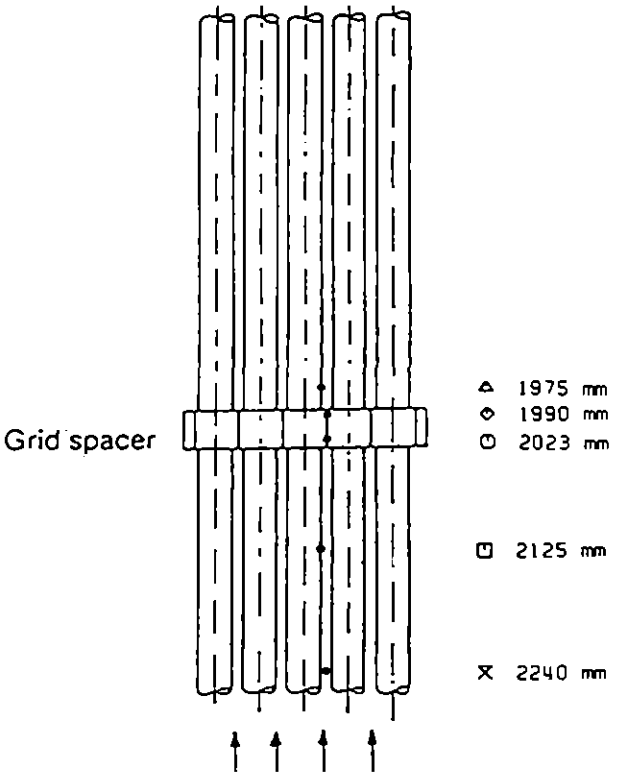

Flooding rate 3.8 cm/s
System pressure 4.1 bar

SEFLEX test No. 03
REBEKA rod bundle
Helium-filled gaps

Axial levels:
□ Cladding, 2125 mm
△ Cladding, 1975 mm
○ Grid spacer, leading edge, 2023 mm
◇ Grid spacer, trailing edge, 1990 mm
X Fluid TC signal, 2240 mm

Figure 44. Cladding and grid spacer temperatures, and fluid TC signal on enlarged time scale at quenching of grid spacer (test No. 03).

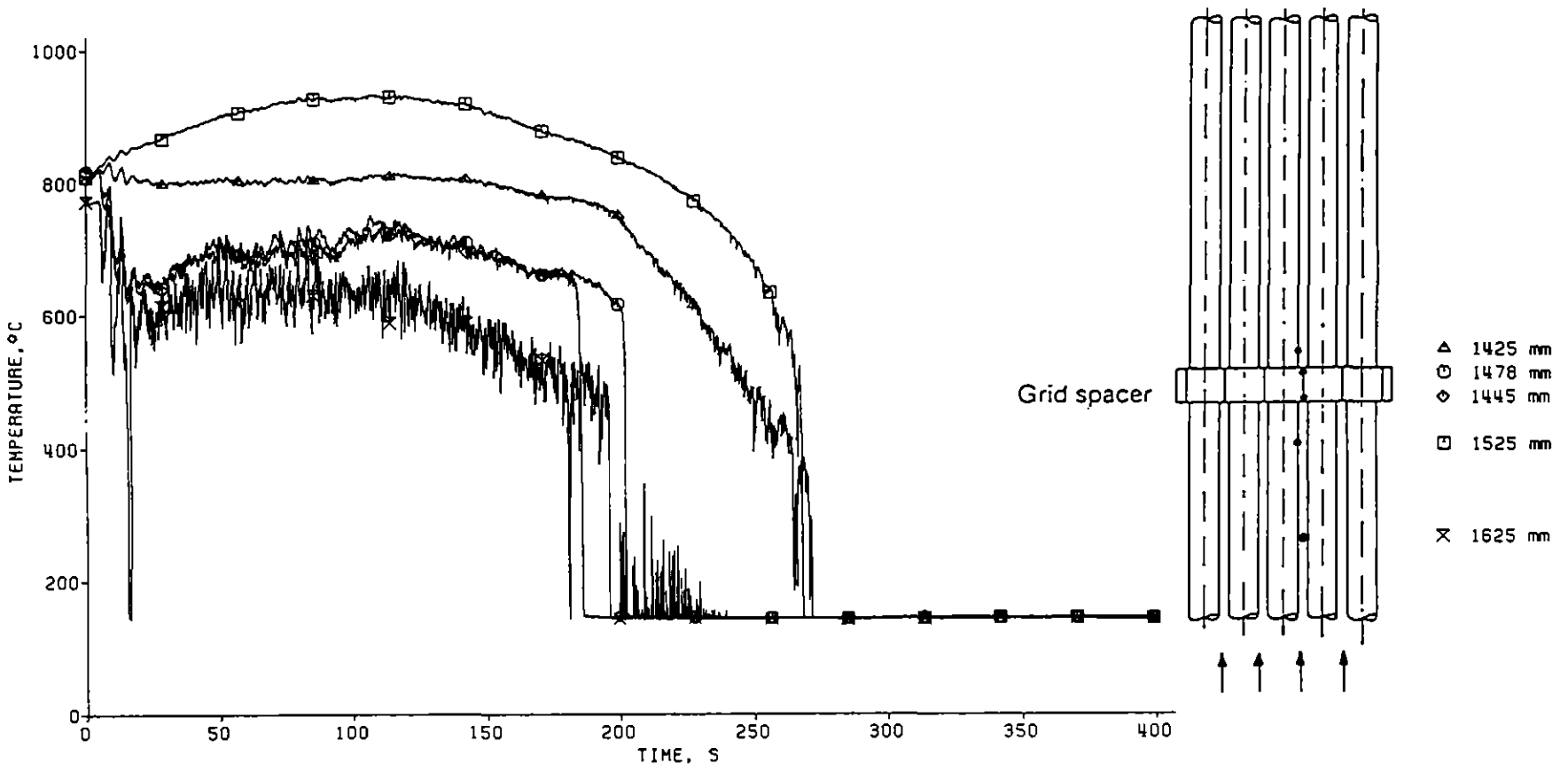

Flooding rate 3.8 cm/s
System pressure 4.1 bar

SEFLEX test No. 03
REBEKA rod bundle
Helium-filled gaps

Axial levels:
□ Cladding, 1525 mm
△ Cladding, 1425 mm
○ Grid spacer, leading edge, 1478 mm
◇ Grid Spacer, trailing edge, 1445 mm
X Fluid TC signal, 1625 mm

Figure 45. Cladding and grid spacer temperatures, and fluid TC signal above the bundle midplane (test No. 03).

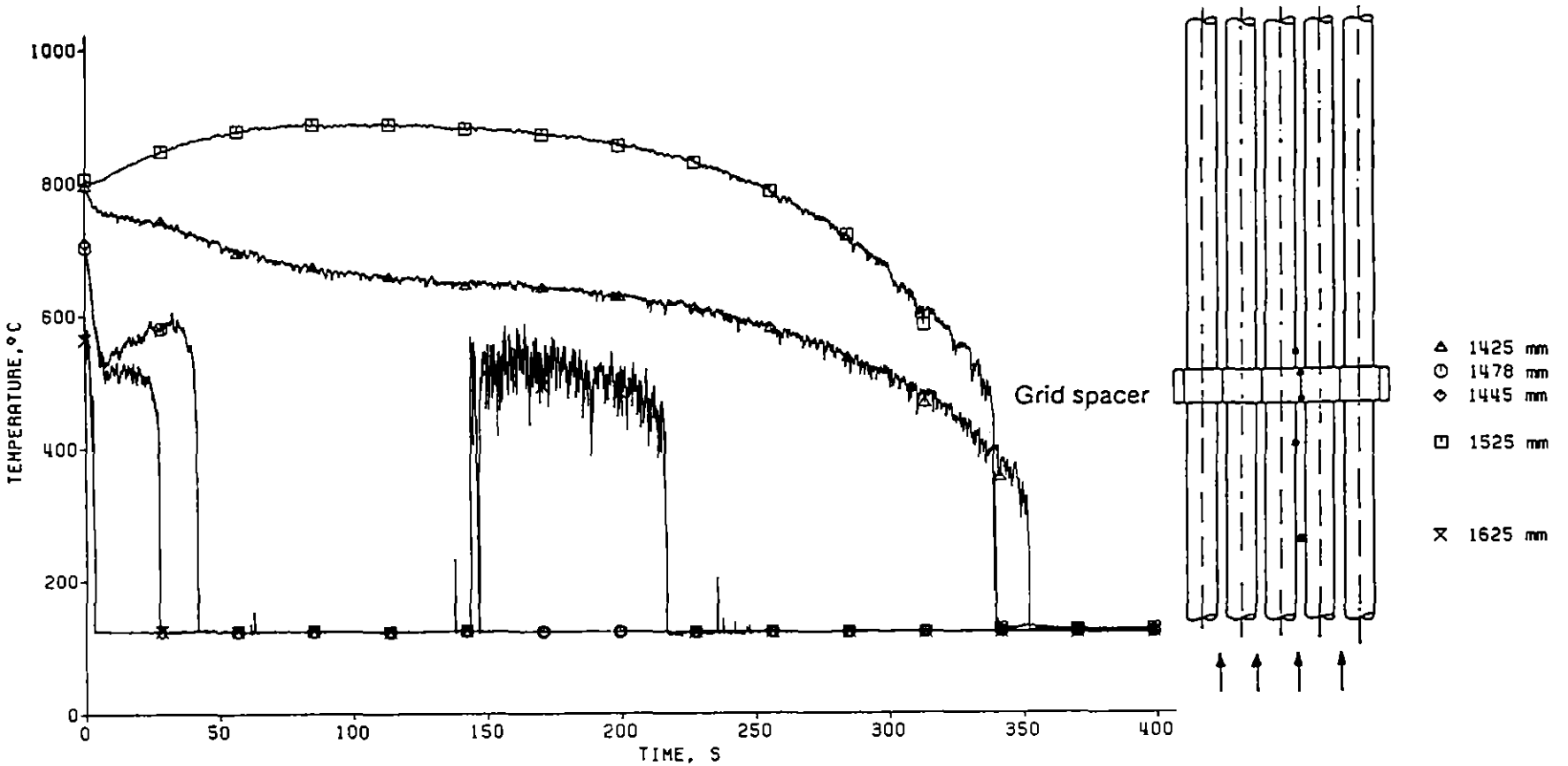

Flooding rate 3.8 cm/s
System pressure 2.1 bar

SEFLEX test No. 05
REBEKA rod bundle
Helium-filled gaps

Axial levels:
□ Cladding, 1525 mm
△ Cladding, 1425 mm
○ Grid spacer, leading edge, 1478 mm
◇ Grid spacer, trailing edge, 1445 mm
⧖ Fluid TC signal, 1625 mm

Figure 46. Cladding and grid spacer temperatures, and fluid TC signal above the bundle midplane (test No. 05).

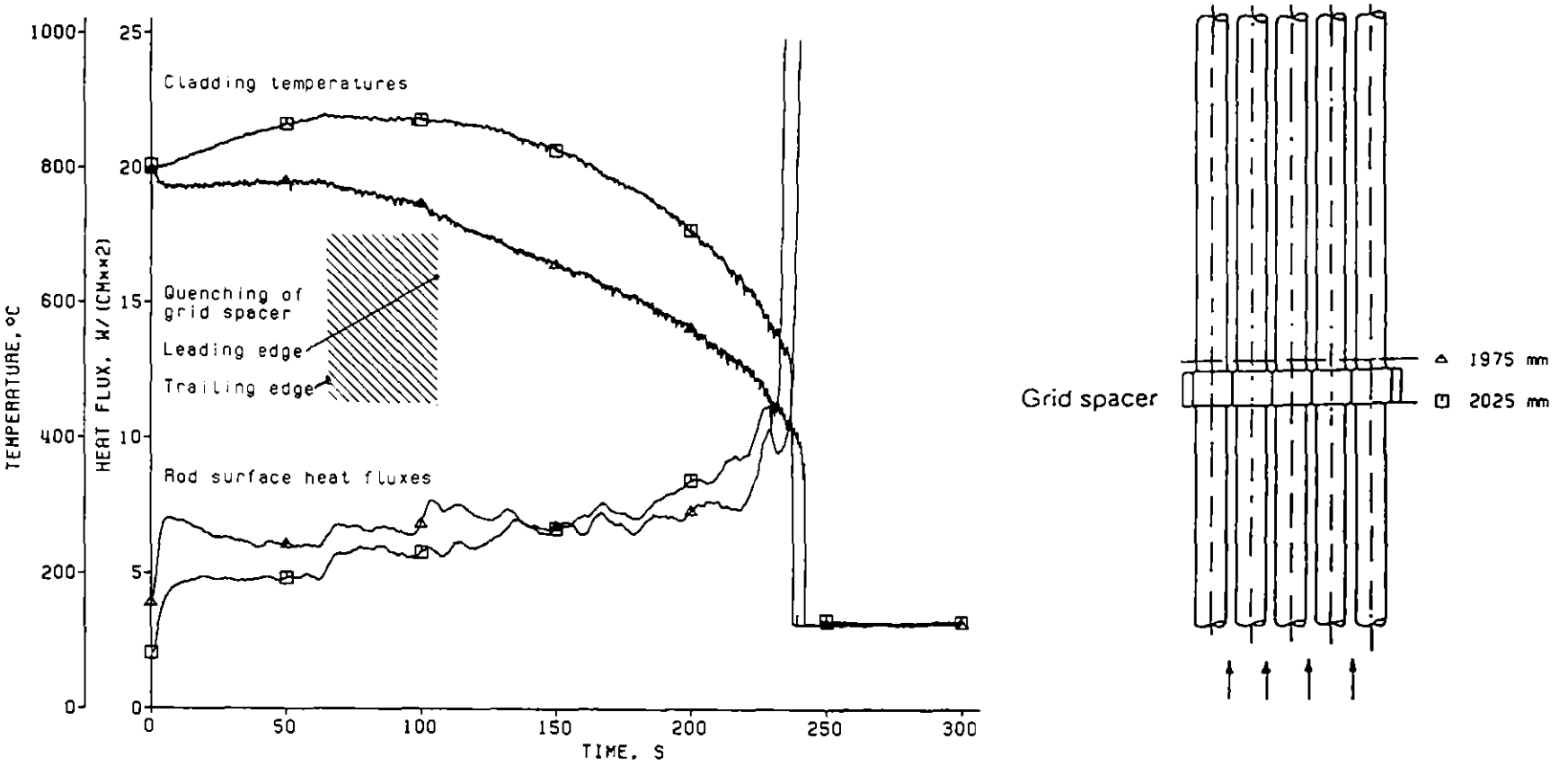

Flooding rate 3.8 cm/s
System pressure 2.1 bar

SEFLEX test No. 05
REBEKA rod bundle
Helium-filled gaps

Axial levels:
□ At leading edge of grid spacer (2025 mm)
△ 12 mm downstream of trailing edge of grid spacer (1975 mm)

Figure 47. Cladding temperatures and surface heat fluxes at leading edge and 12 mm downstream of bundle midplane grid spacer (test No. 05).

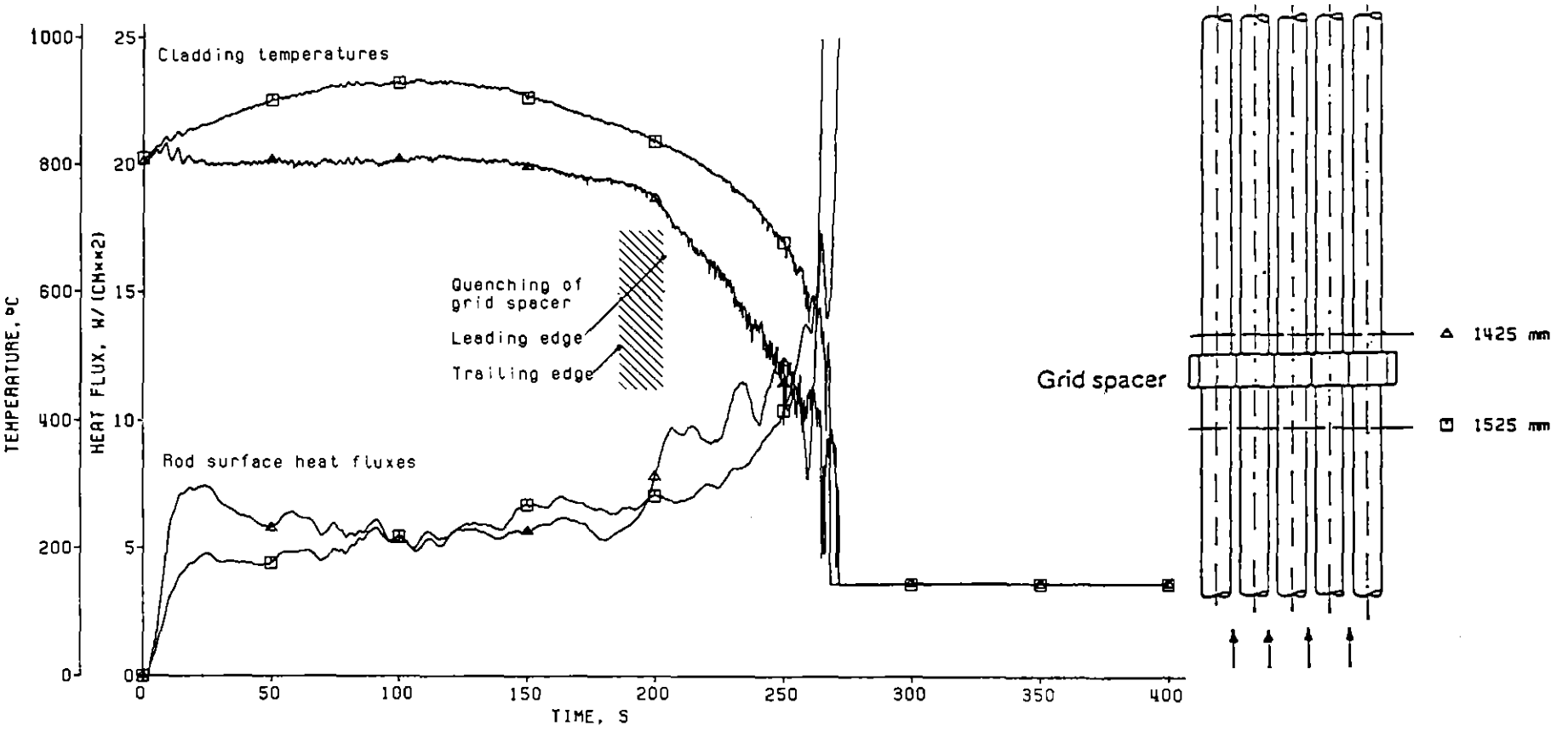

Flooding rate 3.8 cm/s
System pressure 4.1 bar

SEFLEX test No. 03
REBEKA rod bundle
Helium-filled gaps

Axial levels:
□ 45 mm upstream of grid spacer (1525 mm)
△ 17 mm downstream of grid spacer (1425 mm)

Figure 48. Cladding temperatures and surface heat fluxes upstream and 17 mm downstream of the grid spacer above the bundle midplane (test No. 03).

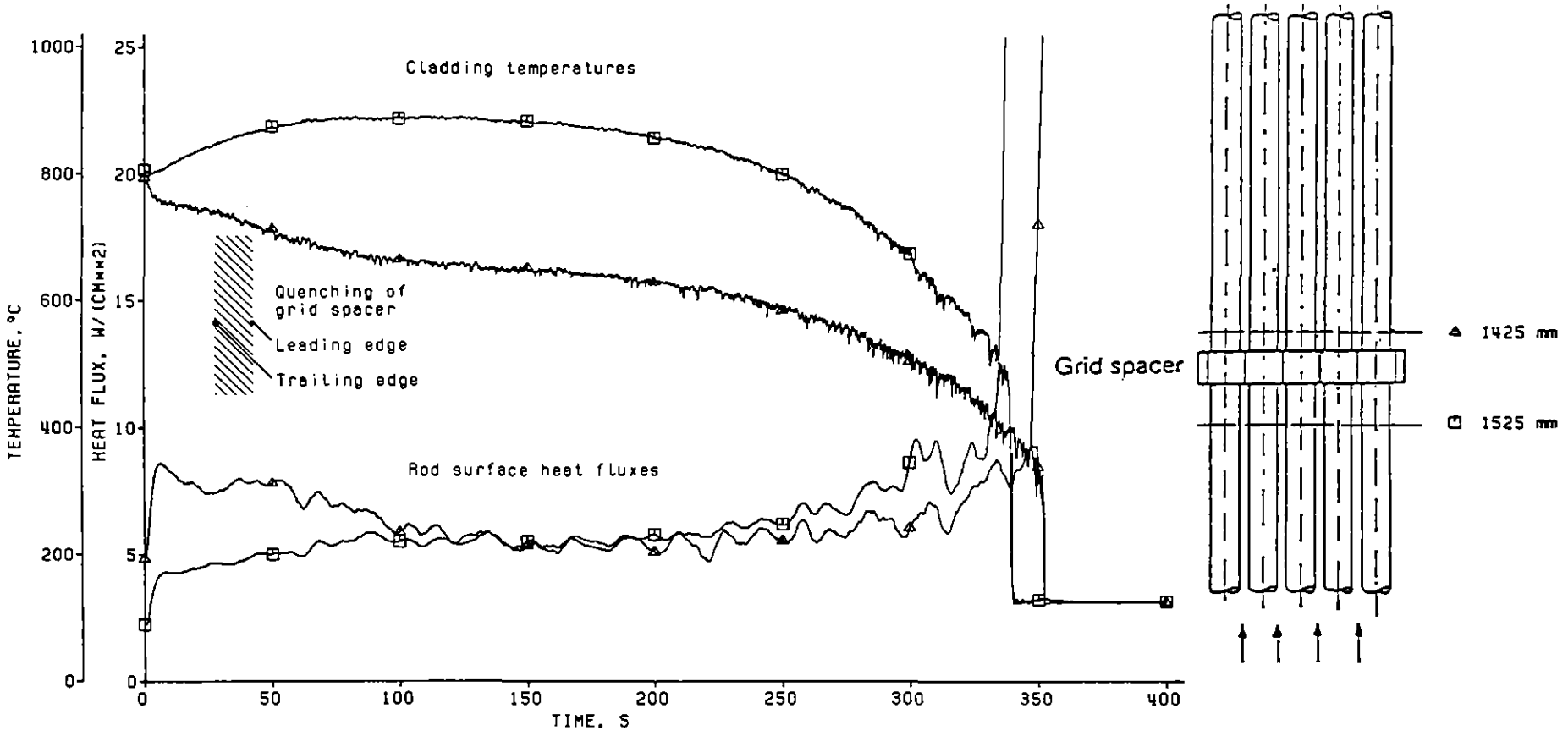

Flooding rate 3.8 cm/s
System pressure 2.1 bar

SEFLEX test No. 05
REBEKA rod bundle
Helium-filled gaps

Axial levels:
□ 45 mm upstream of grid spacer (1525 mm)
△ 17 mm downstream of grid spacer (1425 mm)

Figure 49. Cladding temperatures and surface heat fluxes upstream and 17 mm downstream of the grid spacer above the bundle midplane (test No. 05).

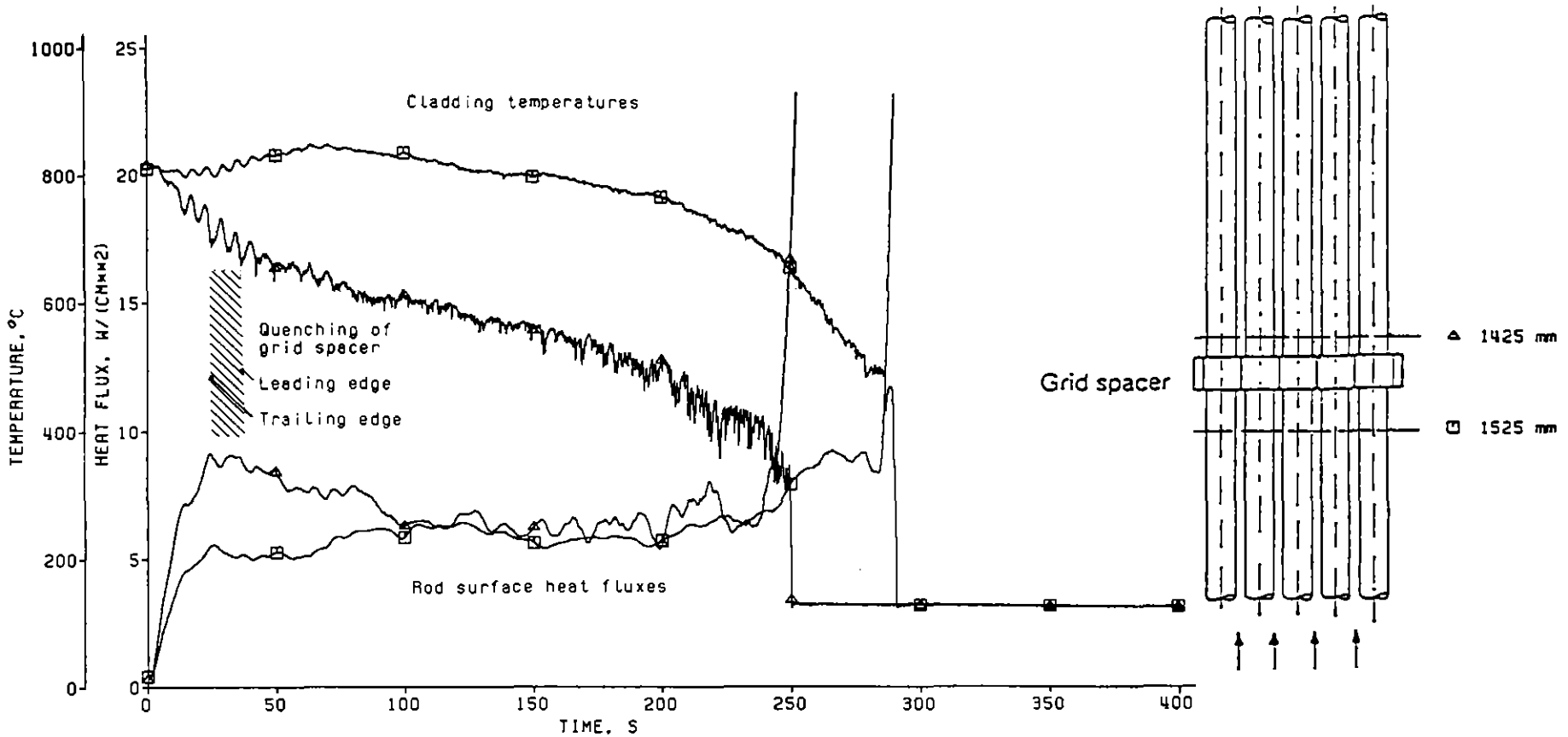

Flooding rate 3.8 cm/s
System pressure 2.1 bar

SEFLEX test No. 07
REBEKA rod bundle
Argon-filled gaps

Axial levels:
□ 45 mm upstream of grid spacer (1525 mm)
△ 17 mm downstream of grid spacer (1425 mm)

Figure 50. Cladding temperatures and surface heat fluxes upstream and 17 mm downstream of the grid spacer above the bundle midplane (test No. 07).

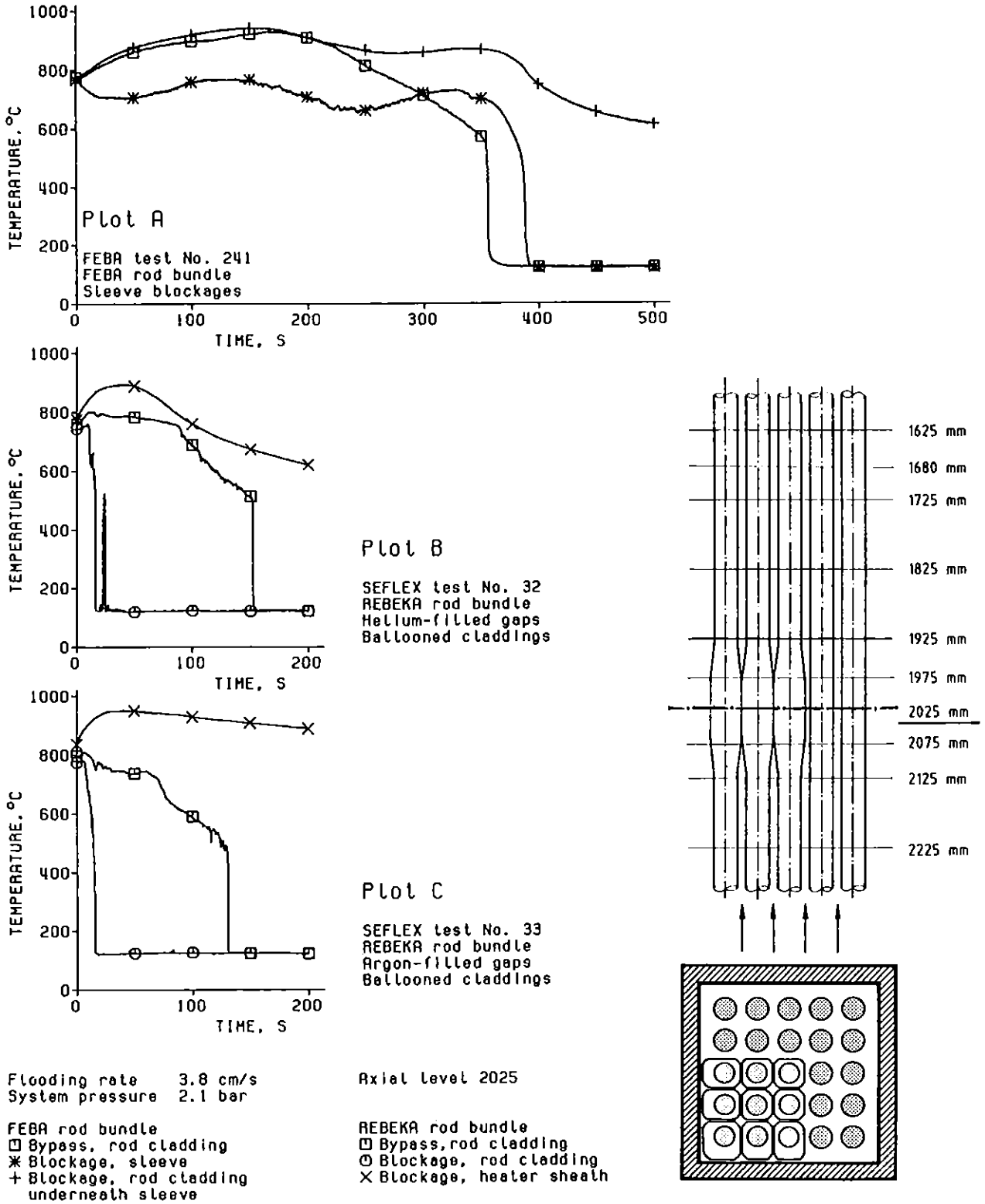

Figure 51. Temperatures measured at the midplane of a 90 percent blockage and in the blockage bypass of FEBA and REBEKA rod bundles.

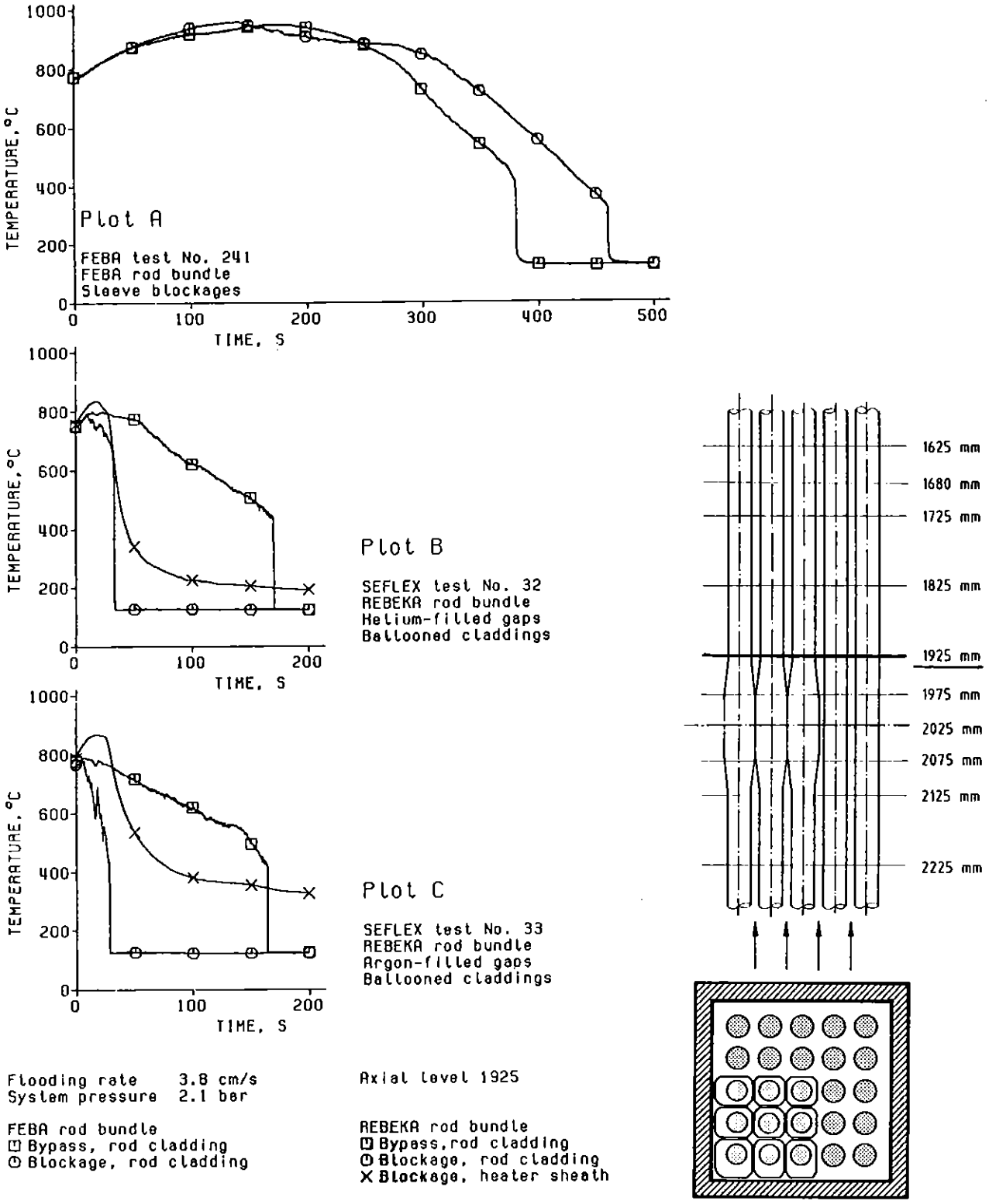

Figure 52. Temperatures measured 10 mm downstream of a 90 percent blockage and in the blockage bypass of FEBA and REBEKA rod bundles.

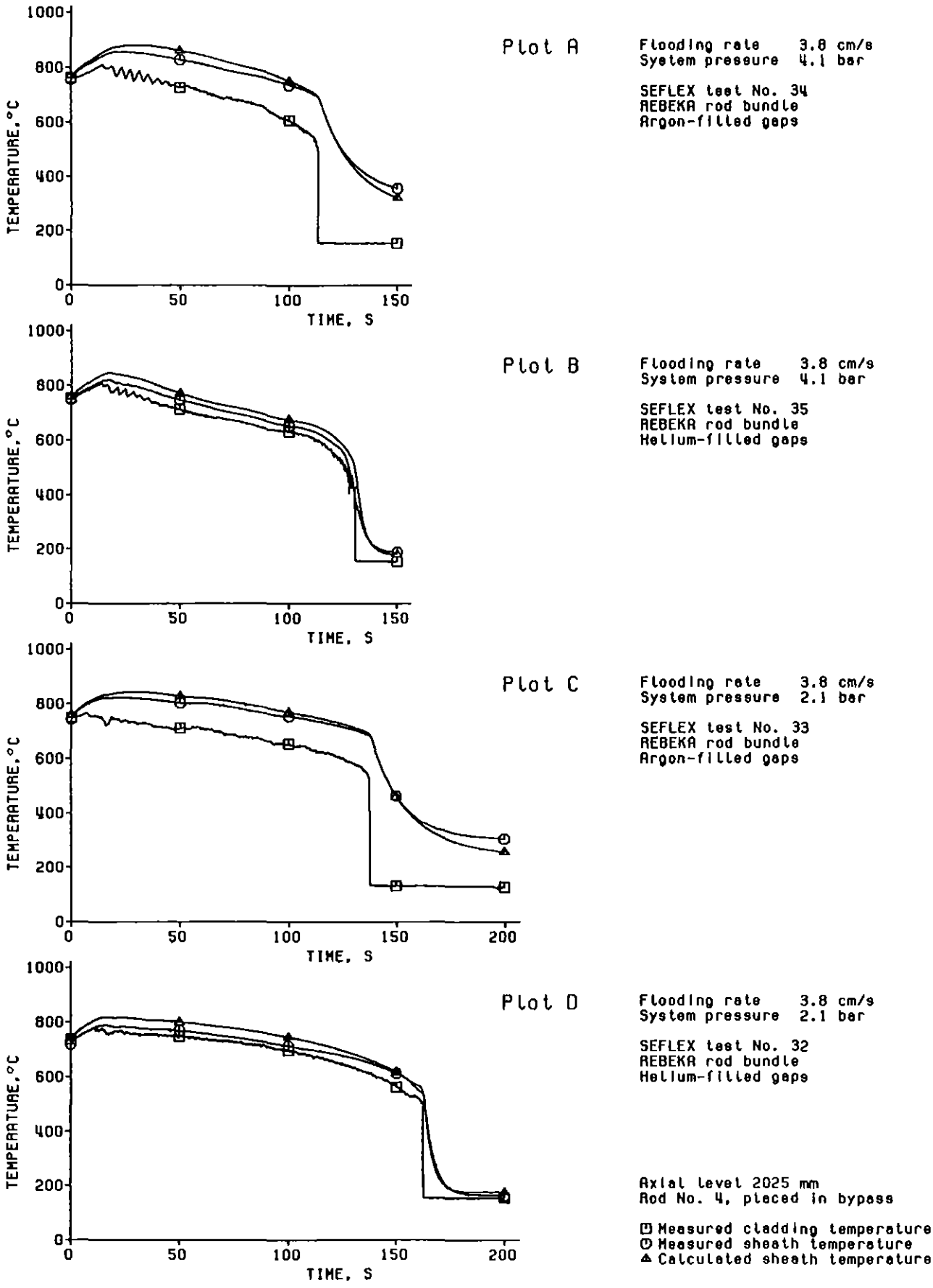

Figure 53. Comparison of measured and calculated heater sheath temperatures and corresponding cladding temperatures measured at the bundle midplane in the blockage bypass of a REBEKA rod bundle.

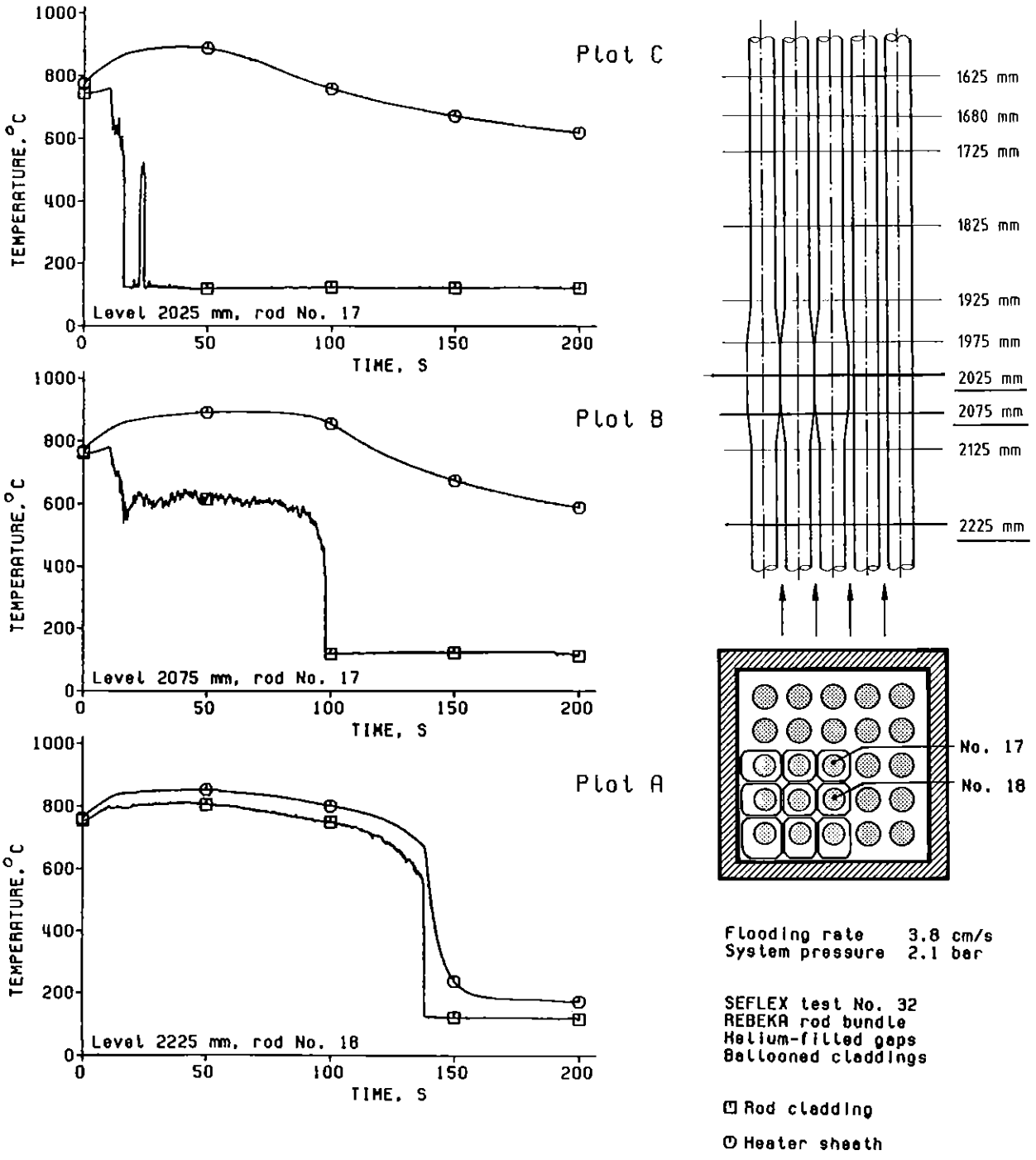

Figure 54. Cladding and heater sheath temperatures measured upstream and at the bundle midplane in the blocked rod cluster of a rod cluster of a REBEKA rod bundle.

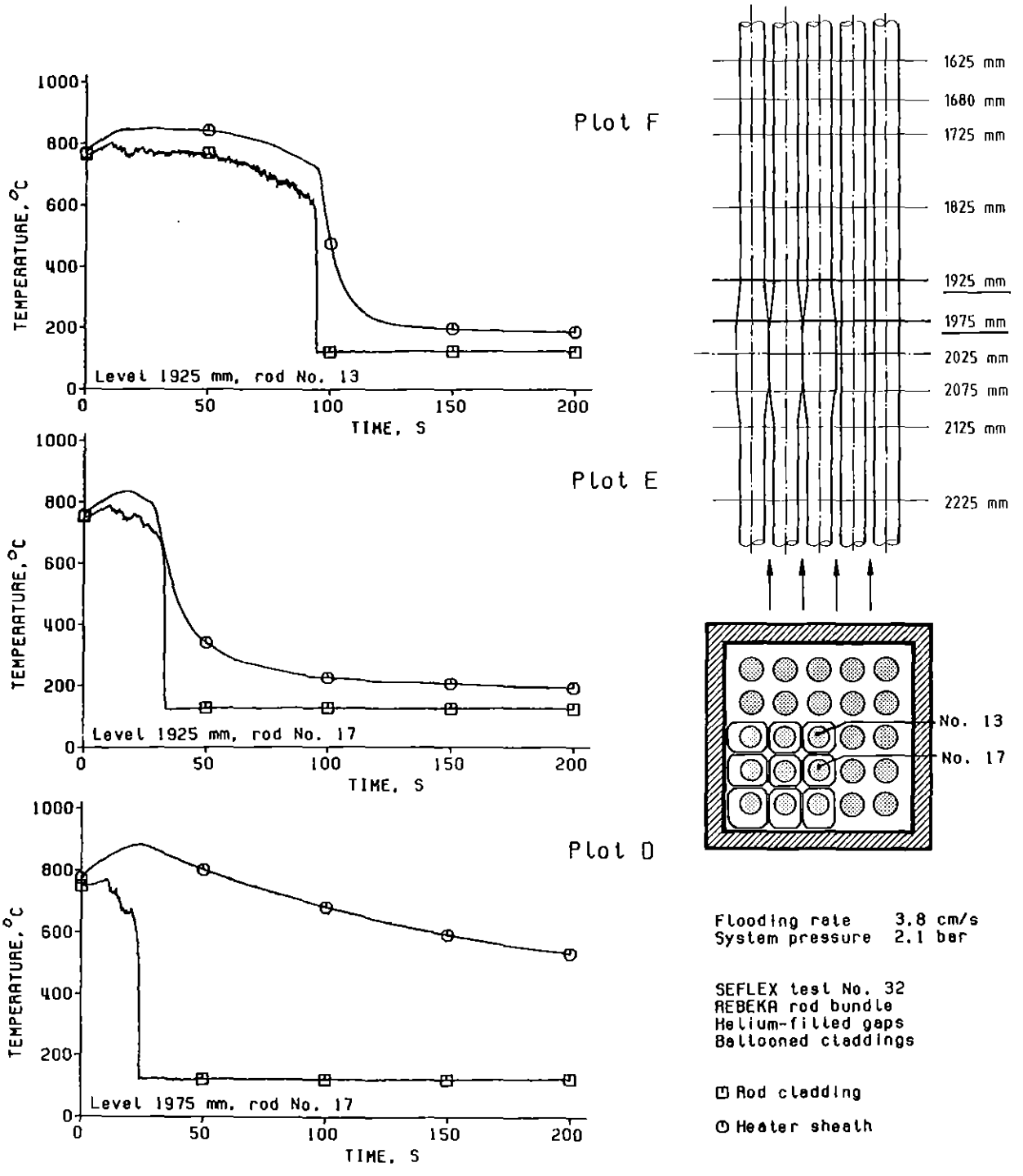

Figure 55. Cladding and heater sheath temperatures measured downstream of the bundle midplane in the blocked rod cluster of a REBEKA rod bundle.

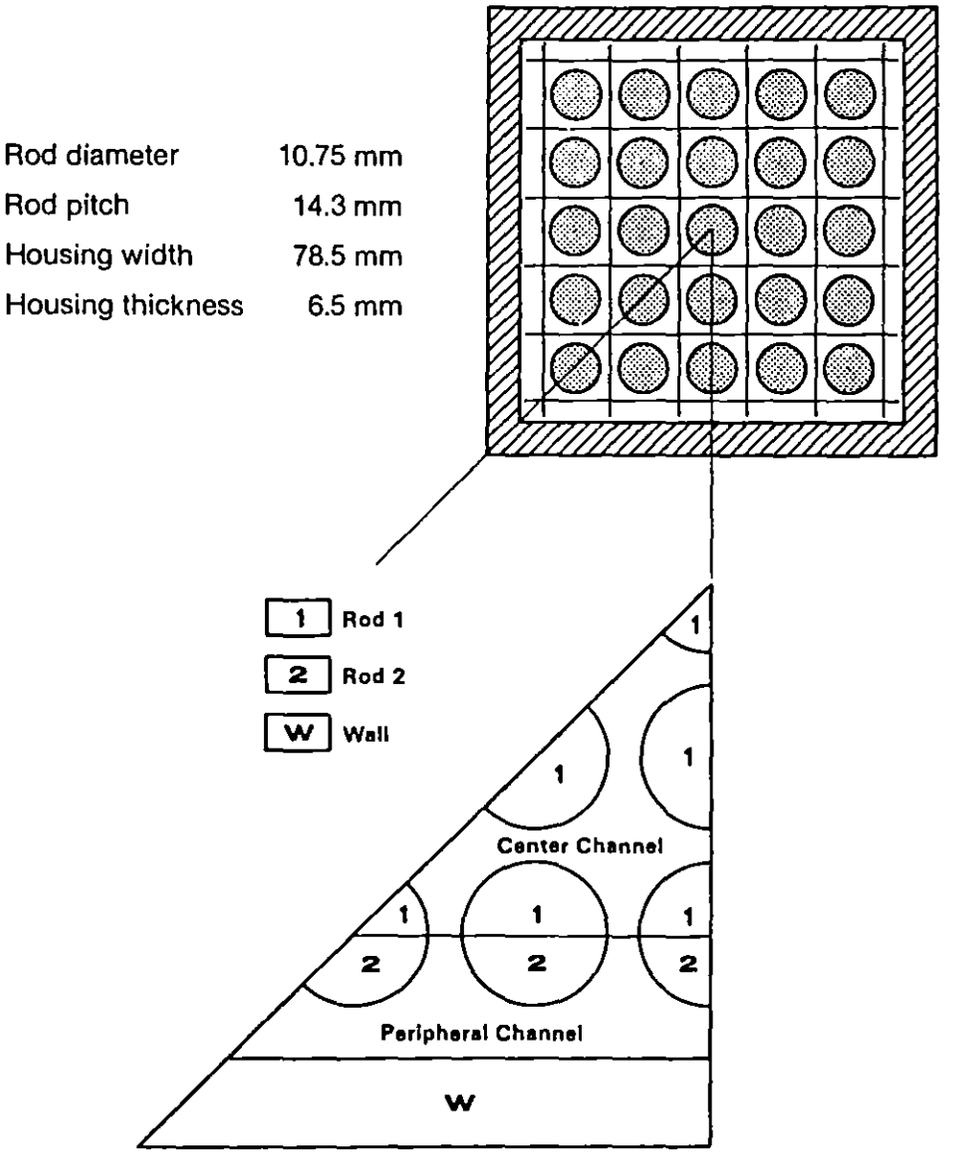

Figure 56. Radial noding scheme of the FEBA test section for COBRA-TF calculations.

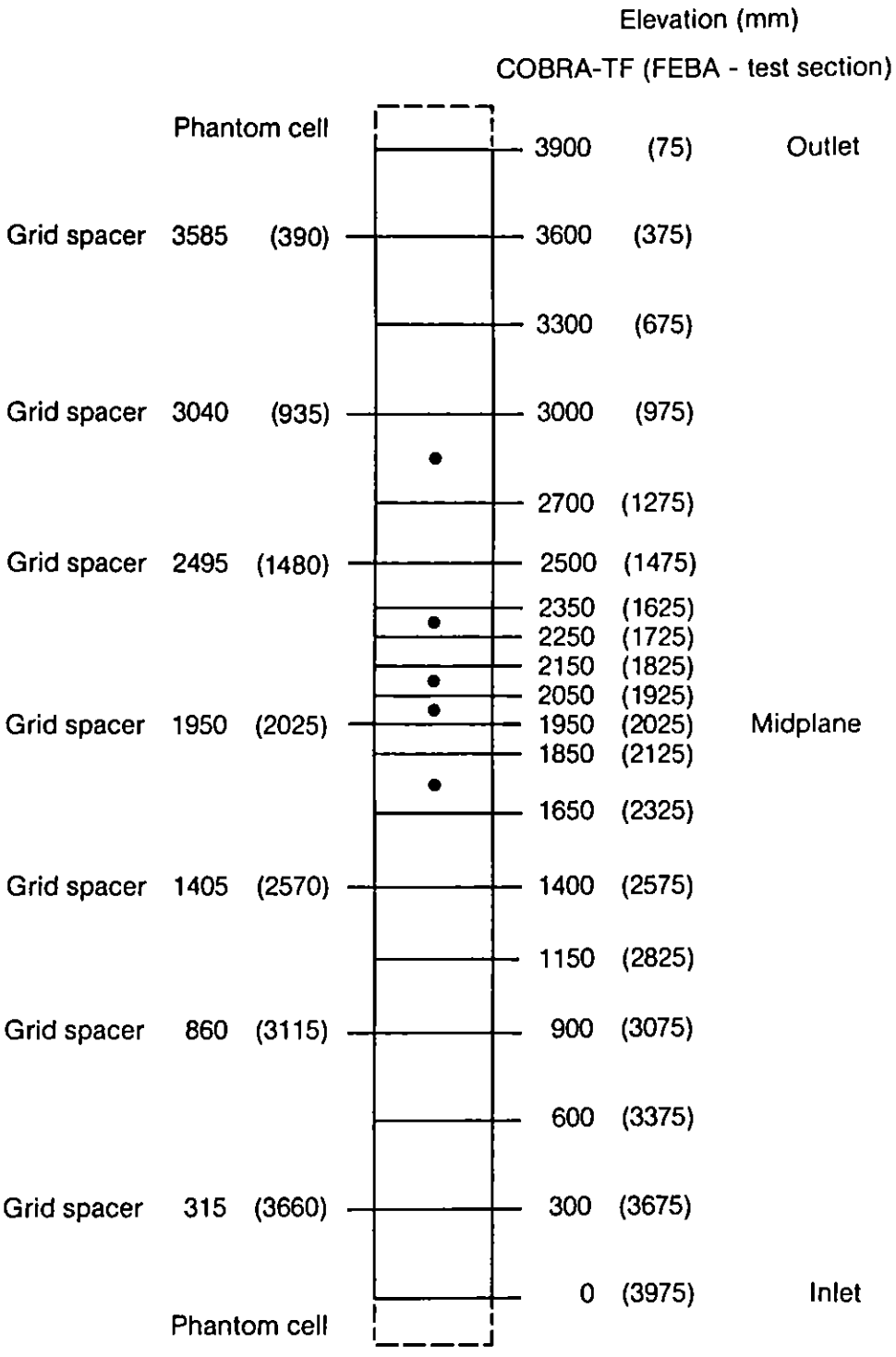

Figure 57. Axial noding scheme of the FEBA test section (fluid cells) for COBRA-TF calculations.

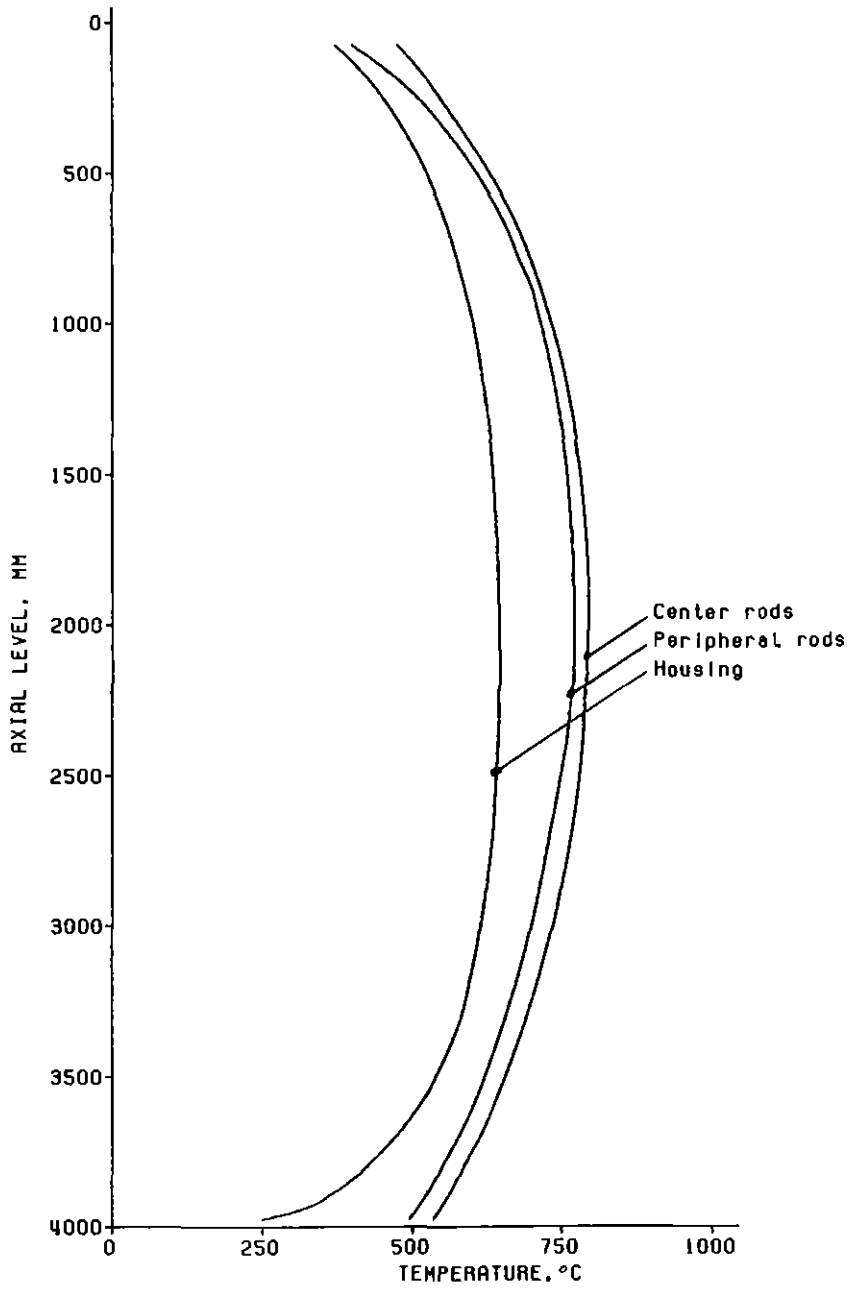

Figure 58. Initial axial temperature profiles of claddings and housing (SEFLEX test No. 03).

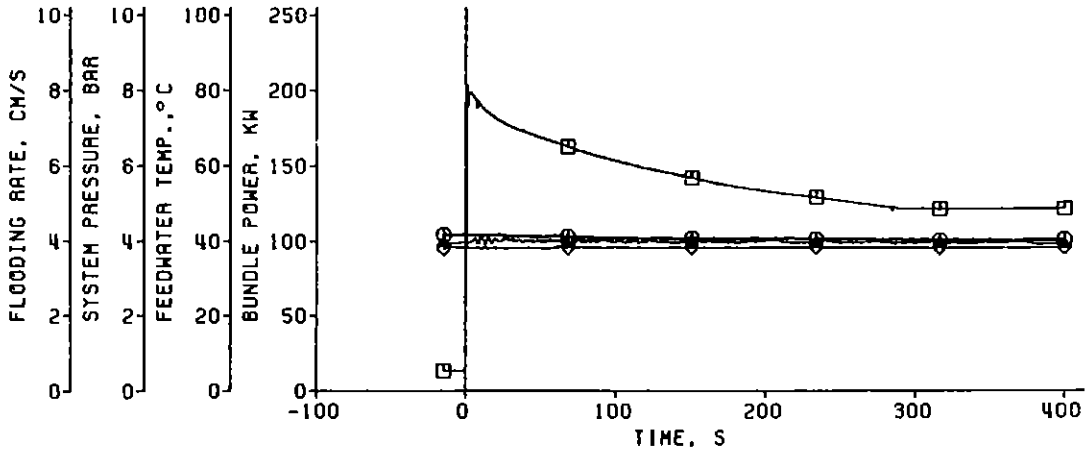

Flooding rate 3.8 cm/s
System pressure 4.1 bar

SEFLEX test No. 03
REBEKA rod bundle
Helium-filled gaps

◇ Flooding rate, (in cold bundle)
△ System pressure
⏲ Feedwater temperature
⊡ Bundle power

Figure 59. Flooding parameters (SEFLEX test No. 03).

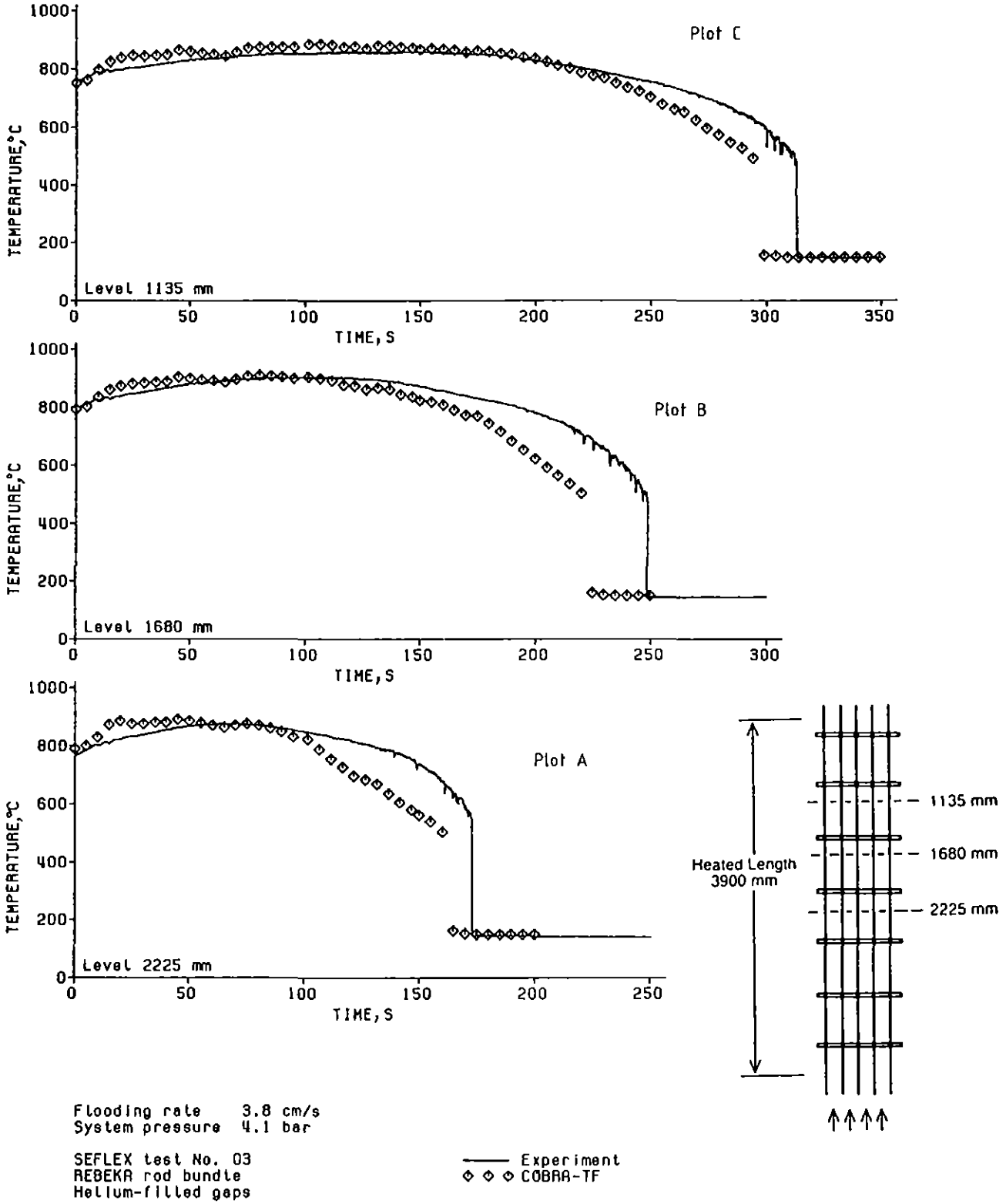

Figure 60. Comparison of measured and calculated center rod cladding temperatures (SEFLEX test No. 03).

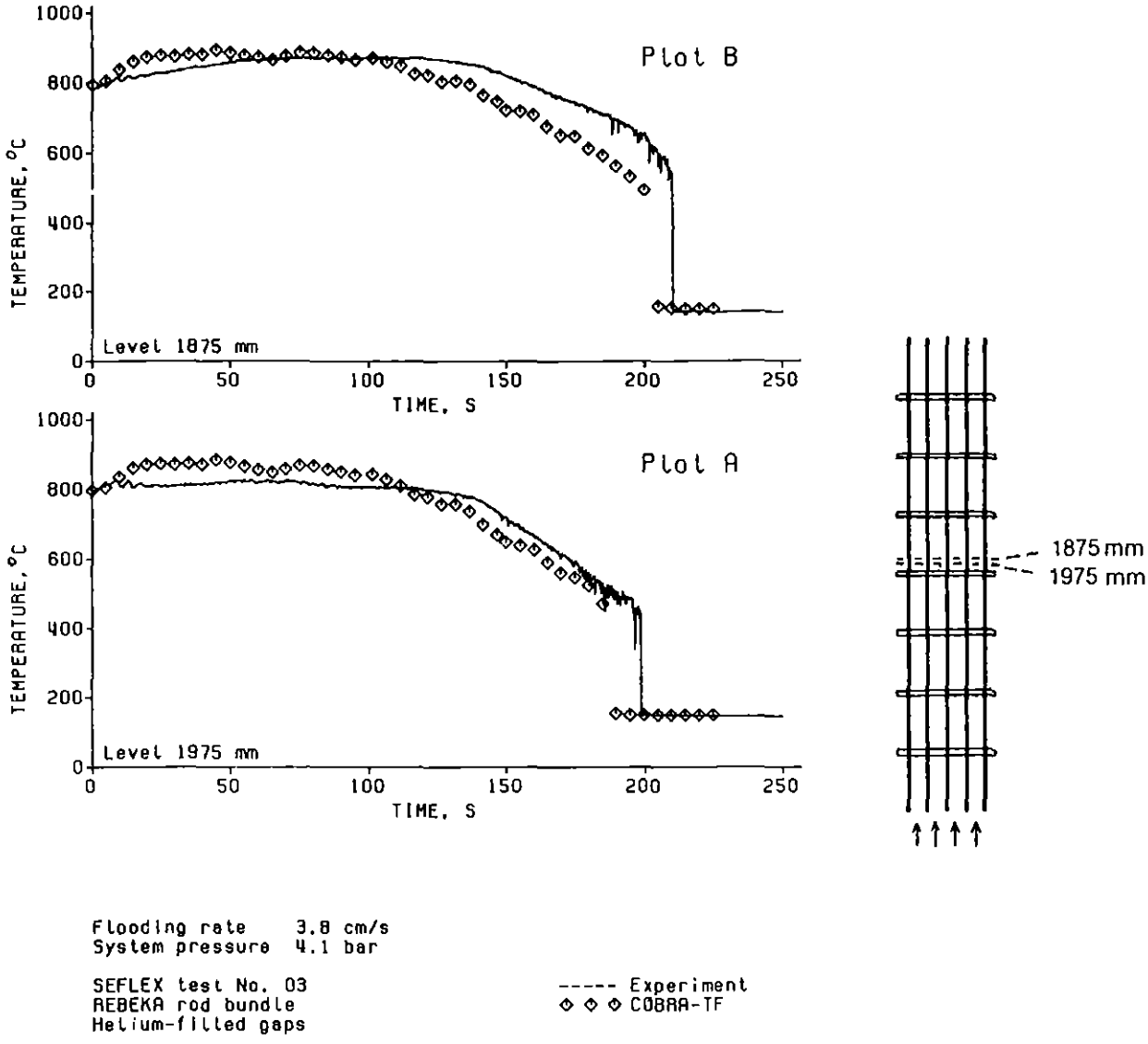

Figure 61. Comparison of measured and calculated center rod cladding temperatures downstream of the bundle midplane grid spacer (SEFLEX test No. 03).

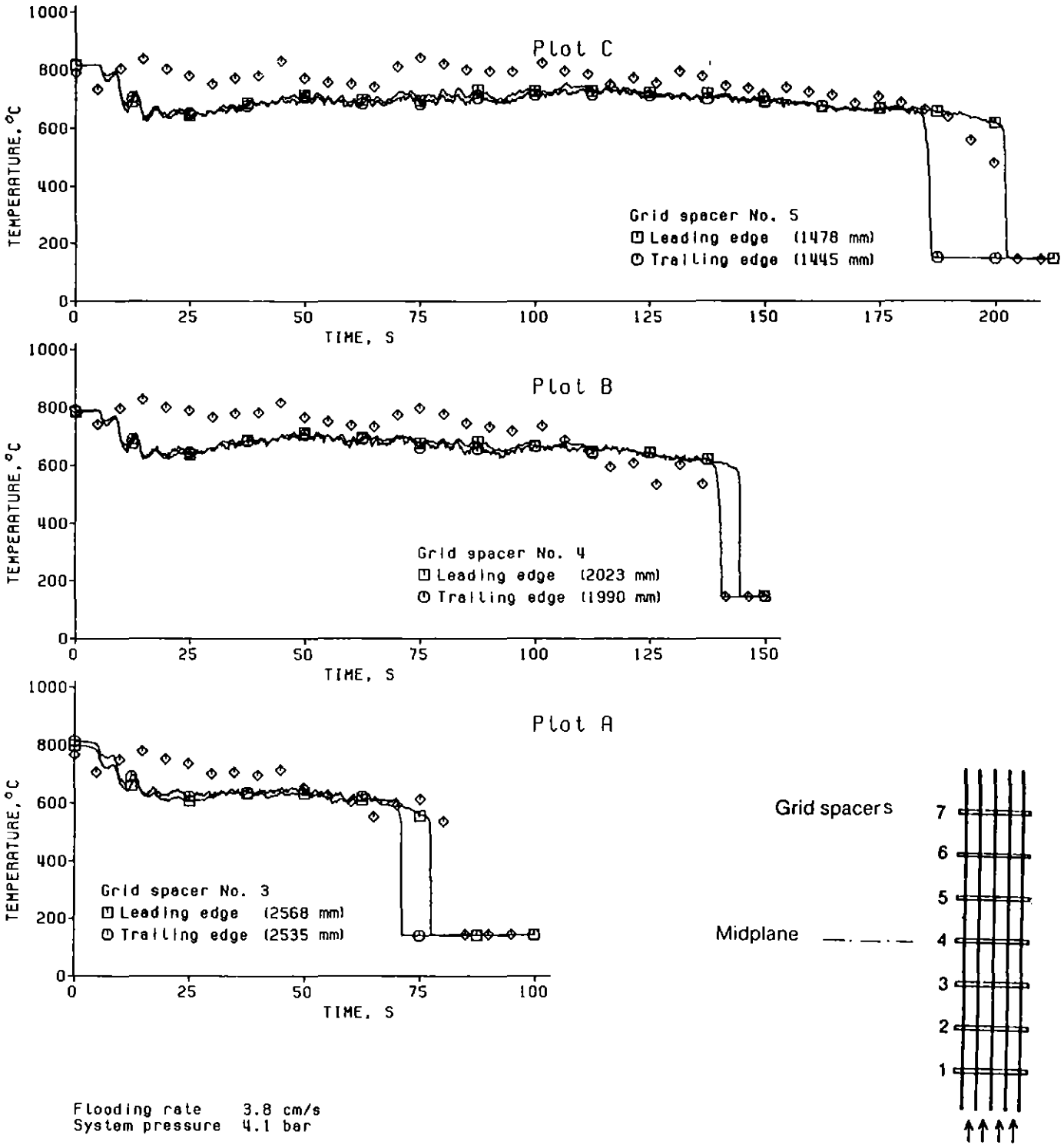

Figure 62. Comparison of measured and calculated grid spacer temperatures (SEFLEX test No. 03).

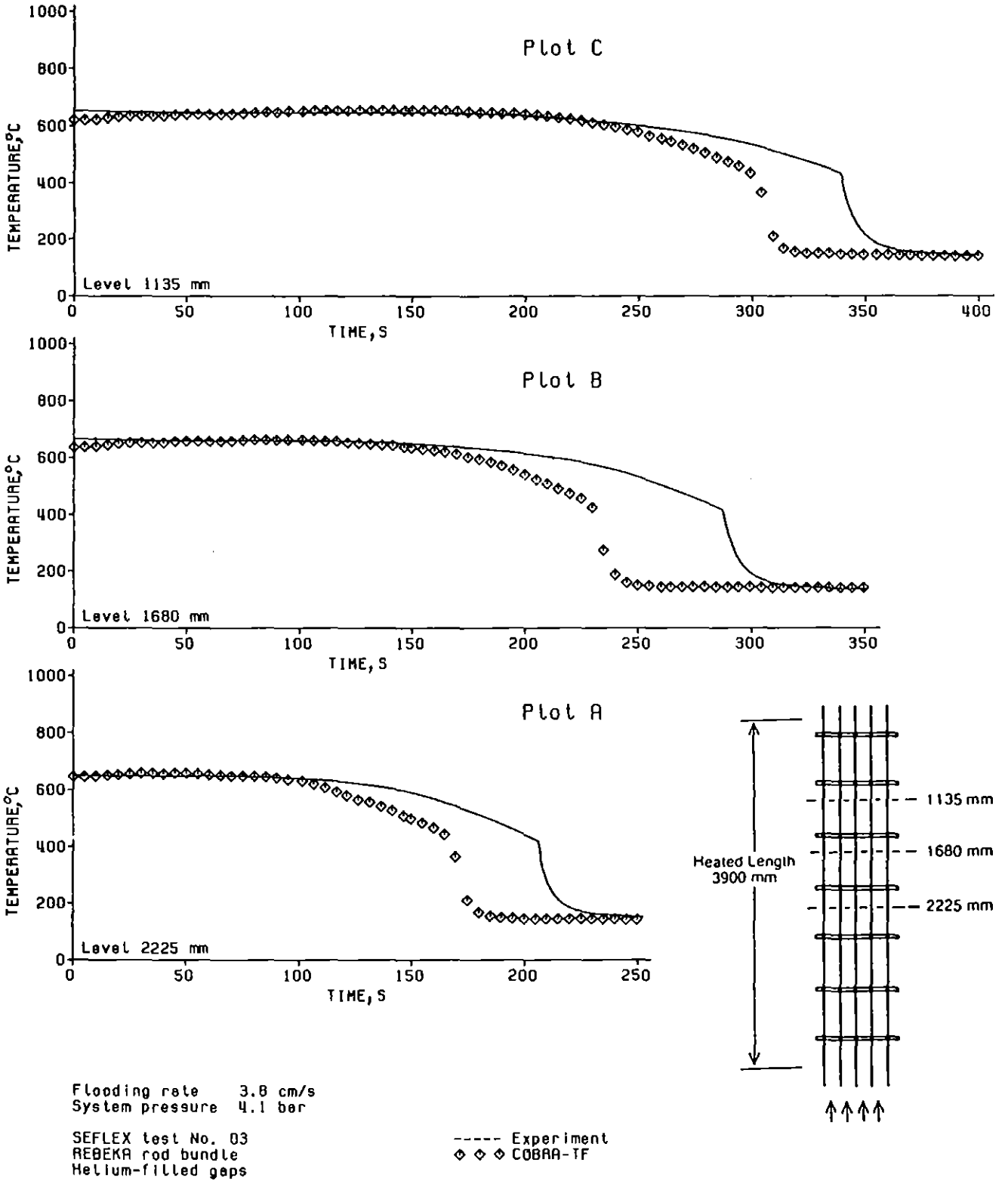

Figure 63. Comparison of measured and calculated housing temperatures (SEFLEX test No. 03).

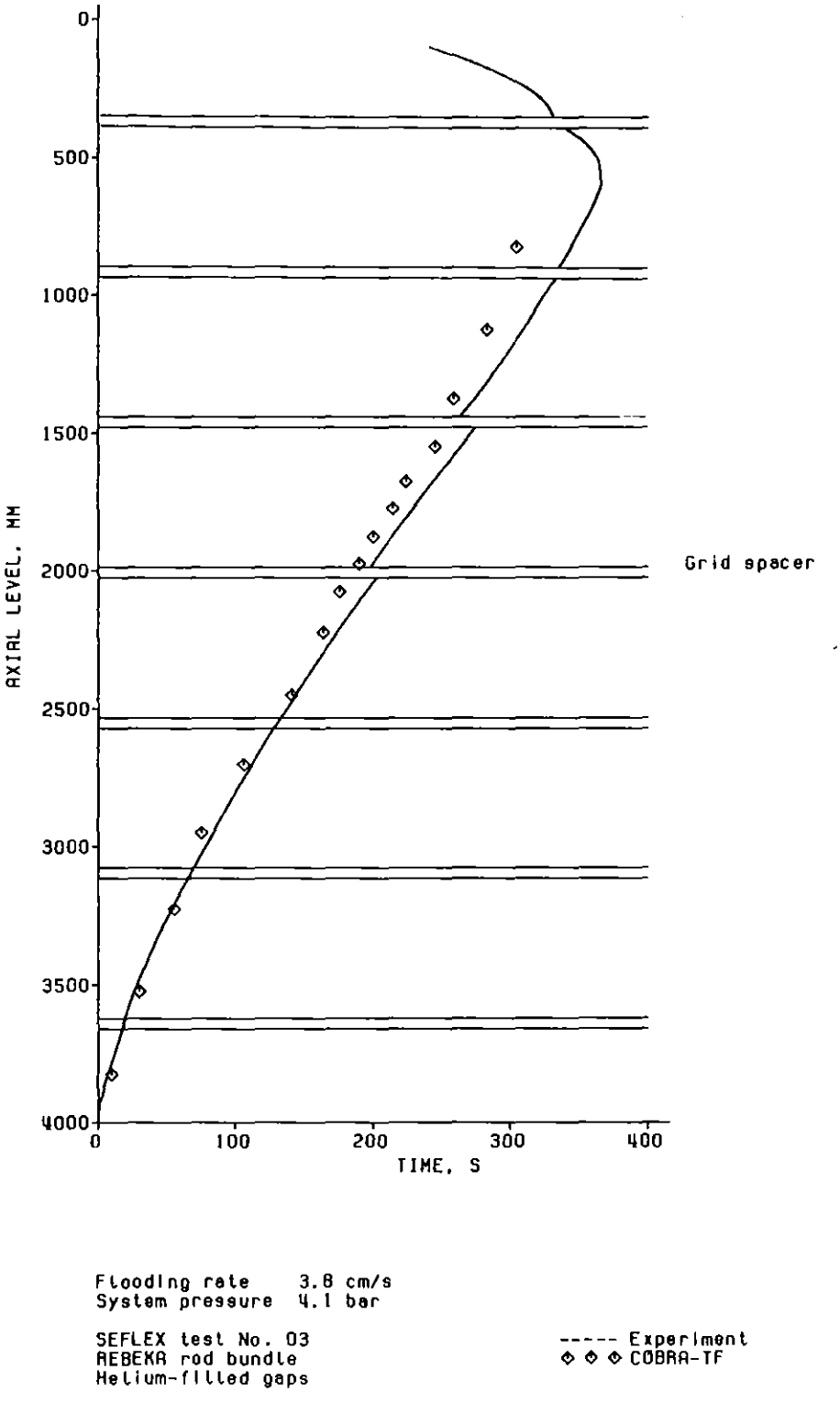

Figure 64. Comparison of measured and calculated quench front progression (SEFLEX test No. 03).

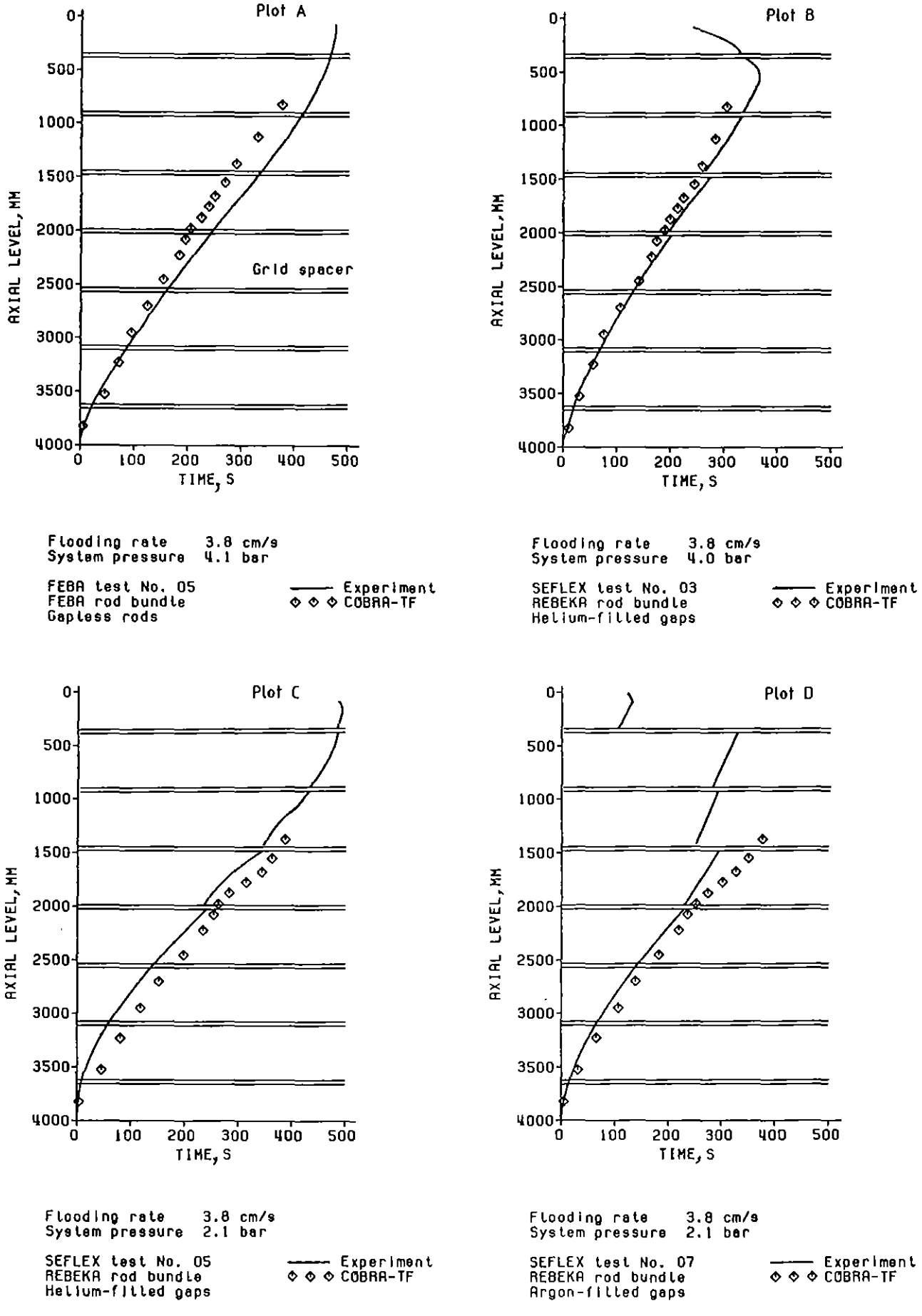

Figure 65. Comparison of measured and calculated quench front progression (FEBA test No. 223, SEFLEX tests No. 03, 05, and 07).